On the Distance-Independent Hole Transfer over Long (A–T)$_n$-Sequences in DNA

_____

Inauguraldissertation

zur

Erlangung der Würde eines
Doktors der Philosophie

vorgelegt der
Philosophisch-Naturwissenschaftlichen Fakultät
der Universität Basel

von

Ernst Furrer
aus Basel (BS)

Basel, 2004

Genehmigt von der Philosophisch-Naturwissenschaftlichen Fakultät der Universität Basel auf Antrag der Herren

Prof. Dr. Bernd Giese

Prof. Dr. Wolf-D. Woggon

Basel, den 28. September 2004

Prof. Dr. M. Tanner
(Dekan)

The work presented herein was initiated and guided by Prof. Dr. Bernd Giese at the Institute of Organic Chemistry of the Philosophic-Scientific Faculty of the University of Basel, during the time period from September 2000 to September 2004.

For my parents

„Experience: that most brutal of teachers. But you learn, my God you learn.”

--- C. S. Lewis

„Art is born of the observation and investigation of nature.“

--- Cicero

Experimental Part

Abbreviations and Acronyms

A	adenine within structural formulas, adenosine within text
A*	4'-pivaloyl modified adenosine
APT	attached proton test (NMR)
arom.	aromatic (NMR)
ATP	adenosine triphosphate
B	any base (adenine, cytosine, guanine or thymine)
Bn	benzyl
Boc	(*tert*-butoxy)carbonyl
B^P	any protected base (adenine, cytosine or guanine)
Bz	benzoyl
C	cytosine within structural formulas, cytidine within text
°C	degree centigrade
CD	circular dichroism
CMC	1-cyclohexyl-3-(2-morpholinoethyl)carbodiimide-*p*-toluenesulfonate
CPG	controlled pore glass
CPM	counts per minute
CSA	(±)-camphorsulfonic acid
d	deoxy-
DCC	dicyclohexyl carbodiimide
DEPT	distortionless enhancement by polarization transfer (NMR)
DMAP	(4-dimethylamino)pyridine
dmf	(dimethylamino)methylidene
DMF	dimethylformamide
DMT	4,4′-dimethoxytrityl (=bis(4-methoxyphenyl)(phenyl)methyl)
DNA	deoxyribonucleic acid
EA	elementary analysis
EDTA	ethylendiamine tetraacetate
ESI	electrospray ionization

ET	electron transfer
FAB	fast-atom bombardment
FC	flash column chromatography
G	guanine within structural formulas, guanosine within text
H	reduced abasic site
HPCE	high performance capillary electrophoresis
HPLC	high performance liquid chromatography
Hz	Hertz
IR	infrared / infrared spectroscopy
J	coupling constant
k	rate constant
MALDI-TOF	matrix-assisted laser desorption ionization time-of-flight
MO	molecular orbital
M.p.	melting point
MS	mass spectrometry
NHE	normal hydrogen electrode
NMR	nuclear magnetic resonance
NOE	nuclear overhauser effect (NMR)
$\tilde{\nu}$	wavenumber
PAGE	polyacrylamide gel electrophoresis
PE	polyethylene
PMMA	polymethyl methacrylate
ppm	part(s) per million
py	pyridine
R_f	Retention factor (TLC)
RP	reversed-phase
r.t.	room temperature
T	thymine within structural formulas, thymidine within text
TBAF	Bu_4NF
TBDMS	t-$BuMe_2Si$

TBE	*Tris*-borate-EDTA buffer
TEAA	tetraethylammonium acetate
TFA	trifluoroacetic acid
THF	tetrahydrofuran
TLC	thin layer chromatography
T_m	DNA melting temperature
TMEDA	N,N,N',N'-tetramethylethylene-1,2-diamine
Tris	tris(hydroxymethyl)aminomethane (=2-amino-2-(hydroxymethyl)propane-1,3-diol)
UV	ultraviolet
UV/VIS	ultraviolet/visible spectroscopy
Å	Ångström (1 Å $= 10^{-10}$ m)

Theoretical Part

1 Introduction and Basics

1.1 Structure and Function of Deoxyribonucleic Acid (DNA)

1.1.1 The Molecular Structure of DNA

Carrying the hereditary information of all living cells, DNA came into the researchers' focus in the early 1950s, when its molecular structure was elucidated.[1] In 1953, *Watson* and *Crick* succeeded in interpretating an X-ray scattering pattern of native DNA, and, together with previous results, proposed its structure to be a right-handed, double-stranded helix.[2] DNA is built up of monomeric units called nucleotides. A nucleotide consists of three molecular fragments: sugar, heterocycle, and phosphate. The sugar, or deoxyribose, is in a cyclic, furanoside form and is connected by a β-glycosyl linkage with one of four heterocyclic bases to produce the four normal nucleosides: adenosine, guanosine, cydidine, and thymidine. In DNA, the nucleosides are linked by 3',5'-phosphodiester bonds to form a linear polymer. Specific, hydrogen-bonded base-pairs of adenine with thymine (A−T) and guanine with cytosine (G−C) (*Figure 1.1*) are stacked like rolled coins at 3.4 Å distance (pitch). Right-handed rotation of approximately 36° between adjacent base-pairs produces a double helix of two antiparallel strands with 10.5 base-pairs per turn and 20 Å diameter. The arrangement of the two strands generates two grooves of similar depth but different width along the double helix, denominated as the minor and major grooves. (*Figure 1.2*).[3]

A   **T**   **G**   **C**
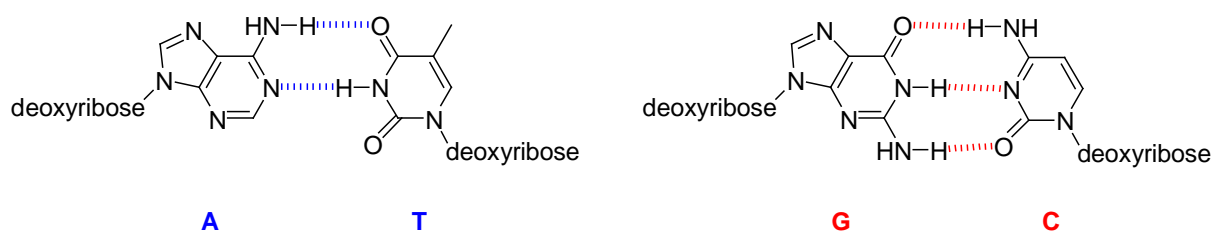
Figure 1.1. Hydrogen-bonded base-pairs after Watson and Crick

hydrogen-bonded nucleobases
5'
3'
20 Å
minor groove
34 Å
major groove
5'
3'
sugar-phosphate backbone
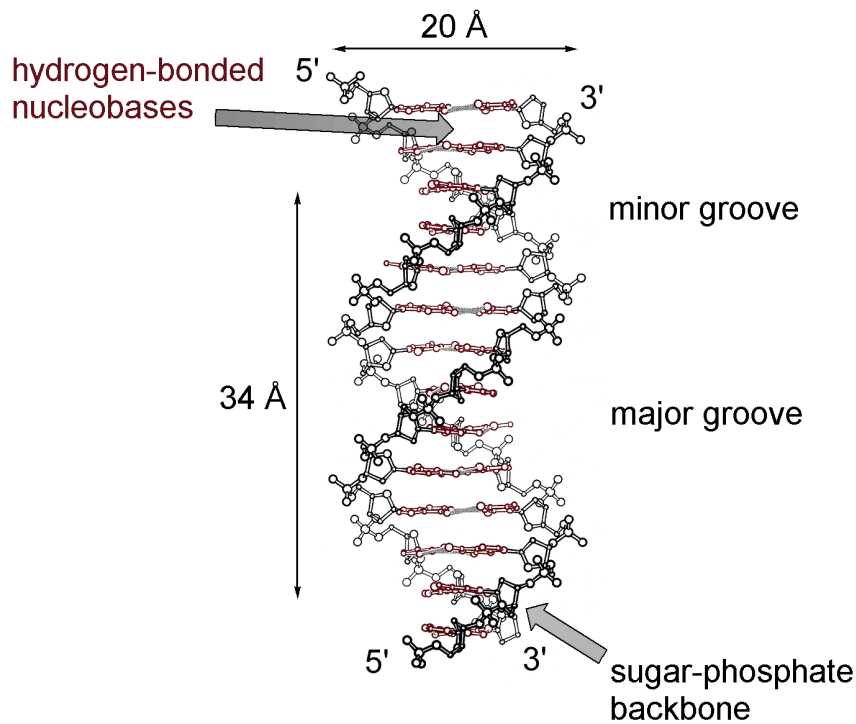
Figure 1.2. *Three-dimensional structure of B-DNA*

There are numerous secondary structures of DNA, which depend upon of the environment and base sequence. They differ in density, diameter and helical structure. The most common DNA secondary structures are the A-, B-, or Z-types (*Figure 1.3*), of which the B-type is the most commonly found in living cells. For example, a poly(G)−poly(C) sequence preferably forms an A-type helix in a low-water environment. For a defined sequence, A-DNA is shorter and has a wider diameter than the corresponding B-DNA.[4,5] In high-salt environment, poly(G−C) sequences preferably form Z-DNA, which is also features two antiparallel strands, but in opposite direction, which leads to a left-handed helix.[6] There has been considerable discussion about the conformation of poly(A)−poly(T) sequences, which form a different helix type called B'-DNA. This will be discussed in *Chapter 8*.[7]

A-DNA   B-DNA   Z-DNA
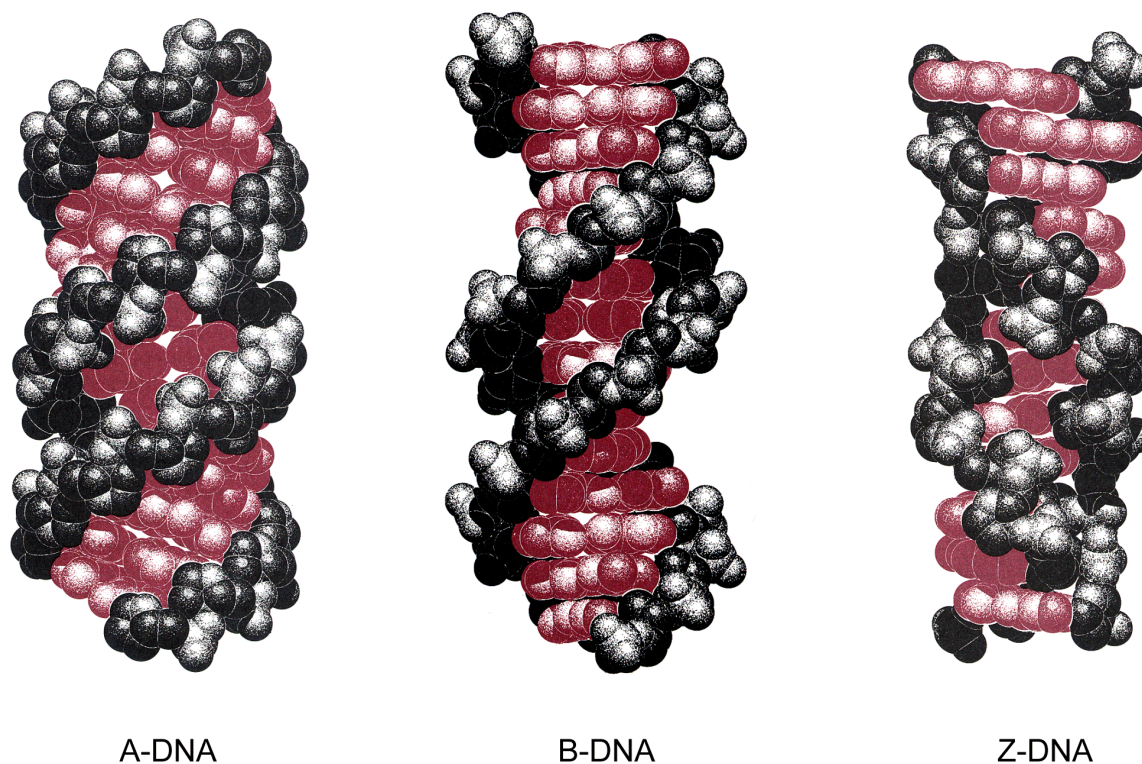
Figure 1.3. Space-filling structures of A-, B-, and Z-DNA

1.1.2 Stability of the DNA Double Helix

There are several independent stabilizing effects, which occur depending on the environment and the sequence of the DNA strand. Its three-dimensional structure shows a much wider variety than initially proposed by Watson and Crick. The rotation angle between adjacent bases, the position of the helical axis, or the "propeller twist" (the twist angle between the π-system planes of two hydrogen-bonded bases) provide additional stability to the double helix.[3] The propeller twist enables a more compact base stacking which contributes to the stability of the double helix.[8] The hydrogen bonds contribute 15–25 kJ mol^{-1} and 25–40 kJ mol^{-1} per base-pair to the stabilization for A–T and G–C pairs, respectively.[9] The stacking of the aromatic bases yields another contribution to the helical stability, by means of the partial overlap of the π-systems of two neighbouring bases. For two π-stacked bases, gas-phase

quantum-chemical calculations by *Šponer* and co-workers yielded a stabilization energy of 10–30 kJ mol^{-1} per base-pair, for an idealized B-DNA structure.[10] In a neutral aqueous solution, a stabilization energy of 2–8 kJ mol^{-1} was calculated.[11] In addition, the negatively-charged phosphate backbone is strongly solvated in water.[12]

1.1.3   DNA as Carrier of Hereditary Information

The genetic code of all living organisms is stored in the DNA, long chain molecules of numerous stacked building blocks, which in eucaryotic cells are located in the nucleus of the cell. The hereditary information is generated through the sequence of the four nucleobases, like a text which contains a distinctive sequence of four different letters. A gene is a section of a DNA chain, which delivers the information about the amino acid sequence of one protein. At the translation process, the genetic information is translated from the "language" of nucleic acids, whose alphabet contains only four letters, into the "language" of proteins, which comprises 20 different letters (amino acid building blocks). This translation is achieved by the genetic code, whose decoding has caused a decisive breakthrough in the understanding of living processes.[13] As they are self-complementary, the two antiparallel DNA strands can both serve separately as templates for the replication of the genetic code, achieved by template-directed synthesis of a new complementary strand. The universality of the genetic code ("language of life") from prokaryotes up to humans, points towards the relationship of all known livings and their joint origin in an intelligent creation.[14]

1.2   Damaging Processes to DNA

1.2.1   Physical and Chemical Mutagenesis

X-rays and nuclear radiation (α-, β-, γ-rays, n) are ionizing, and hence can generate reactive radicals in biological systems. Generally, the increase of recessive lethal mutations in DNA is

directly proportional to the radiation dose, and shows that a mutation usually results from one single hit of ionizing radiation. [15]

Short-wave ultraviolet light (UV−A) is mutagenic, especially for bacteria. In higher organisms, its effect is limited to the skin, due to its poor penetration through tissue. At 260 nm, the absorption maximum of DNA, its mutagenic effect is maximal. The main mutagenic effect of UV radiation is the formation of dimers of two neighbouring thymines, which inhibit DNA synthesis.[13] "Photoreactivation" is one known repair process for thymine dimers. Interestingly, this enzymatic reaction depends upon UV light of 310–400 nm wavelength.[16] Enzymatic excision of thymine dimers, followed by insertion of new monomers, or long-range charge transfer through DNA is another possible pathway of thymine dimer repair, as shown by the groups of *Barton*[17] and *Giese*.[18]

High temperature and especially low pH values, lead to depurination of DNA. The purine bases are hydrolytically cleaved off the deoxyribose backbone. With the next DNA replication, the missing bases are replaced by random bases, or the strand is cleaved by phosphate elimination.[19]

Numerous chemicals show direct or indirect mutagenity (*via* metabolically generated derivatives). Three main classes of direct chemical mutagens are common: modifying/ alkylating, base analogs, and intercalating substances.[13]

1.2.2 Oxidative Stress

Mainly through the mitochondrial process of oxidative phosphorylation, involving enzymes NADPH oxidase and cytochrome P450 oxidase, reactive oxygen species (ROS) are permanently generated within the cell. ROS include the hydroxyl radical ($HO^\bullet$), the superoxide radical ($O_2^{-\bullet}$), as well as hydrogen peroxide (H_2O_2) and singulet oxygen ($^1O_2$). Their concentration is regulated by several proteins such as superoxide dismutase (SOD), catalase (CAT), and the glutathione reductase (GPx). For example, SOD converts $O_2^{-\bullet}$ to H_2O_2, which is then reduced to H_2O and O_2 by CAT. There are also several antioxidizing cofactors like glutathione, or the vitamins A, C, and E.[20] If there is an excess of ROS in the

cell, for example by underregulation, the cell suffers from "oxidative stress", which poses a chemical threat for lipids, proteins and DNA.[13,21]

One of the main targets of these oxidants is the nucleobase guanine, because it has the lowest oxidation potential (+1.49–1.58 V *vs.* NHE) of the four DNA bases.[22] In the first step of this process, the guanine radical cation **2** is generated, and subsequently either reacts with water to form 8-hydroxyguanine **4** or 8-oxoguanine **5**, or deprotonates to form a neutral radical, which reacts with oxygen to the products 2-amino-imidazolone **8**, as well as 2,2-diamino-oxazolone **9** (*Scheme 1.1*).[23] There are several other pathways of formation of 8-oxoguanine **5**, *e.g. via* direct addition of a hydroxyl radical at position 8, or by a [2+4]-cycloaddition of singulet oxygen to the imidazole moiety of guanine, followed by ring opening and reduction ot the intermediary endoperoxide **1**.[24] Under anerobic conditions, it was found that 8-oxoguanine **5** is preferably formed, whereas under atmospheric conditions, mainly the imidazolone **8** and oxazolone **9** are formed.[25]

Scheme 1.1
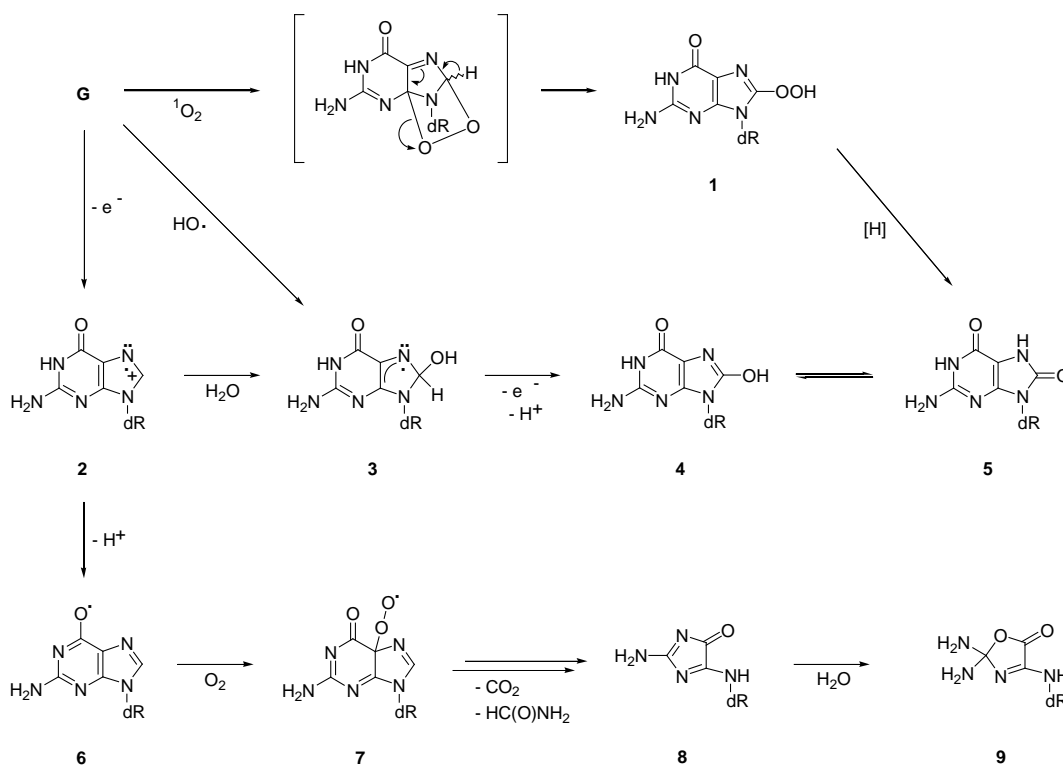
dR = 2'-deoxyribose

In the replication process, 8-oxoguanine **5** is no longer recognized as guanine, which leads to the insertion of adenine instead of cytosine into the newly synthesized complementary strand. Following another replication, a G−C → A−T transversion mutation results (*Figure 1.4*).[26]
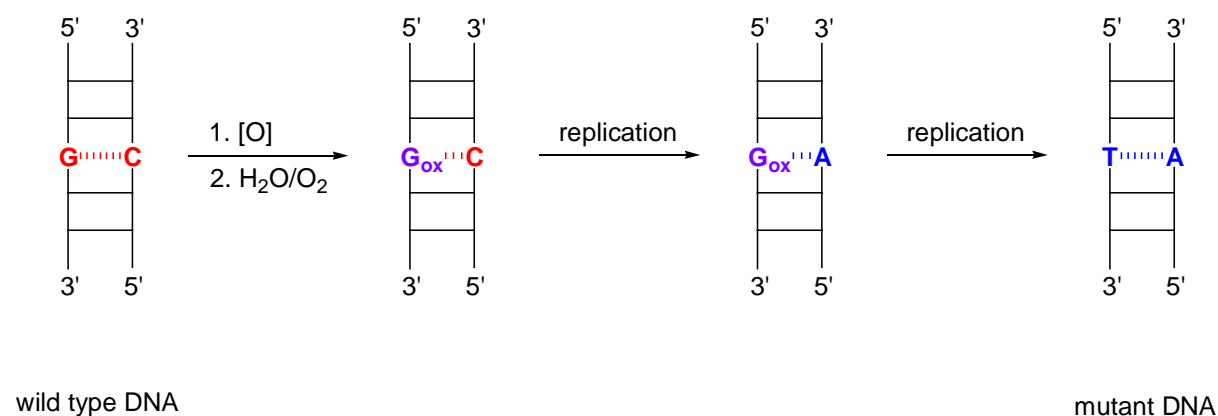
Figure 1.4. Transversion of a base-pair, caused by oxidative damage of a guanine base

Studies over the past decade have shown that DNA is capable of long-range charge transfer.[27-30] The thermodynamic driving force for this process is the dependence of the guanine oxidation potential upon the DNA sequence. The oxidation potential of guanine is lowered by a maximum of 0.7 V within the series G > GG > GGG.[31] Hence, more damage is to be expected in guanine-rich regions of DNA. Many GG units have been found within the p53 tumor suppressor gene and the H-*ras* proto-oncogene, thus suggesting that these genes should show a higher susceptibility for mutations, and thus play a crucial role in the development of cancer for an affected organism.[32] However, in the case of the GG and GGG units being preferably located outside the encoding regions of the DNA, such sequences may offer the possibility of a guanine radical cation repair by long-range electron transfer (ET) (*Figure 1.5*).[33] Non-encoding, guanine-rich sequences are found at the ends of eucaryotic chromosomes, and such sequences are called telomers. For example, in human telomeric DNA, the sequence 5'-TTAGGG-3' is repeated dozens or thousands of times and several genes possess guanine-rich sequences outside the encoding area.[34,35] These poly(G−C)

domains are sinks for the positive charge and may serve as a cathodic corrosion protection for essential gene sequences.[36]
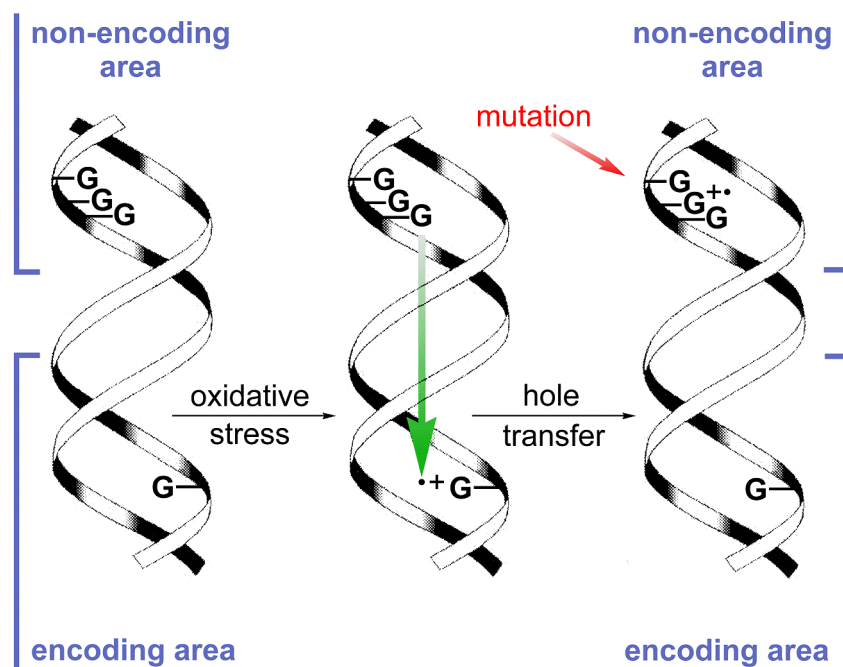
Figure 1.5. *Oxidation of a G in the encoding area and the transport of the positive charge into a G-rich sequence in the non-encoding area.*

1.2.3   DNA Strand Cleavage

Single- or double-strand cleavage caused *via* deoxyribose radicals is another critical hazard to DNA. In eucaryotic cells, it takes about 40 to 50 strand breaks for a lethal incident, in case the enzymatic repair mechanism (DNA-Ligase) is defective or missing.[37] Reactive oxygen species (ROS) are capable of abstracting any of the seven hydrogen atoms from the deoxyribose moiety. The five possible deoxyribose radicals generate reactive intermediates which normally lead to strand cleavage. However, the C-4' radical is the only known furanosyl radical which leads to strand cleavage under anaerobic conditions.[38] Abstraction of a hydrogen atom at the 4'-position of deoxyribose in DNA **10** by a ROS leads to radical **11**,

which undergoes a heterolytic β-elimination to form the 5'-phosphate **12** and the reactive deoxyribose radical cation **13** (*Scheme 1.2*).

Scheme 1.2
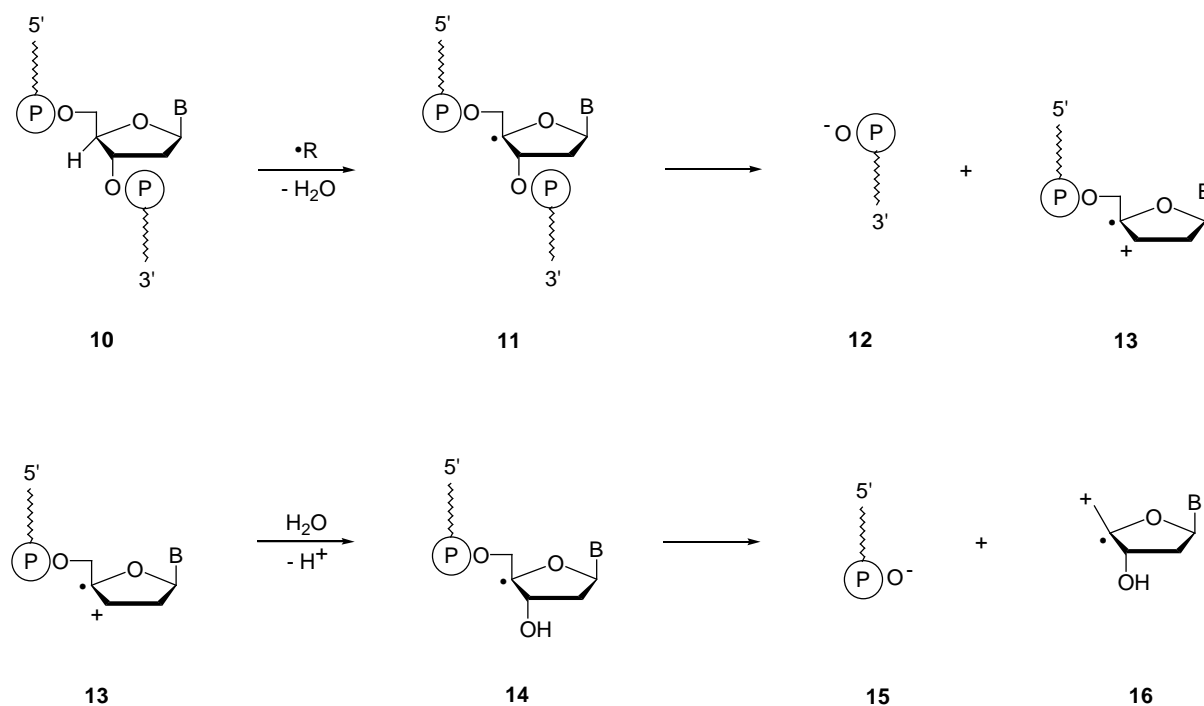
Due to having a phosphate substituent as a leaving group, and due to the formation of a more stable secondary carbocation, initial 3'-cleavage is favoured and proceeds at a 15 times faster rate than 5'-cleavage.[38] Water addition to C-3' of **13**, followed by a second β-elimination, leads to formation of 3'-phosphate **15** and deoxyribose radical cation **16**. As enol ether radical cations are known to be strong oxidants,[39] radical cation **13** is a suitable electron acceptor for studying electron transfer reactions in DNA.[40]

1.3   Electrical Conductivity or Long-Distance Redox Chemistry in DNA?

1.3.1   A Controversy

In 1962, *Eley* and *Spivey* suggested that DNA may provide an efficient one-dimensional π-way charge transport.[41] However, it took years until methods for synthesis and probing of custom DNA sequences were developped. Both extremes, DNA as an insulator or as a molecular wire, were initially supported by theoretical assays.[42] In 1993, an experiment by attention of *Turro*, *Barton* and co-workers brought the question of the conductivity of DNA back to the researchers.[43] They reported a photoinduced electron transfer in DNA between two metal complexes, where the electrons moved over a distance of approximately 40 Å at a rate of 10^9 s^{-1}, from which they concluded that DNA acts as a molecular wire. Intercalating metal complexes were attached at both ends of a 15mer double-stranded DNA. A ruthenium(II) and a rhodium(III)-complex served as electron donor and acceptor, respectively. The intercalating rhodium complex quenched the fluorescence of the ruthenium complex, which was interpretated to be due to electron transfer, because the fluorescence persisted in the absence of intercalating agents. Their quantitative results were queried[44] due to the limitations of the experimental setup. The reported shallow distance dependence ($\beta < 0.2$ Å^{-1}; see *Chapter 1.3.2*) was in contrast to other reports of DNA-mediated ET, which did not observe a similarly shallow distance dependence, thus demonstrating that long-range ET in DNA or proteins and saturated hydrocarbons is not a general phenomenon.[45,46] The results from different assays remained contradictory[47] and the conclusions ranged from seeing DNA as an insulator[48] to either considering DNA as a conducting material behaving in accordance to Ohm's law[49] or as a large-bandgap semiconducting material with nonlinear current-voltage behaviour.[50] However, all these electrical measurement setups lacked an essential experimental feature: in order to avoid two large-bandgap barriers due to non-covalent attachment of both ends of the DNA strand, its covalent bonding to the electrodes by a conjugated π-system is mandatory. If this is not performed the experiment will mainly or exclusively show the electric behaviour of these barriers.[51]

Barton and co-workers finally provided a proof for long-range ET through DNA by an experiment in which they observed the repair of a thymine dimer by long-range hole transfer, triggered by photoreduction of an intercalating rhodium(III) complex.[17]

The nature of electric conductivity of DNA is still to be elucidated, as the reports remain contradictory and no experiments have yet been achieved, which do not contain limitations in their the experimental setups. So far DNA has been proven to at least enable long-range redox chemistry. Furthermore, all these reports have shown that the data obtained is crucially depending on the experimental setup and that the results obtained are strongly dependent on the nature of the charge injection assay.[52] In conclusion, for building models of charge transfer in DNA, the necessity of systematic investigation of geometrically well-defined systems, including precise charge injection systems, remains compelling.

1.3.2 Charge Transfer in DNA

The Marcus Theory

Electron transfer (ET) is the most elementary and ubiquitous of all chemical reactions, playing a key role in many essential biological processes. Theoretical efforts initiated by *Marcus* in the late 1950s and continuing to the present day have provided a remarkably detailed description of ET reactions.[53] *Marcus* was honoured with the Nobel prize in Chemistry in 1992 "for his contributions to the theory of electron transfer reactions in chemical systems". *Marcus'* model is based on the activated complex theory.[54] Accordingly, the rate constant of a single-step electron transfer reaction, k_{et} , depends on the energy barrier to pass the transition state (= free enthalpy of activation, $\Delta^{\ddagger}G_{et}$) in the following way (Eq. 1-1):

$$k_{et} = A \cdot e^{-\dfrac{\Delta^{\ddagger}G_{et}}{RT}} \tag{1-1}$$

In Eq. 1-1, R is the gas constant, and T is the temperature of the reaction. The term A depends on the nature of the charge transfer reaction (*e.g.* intramolecular, bimolecular, etc.). In conventional chemical reactions bonds are broken and/or formed and the transition state corresponds to a particle with intermediate bonds. In charge transfer reactions however, no chemical bonds are broken or formed and so a somewhat different model for the reaction is needed.

If we consider the exothermic hole transfer from a radical cation $\mathbf{D^{\bullet+}}$ (hole donor) to a neutral molecule $\mathbf{A}$ (hole acceptor), according to *Marcus'* theory[53] the theoretical framework for most ET reactions is based on a simple two-state model (*Figure 1.6*).

$$\mathbf{D^{\bullet+}} + \mathbf{A} \longrightarrow \mathbf{D} + \mathbf{A^{\bullet+}} \qquad \text{thermal}$$
$$\mathbf{*D^{\bullet+}} + \mathbf{A} \longrightarrow \mathbf{D} + \mathbf{A^{\bullet+}} \qquad \text{photoinduced}$$

Figure 1.6. Electron transfer process according to Marcus' *two-state model, depicted as a charge shift. The chromophore bearing an asterisk (*D) indicates that it is in an electronically excited state, generated by absorption of light*

The energy surface for an ET process, conveniently represented by a one-dimensional reaction coordinate which is supposed to describe changes in both geometry of the $\mathbf{D}$–$\mathbf{A}$ system and solvent orientation, may be regarded in terms of two diabatic surfaces. One represents the electronic configuration of the reactant, $\mathbf{D^{\bullet+}}$ and the other represents the electronic configuration of the product, $\mathbf{A^{\bullet+}}$. In the region where the diabatic surfaces intersect, the two configurations mix (symmetry permitting) and this results in an avoided crossing (or tunneling). The magnitude of the avoided crossing is given by approximately H_{AB}, where H_{AB} is the electronic coupling matrix element and may be regarded as a rough measure of the strength of orbital interactions between $\mathbf{D}$ and $\mathbf{A}$. In *Figure 1.7*, ΔG_{et} is the free enthalpy change associated with the ET process and λ is the reorganization energy. The reorganization energy is approximately given by the sum of vibrational contributions from the

donor and acceptor chromophores (internal reorganization energy, λ_i) and low-frequency contributions from the solvent (solvent reorganization energy, λ_s).[53,55]
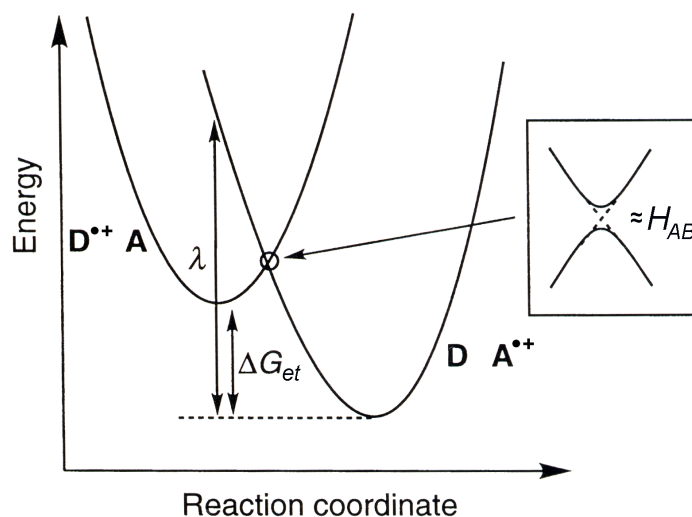
Figure 1.7. Energy diagram for charge transfer resolved into reactant-like and product-like surfaces. The two diabatic curves do not intersect, but interact to give an avoided crossing, whose energy gap is about the electronic coupling (H_{AB}) for the interaction.

In case of long-range ET, where the donor and acceptor chromophores are separated by distances which exceed the sum of their Van der Waals radii, H_{AB} is generally very small (< 300 cm^{-1}). ET then occurs nonadiabatically and theoretical calculations by *Levich*,[56] *Jortner* and co-workers[57] as well as *Marcus* and *Sliders*[58,59] have shown, that for a charge transfer reaction with frozen distance between donor and acceptor, the term *A* may be expressed according to Eq. 1-2, where *h* is the Planck constant:

$$A = \frac{4\pi^2}{h} \cdot \frac{H_{AB}{}^2}{\sqrt{4\pi\lambda RT}} \tag{1-2}$$

The energy of the intersection point of the diabatic curves, corresponding to the free enthalpy of activation, $\Delta^{\ddagger}G_{et}$ in Eq. 1-1, can be easily calculated using Eq. 1-3:[53]

$$\Delta^{\ddagger}G_{et} = \frac{(\Delta G + \lambda)^2}{4\lambda} \qquad (1\text{-}3)$$

The combination of *Marcus'* classical electron transfer theory with the results of the quantum mechanical treatments leads to the semi-classical *Marcus-Levich-Jortner* equation 1-4:[53,60]

$$k_{et} = \frac{4\pi^2}{h} \cdot \frac{H_{AB}{}^2}{\sqrt{4\pi\lambda RT}} \cdot e^{-\frac{(\Delta G_{et} + \lambda)^2}{4\lambda RT}} \qquad (1\text{-}4)$$

As a consequence of Eq. 1-3, electron transfer reactions for which $-\Delta G_{et} < \lambda$ are said to take place in the *Marcus normal region* and their rates increase with increasing exergonicity, becoming optimal (barrierless) when $-\Delta G_{et} = \lambda$. When the reaction becomes even more exergonic, then $-\Delta G_{et} > \lambda$ and an activation barrier reappears; the reaction is now in the *Marcus inverted region*, and the ET rate is predicted to decrease with increasing exergonicity. This prediction was elegantly verified by *Miller* and co-workers for thermal charge shift reactions in the radical anions of the rigid **D–steroid–A** dyads (shown in *Figure 1.8*) which were generated by pulse radiolysis.[61] The driving force ($-\Delta G_{et}$) for the reaction was adjusted by changing the acceptor. It was found that, in qualitative agreement with classical Marcus theory, the ET rate increased with increasing exergonicity, peaked and then dropped.
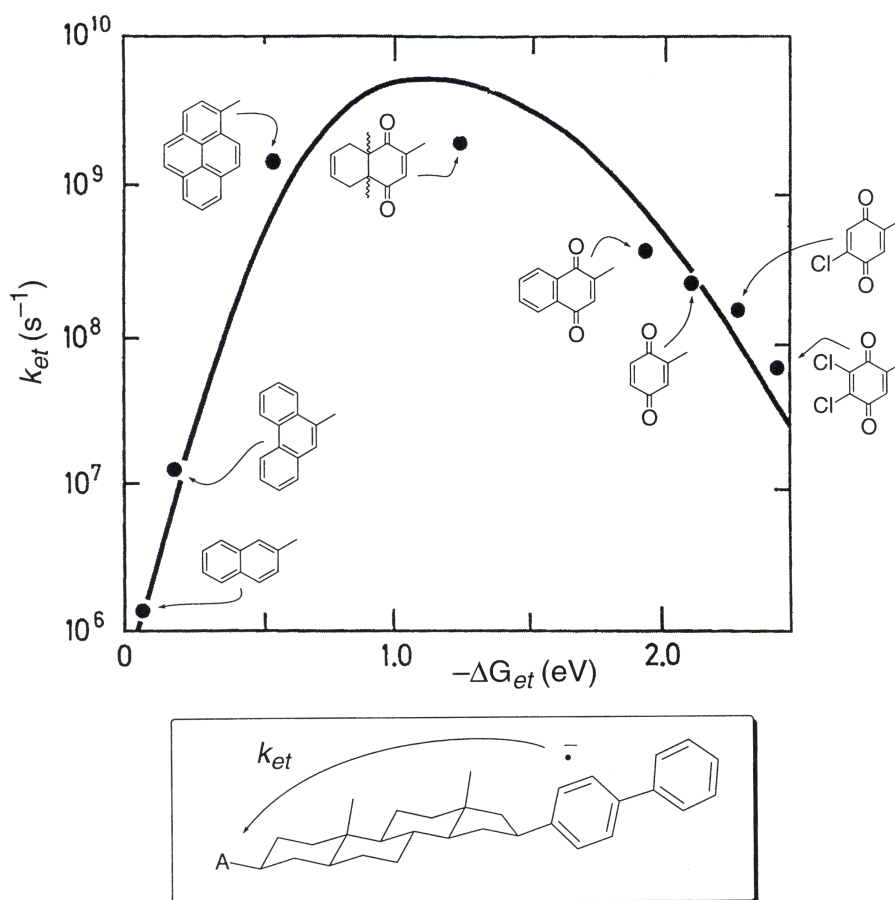
Figure 1.8. *Schematic of the plot of the rate of ET from a biphenyl radical anion to an acceptor, A, as a function of driving force.*[61]

Thus, within the context of Marcus theory, the three important variables that determine the ET rate constant are H_{AB}, λ, and ΔG_{et}. If the charge transfer occurs through vacuum (through-space) H_{AB} solely depends on the relative energies of the molecular orbitals of the donor and acceptor and the subsequent overlap of these orbitals. The strength of orbital overlap shows an exponential distance dependence and therefore the electronic coupling element decays exponentially upon increase of the charge transfer distance d:[53,62]

$$H_{AB}^{2} = H_{AB,o}^{2} \cdot e^{-\beta(d-d_o)} \tag{1-5}$$

In Eq. 1-5, $H_{AB,o}$ is the electronic coupling matrix element for the reference distance d_o. The exponential decay parameter β characterizes the extent of the distance dependence. For vacuum, β–values of 3.4 Å^{-1} [63] and of about 5 Å^{-1} [64] have been estimated. Thus, the increase of the separation distance by 1 Å reduces k_{et} by a factor of 30–150. The combination of Eq. 1-4 and Eq. 1-5 results in the general distance dependence of the charge transfer rate:

$$k_{et} = k_{et,o} \cdot e^{-\beta(d-d_o)} \tag{1-6}$$

with

$$k_{et,o} = \frac{4\pi^2}{h} \cdot \frac{H_{AB,o}^2}{\sqrt{4\pi\lambda RT}} \cdot e^{-\frac{(\Delta G_{et} + \lambda)^2}{4\lambda RT}}$$

The Superexchange Mechanism

If a charge transfer does not occur through-space, but inside a molecule, where charge donor and acceptor are separated by molecular material (*e.g.* protein, nucleobases, solvent molecules etc.) according to *Meggers* and co-workers,[27] and *Jortner*, *Bixon* and co-workers,[65] two mechanisms must be distinguished: a) single-step superexchange-induced charge transfer, or b) multi-step charge hopping involving the bridge as charge carrier. The first case is illustrated in *Figure 1.9* for the intramolecular charge transfer between a radical cation as charge donor ($\mathbf{D}^{\bullet+}$) and a neutral moiety as charge acceptor ($\mathbf{A}$) that are separated by a bridge medium containing physical subunits $\mathbf{B_1}$, $\mathbf{B_2}$,…$\mathbf{B_n}$ (*e.g.* protein side-chains or intervening DNA base pairs). It is important to note that in the superexchange mechanism, the ionic bridge configurations should be considered as one large, delocalized molecular orbital; they are not intermediates in the charge shift process since their energies are much higher than those of the reactant and product states. The energy gap (Δ) is very large (at least 2 eV) and so the charge cannot be thermally injected into the bridge. Instead, the electron moves

coherently in one sudden "jump" from donor to acceptor and it never becomes localized within the bridge.
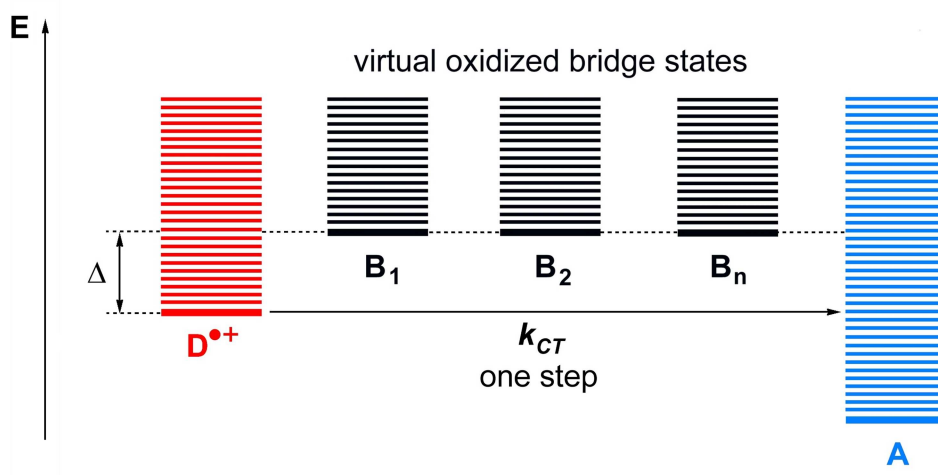
Figure 1.9. Single-step superexchange mechanism. The charge transfer occurs via *a tunneling process between donor, D, and acceptor, A.*

The distance dependence of the charge transfer rate for this mechanism is exponential decay (Eq. 1-6).[55] However, in contrast to the through-space charge transfer, the intervening bridge medium *enhances* the electronic coupling between $\mathbf{D}^{\bullet+}$ and $\mathbf{A}$ *via* virtual states. The oxidized brigde subunits $\mathbf{B_1}$, $\mathbf{B_2}$,…$\mathbf{B_n}$ interact with the reactant state and product state. It was found that β–values in materials are considerably smaller than *in vacuo*, *e.g.* protein media feature β–values in the range of 0.8 to 1.4 Å^{-1}.[62,66] For charge transfer reactions in DNA following the superexchange mechanism, *Lewis* and *Wasielewski*,[67] *Harriman*,[45a] *Tanaka*[48] and *Giese*[68] found reasonably similar β–values in the range of 0.64 to 1.42 Å^{-1}. In the superexchange mechanism case, the β–value can be regarded as a material constant of the bridging medium and it reflects the extent of electronic coupling within the bridge. The superexchange mechanism reflects the strong distance dependence found in experiments by *Meggers*[40] and *Wessely*.[69] A distant GGG unit is oxidized by a guanine radical cation ($G^{\bullet+}$),

separated by a bridge of up to 3 A−T pairs, before the radical cation is irreversibly trapped by water (*Figure 1.10*).[70] Further theoretical treatment of the superexchange mechanism was undertaken by *Beratan*, *Ratner* and co-workers and was in accordance with the previously observed experimental results.[71]
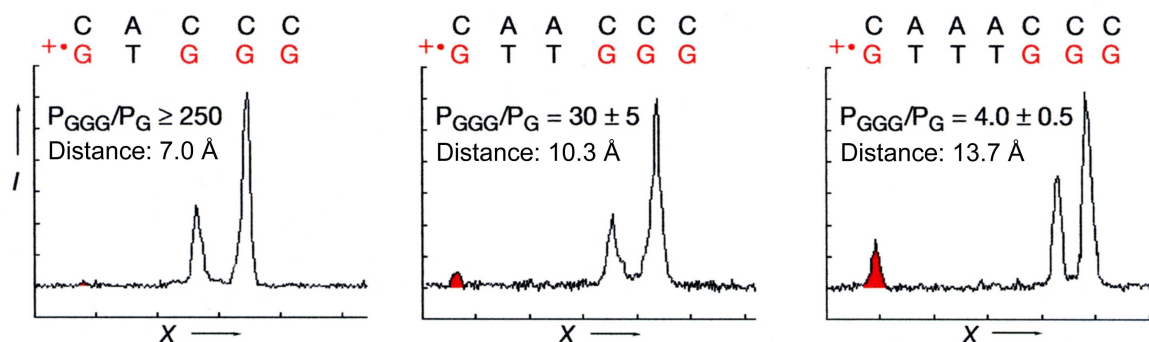
Figure 1.10. *Strong distance dependence for charge transfer following the superexchange mechanism, shown as PAGE lane histograms. P_{GGG}/P_G gives the ratio of yields between damage at the GGG unit (P_{GGG}), and damage at the G unit (P_G, peak shown in red) respectively, obtained by integration of the peak areas. The damage is due to nucleophilic trapping of the guanine radical cations by water. Piperidine treatment leads to strand cleavage and the fragments can be separated and quantified by PAGE and radioactivity measurement. Each peak arises at the nucleotide position (X) shown in the strand depicted at the top of each panel. The nucleotides in red indicate the beginning and the end of the charge transfer process.*

The Hopping Mechanism

In DNA sequences where the water trapping of a guanine radical cation ($G^{\bullet+}$) is slower than the hole transfer between the guanine bases, the charge shift is not expected to not stop after the first step. The fact that single guanines may act as carriers of the positive charge, was demonstrated in experiments by *Giese* (*Figure 1.11*)[69,72] and by *Nakatani* and *Saito*.[73]
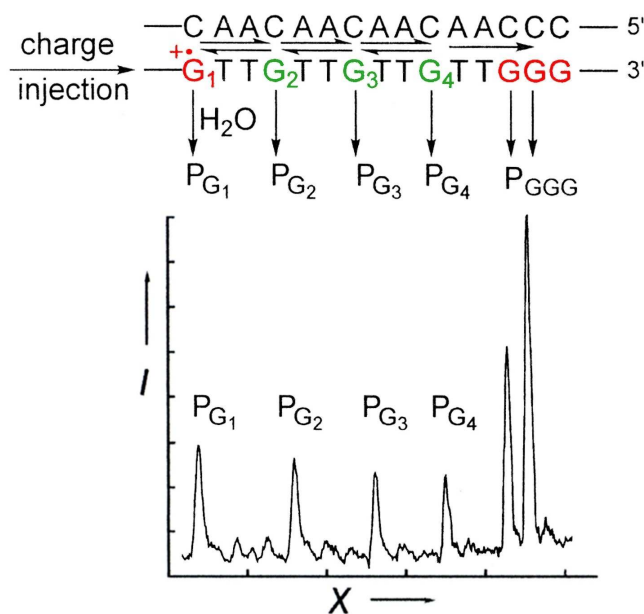
Figure 1.11. *Histogram showing the products P_G and P_{GGG} formed after charge injection into G_1, water trapping of the guanine radical cations and subsequent strand cleavage. All single guanines lead to water trapping products.*

The experiment can be described by a reversible diffusion of the charge between the guanine charge carriers so that the overall charge transport over long distances occurs in a multistep hopping process from donor to acceptor. *Ratner* and co-workers,[71,74] *Jortner*,[75] as well as *Renger* and *Marcus*[76] have theoretically described this mechanism in accordance to the experimental findings. In contrast to the single-step superexchange process, the ionized guanines between the A–T bridges are of similar energy as the hole donor ($G^{\bullet+}$); they are physical intermediates in the charge shift process (*Figure 1.12*) and this explains the damage observed at all gunanines shown in *Figure 1.11*. A multistep-hopping mechanism cannot be described by the *Marcus-Levich-Jortner* equation (Eq. 1-4), since the β-value is defined for a single-step process. The overall charge shift process can be described as a sequence of reversible, single charge hops between neighbouring guanines, each hopping step following a superexchange mechanism, until the charge is irreversibly trapped at a GGG unit.
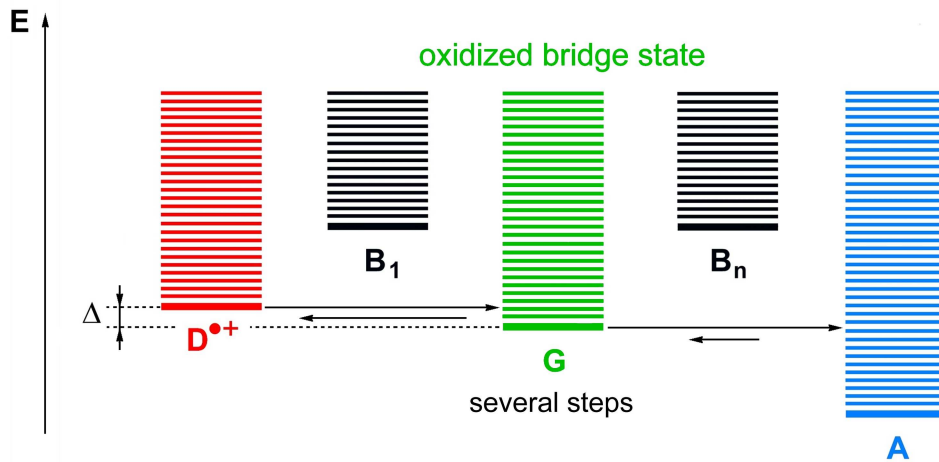
Figure 1.12. *Multistep hopping mechanism. The charge transfer occurs via a sequence of reversible tunneling steps between donor (**D**) and acceptor (**A**). The intervening guanines act as charge carriers.*

Despite the strong distance dependence of superexchange-mediated single hops, efficient long-distance charge transfer is possible, as long as the guanines are separated by only short $(A-T)_n$ bridges. Hence, the longest hopping step will determine the overall charge transfer rate. This multistep hopping process can be physically described as a one-dimensional *random-walk* movement of the charge through the DNA strand. For the simplest case of equidistant hopping steps, the rate can be determined as follows (Eq. 1-7):

$$k_{CT} \propto k_{hop} \cdot N^{-\eta} \qquad (1\text{-}7)$$

The overall rate constant (k_{CT}) is determined by the rate constant (k_{hop}) for a single step, the proportionality factor (η, approximately 2 in the simplest case) and the number of hopping steps (N).[27,65,77]

Further experiments by *Schuster*[78] and *Barton*[79] have demonstrated that efficient charge transport also occurs over long, guanine-free sequences. These controversial results were examined in the *Giese* group by *Wessely*[69] and *Spormann*[80] using a comparable charge injection assay also used in former experiments by the *Giese* group. In a similar system, as

shown in *Figure 1.10*, experiments with longer $(A-T)_n$ bridges between G and GGG were performed, and for bridge lengths with $n \geq 4$, a nearly distance-independent charge transfer efficiency resulted (Figure 1.13).
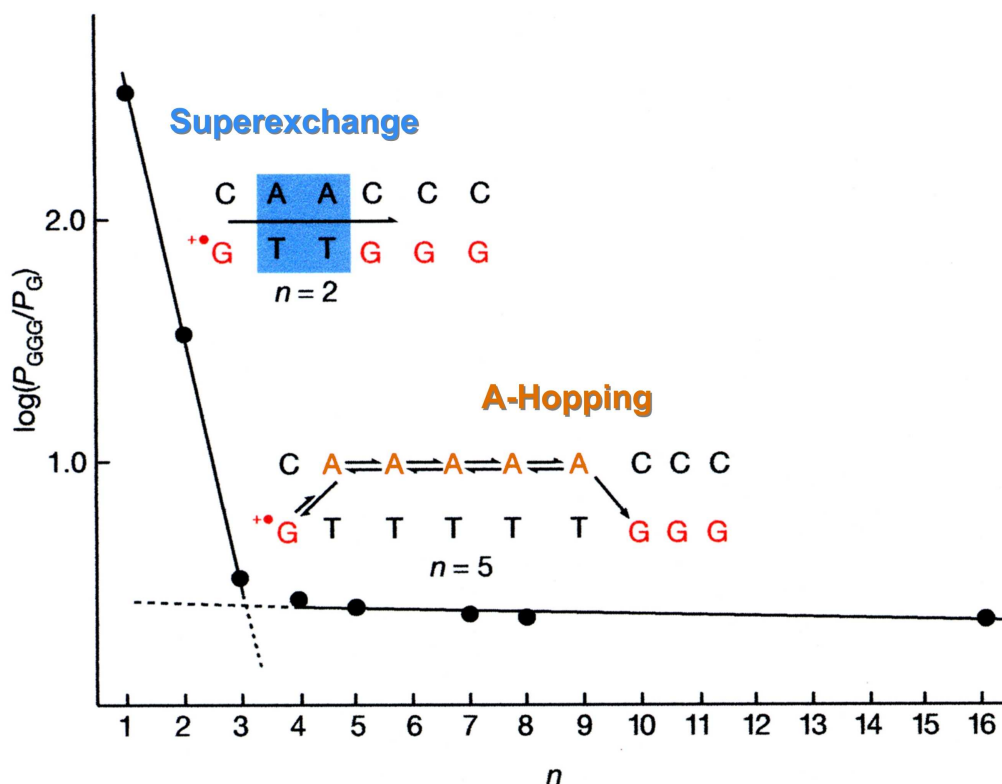
Figure 1.13. *Plot of the yield ratios log(P_{GGG}/P_G) against the number (*n*) of A–T base pairs. Between* n *= 3 and* n *= 4, the mechanism changes from superexchange to A-hopping.*

This experiment established an extended hopping model, that also involves adenines as charge carriers, a behaviour which confirmed theoretical predictions[81−85] and which was validated by experiments where the positive charge was directly injected into an adenine.[86] Tunneling of the charge over 4 A−T pairs is not observed. Conversely, if the lifetime of the guanine radical cation is long enough to oxidize an adjacent adenine, as this is the nucleobase with the second lowest oxidation potential (+1.96−2.03 V *vs.* NHE),[22] then a thermally

induced multistep hopping process involving adenines as charge carriers takes place.[70] The latest experimental data for this "A-hopping" points towards hole transfer rate constants in the range of 10^8–10^{10} s^{-1}.[87]

Summary: Superexchange versus Molecular Wire Behaviour

The rather astonishing revelation that electron transfer can take place rapidly ($> 10^9$ s^{-1}) over inter-chromophore separations exceeding 10 Å through saturated hydrocarbon bridges has led to the oft-asked question: If hydrocarbon bridges are able to strongly mediate ET, may they be considered to possess molecular wire (or electrically conducting) behaviour? The answer is an unequivocal no, they may not be regarded as wires. Electrical conduction through a bridge requires that the electron from the donor becomes thermally injected into the conduction band of the bridge. The electron actually becomes localized within and is transported through the bridge, from donor to acceptor, by an incoherent scattering mechanism, such as a polaron. The distance dependence of the electron transport rate in such a molecular wire is determined by Ohmic scattering and therefore varies inversely with bridge length.[81,82,88] The molecular wire mechanism is summarized in *Figure 1.14*.[55] Molecular wire behaviour is only expected when the energy gap (Δ) between the donor level and the bridge conduction band is very small, of the order of k_BT. This condition is satisfied for long, conjugated bridges such as graphite and doped polyacetylenes, which may be considered as giant chromophores whose MOs are essentially delocalized over the whole bridge (*Figure 1.14*; right-hand inset). The hopping mechanism can be regarded as a variant of wire behaviour, as there is a series of weakly coupling units **B₁, B₂,…Bₙ**, each of which is able to capture the migrating charge for a short period of time before passing it on to one of its neighbouring units (*Figure 1.12*). Assuming that all of the bridge units are energetically nearly degenerate, the migrating charge randomly hops, from bridge unit to bridge unit, up and down the chain, until it is eventually irreversibly trapped by the acceptor which acts as a thermodynamic sink. This mechanism avoids the exponential decay of charge transfer with distance, following a more gentle curve instead (Eq. 1-7).
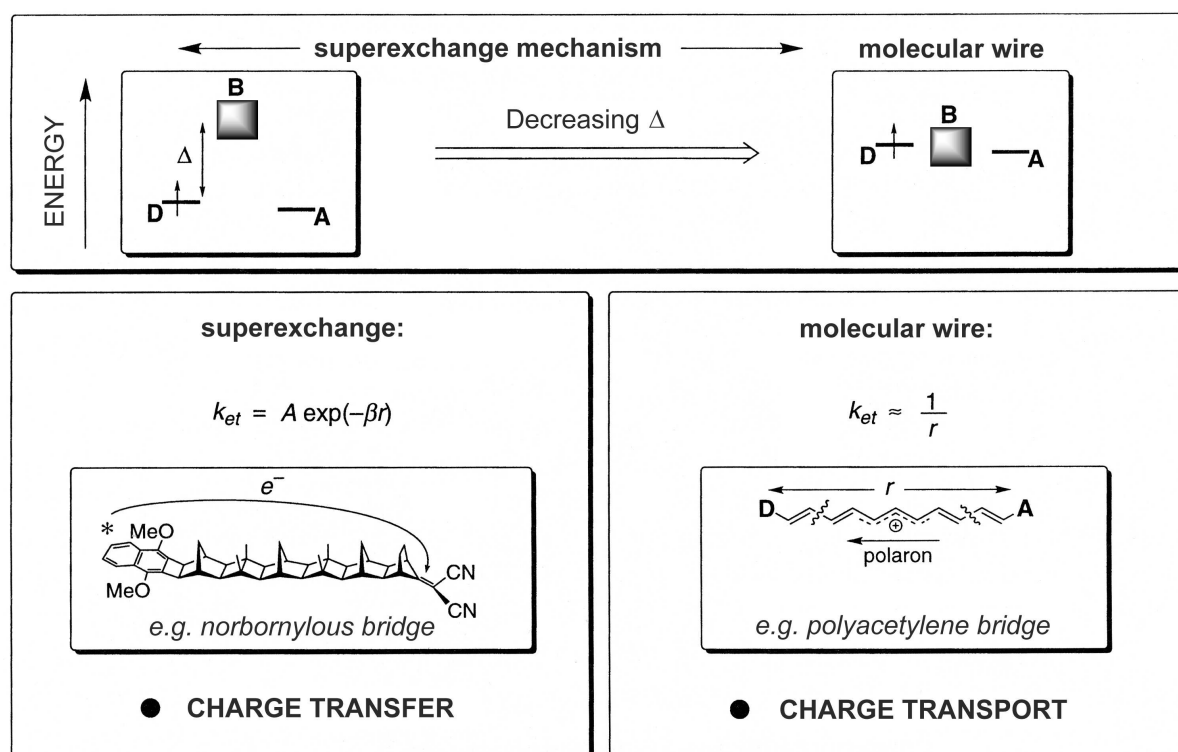
Figure 1.14. *A schematic illustrating the difference between the superexchange mechanism and molecular wire behaviour in a **D−B−A** dyad. Superexchange: the virtual bridge states lie well above the donor level (Δ is large) and consequently, the charge is never localized within the bridge; instead, the charge is transferred from donor to acceptor in one coherent jump. The distance dependence behaviour is exponential decay. Molecular wire behaviour: The bridge states are energetically comparable to the donor level (Δ is very small). In this case, the charge may be thermally injected into the bridge and becomes localized within the bridge, whereupon it moves from the donor to the acceptor incoherently as a defect, such as a polaron. The distance dependence is Ohmic (varies inversely with distance).*

The following work will demonstrate how long $(A−T)_n$ sequences constitute a new situation where more sophisticated models must be applied in order to approach an understanding of the nature of A-hopping, the concept of which will be discussed in *Chapters 6−8*.

1.3.3   Site-Selective Charge Injection into DNA

In order to investigate radical-induced DNA strand cleavage, the *Giese* group developed 4'-acyl modified thymine derivatives, which allowed the generation of radicals selectively at the 4'-position of the carbohydrate moiety by photolysis.[89] The Norrish type I photoreaction of a ketone was applied to generate radicals by the photochemical n → π^* excitation of an electron from a non-binding orbital of the ketone oxygen to the antibinding orbital of the carbonyl bond. One of the α-C,C-bonds is thus cleaved and an alkyl and an acyl radical are formed. this radical can subsequently fragment into a second alkyl radical and carbon monoxide through decarbonylation. The more stabilized the generated radicals are, the easier the α-cleavage occurs. Therefore, *tert*-butylketones are especially suitable for the Norrish type I photoreaction.[90] By photolysis of a DNA sequence containing a 4'-pivaloylated thymidine, a radical at the 4'-position may be selectively generated (*Scheme 1.3*).[89] The semi-occupied atom orbital in radical **18** destabilizes the neighbouring 3'-C,O-bond, which in turn induces heterolysis because the charges generated in the fragments can be stabilized.[91] Cleavage of the 5'-phosphate **20** leads to ribose radical cation **19**, which was characterized by photocurrent measurements and chemically induced dynamic nuclear polarization (CIDNP).[92,93]

Scheme 1.3
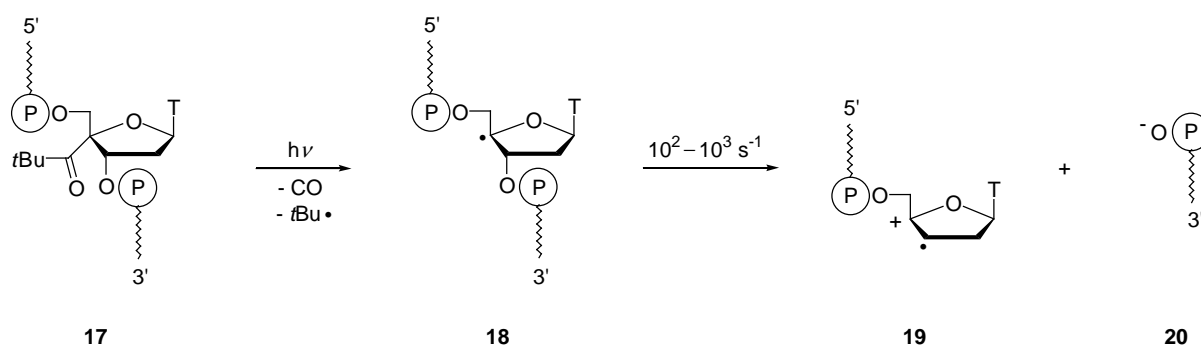
There are several possible reactions for radical cation **19**. Nucleophilic trapping by water leads to 3'-phosphate **22** and ketoaldehyde **25**, or the π-radical cation can act as an oxidant,[39] which leads to enol ether **26** upon reaction with a suitable electron donor (*Scheme 1.4*).

Scheme 1.4
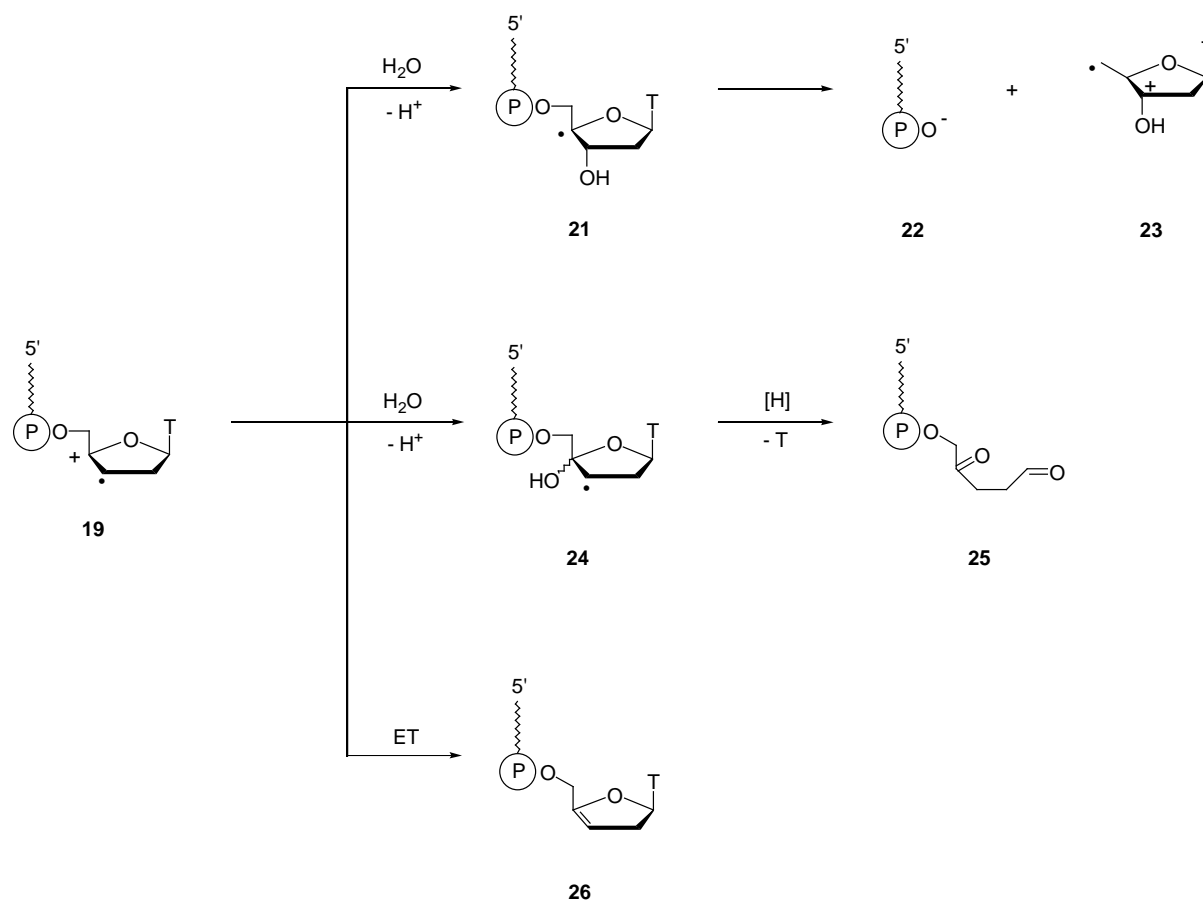
In experiments with DNA strands, *Meggers* found that only enol ether **26** was formed if there was a guanine base close to the radical cation **19**. This observation is explained by the relatively low oxidation potential of guanine (+1.49−1.58 V *vs.* NHE) with respect to the other DNA bases.[22] The yields of enol ether **26** were strongly dependent on the distance to the next guanine base.[94]

Through this superexchange mechanism (see *Chapter 1.3.2*) an electron is transferred from a guanine base to the carbohydrate radical cation **19**, which leads to formation of a guanine radical cation and hence to the generation of a positive charge within the DNA base stack. This charge injection assay is suitable for the investigation of charge transport through DNA.[27,72,77] Firstly, the charge is transferred onto a guanine base in the radiolabelled complementary strand. From there the charge migrates over a bridge to a GGG unit, where it is trapped by water (*Figure 1.15)*. Piperidine treatment leads to strand cleavage and the fragments can be separated and quantified by PAGE and radioactivity measurement.
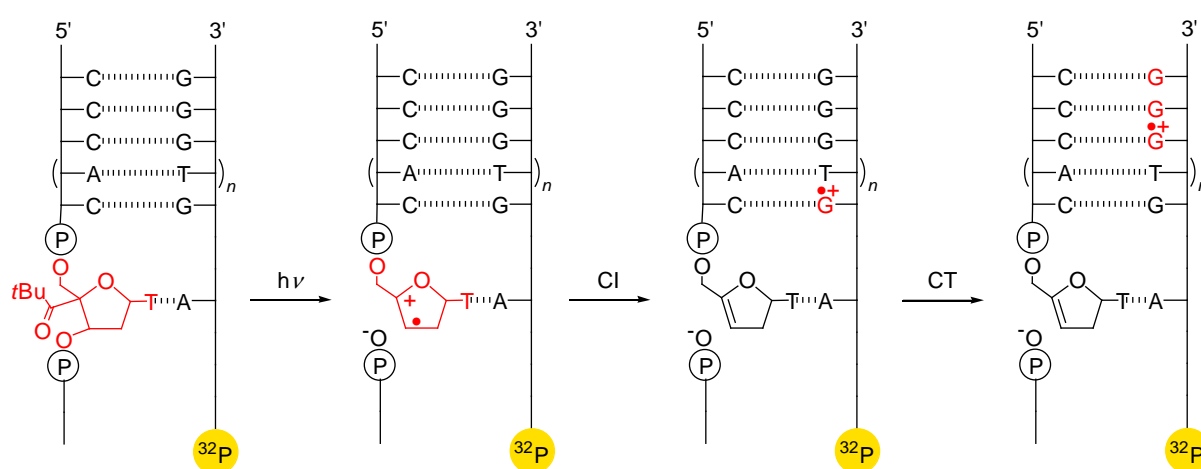
Figure 1.15. *Photolytic generation of a radical cation, charge injection (CI) into DNA by reduction of the ribose radical cation by a guanine base, followed by charge transfer (CT) through the base stack.*

This method of charge injection differs from other methods in several points. Firstly, the 4'-pivaloyl modified thymine derivative can be incorporated at any distinctive position into the DNA strand and shows minimal interference with the local DNA structure.[40] Secondly, the charge injection takes place from the ground state. This assay ensures that only one charge per molecule is generated, as the charge injector cannot be regenerated after its photolysis. Other assays use stilbene derivatives,[67] Rh(III)-complexes,[17,95] anthraquinone derivatives,[29,78b,96] acridine derivatives,[48] which all are either intercalating modifications or are attached to the ends of the DNA strands. Another assay which also enables site-specific charge injection uses

p-cyanobenzophenone substituted uridine derivatives.[73,97] The last assay to be mentioned is pulse radiolysis, which allows the injection of an electron hole into a DNA sequence containing both donor and acceptor moieties.[98,99]

The unique advantage of the 4'-pivaloylated nucleoside assay used by the *Giese* group is that back electron transfer is impossible, because the radical is irreversibly generated by the Norrish type I cleavage of the pivaloyl ketone. *Spormann* improved the charge injection efficiency by replacing the thymidine in precursor **17** by a guanine (precursor **27**, *Scheme 1.5*), to reduce the distance between the ribose radical cation and guanine. This modification accelerated the charge injection step by at least 60-fold, compared to the water trapping reaction, which resulted in literally quantitative charge injection *via* ribose radical cation **28** into guanine, detected as enol ether **29**.[80]

Scheme 1.5
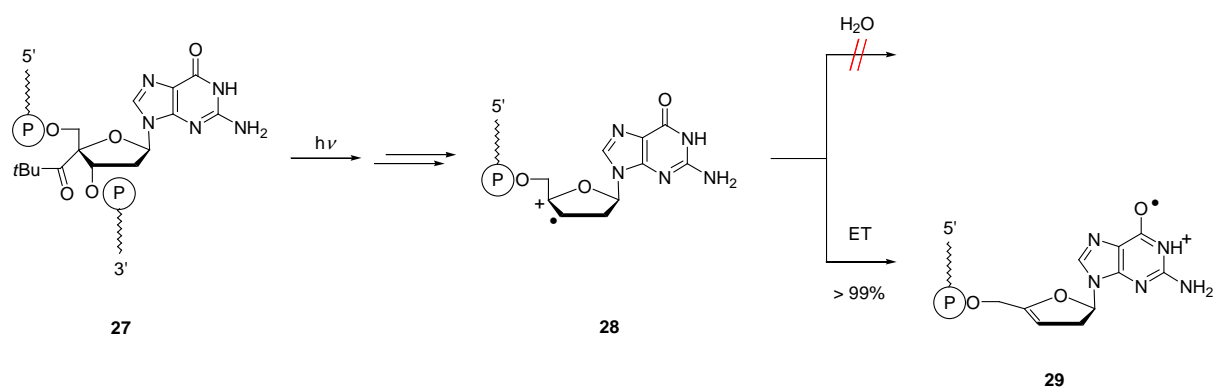
When several experiments pointed towards the contribution of adenines as charge carriers in long (A−T)$_n$ bridges,[79,70] an assay providing direct charge injection into adenine was required, to demonstrate the presence of oxidized adenines within the (A−T)$_n$ bridge during the hole transfer process. *Kendrick* succeeded in synthesizing a 4'-pivaloylated adenosine derivative **30** and thus established the first possibility of a direct charge injection into an adenine (*Scheme 1.6*).[86,100] However, due to the higher oxidation potential of adenine, water trapping of the radical **31** occurs at about the same rate as the hole injection into adenine.

This explains the moderate yield of 40% of enol ether **32**. Addition of KI as a fast hole quencher raised the yield of enol ether **32** to nearly quantitative, showing that the diffusion-controlled reaction with KI efficiently competes with the water trapping reaction.

Scheme 1.6
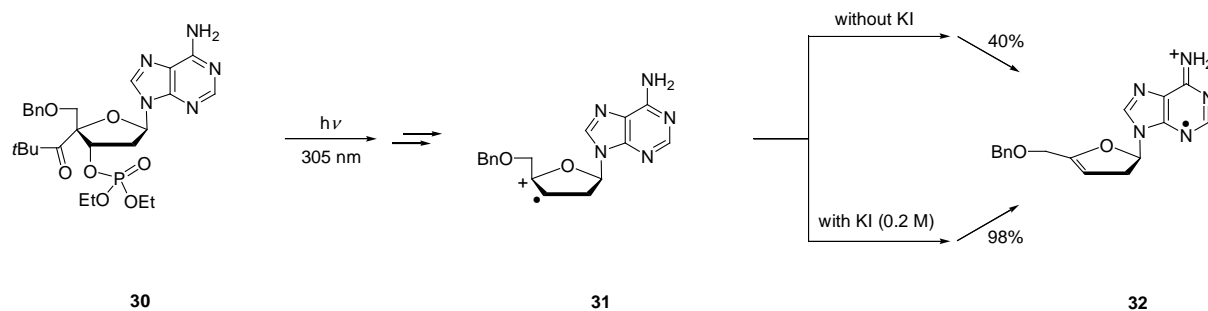
This assay provides the direct hole injection into an adenosine molecule and charge transfer starting at a higher oxidation potential and is the basis for the research presented in this thesis. The following chapters establish the study of the distance-independent hole transfer in DNA.

2 Research Background

2.1 Kendrick's Charge Transfer Experiments

Two important prelimiary experiments with DNA strands modified by the 4'-pivaloylated adenosine were performed by *Kendrick*.[86] The 4'-pivaloylated building block **33** was introduced into DNA double strands **34a**,**b** and the intermediate adenine radical cation in **35a**,**b** was generated by photolysis. The positive charge in **35a**,**b** migrated towards the 3'- and the 5'-end until it was trapped by the GGG sequences. The amount of the charge reaching the guanines was detected by reaction of the guanine radical cations with water, thus affording products P$_{3'}$ and P$_{5'}$ after subsequent strand cleavage (*Scheme 2.1*).

Scheme 2.1

34a: n=1
34b: n=4

35a: n=1
35b: n=4
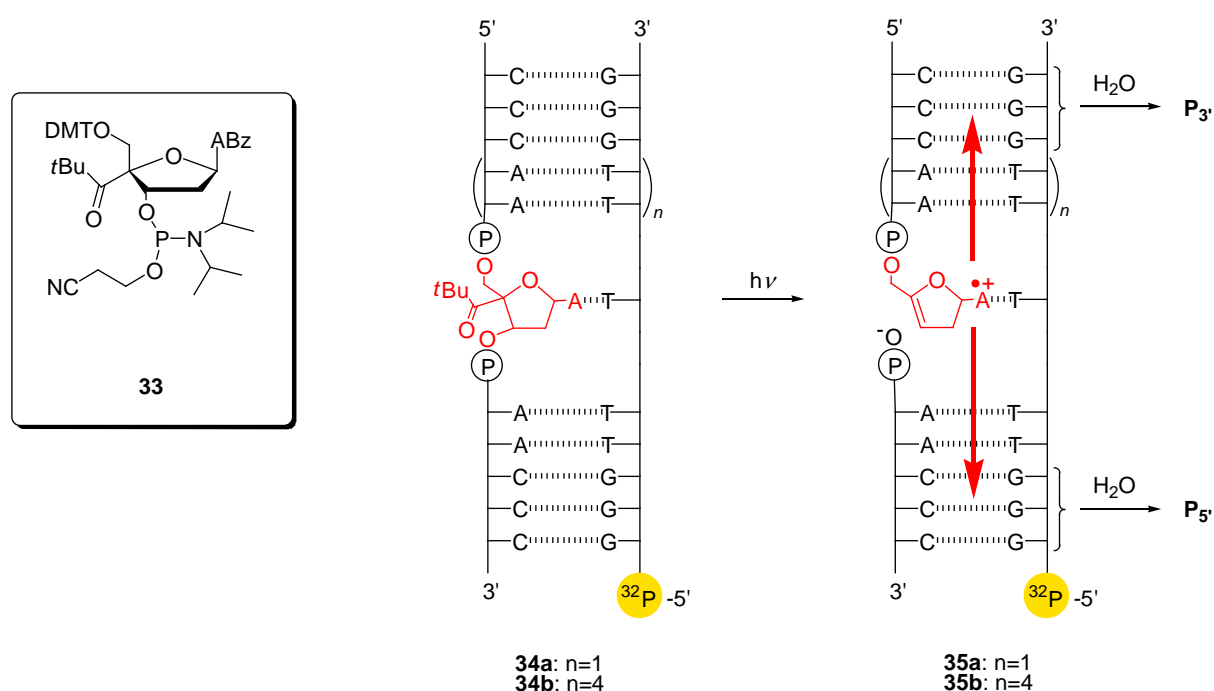
Preliminary experiments were performed to check whether the efficiency of the charge transfer towards the 5'-end is different from that towards the 3'-end. It emerged that photolysis of **34a**,

where both sequences between $A^{\bullet+}$ and the GGG units contain two A−T base pairs, gave about the same amount of products $P_{3'}$ (55%) and $P_{5'}$ (45%). In strand **34b** one of the A−T sequences was extended from two to eight A−T base pairs. Nevertheless, nearly the same ratio of products $P_{3'}/P_{5'}$ was observed (*Figure 2.1*). In these experiments, the efficiency of the charge migration through the A−T sequences altered very little depending on the number of the A−T base pairs.
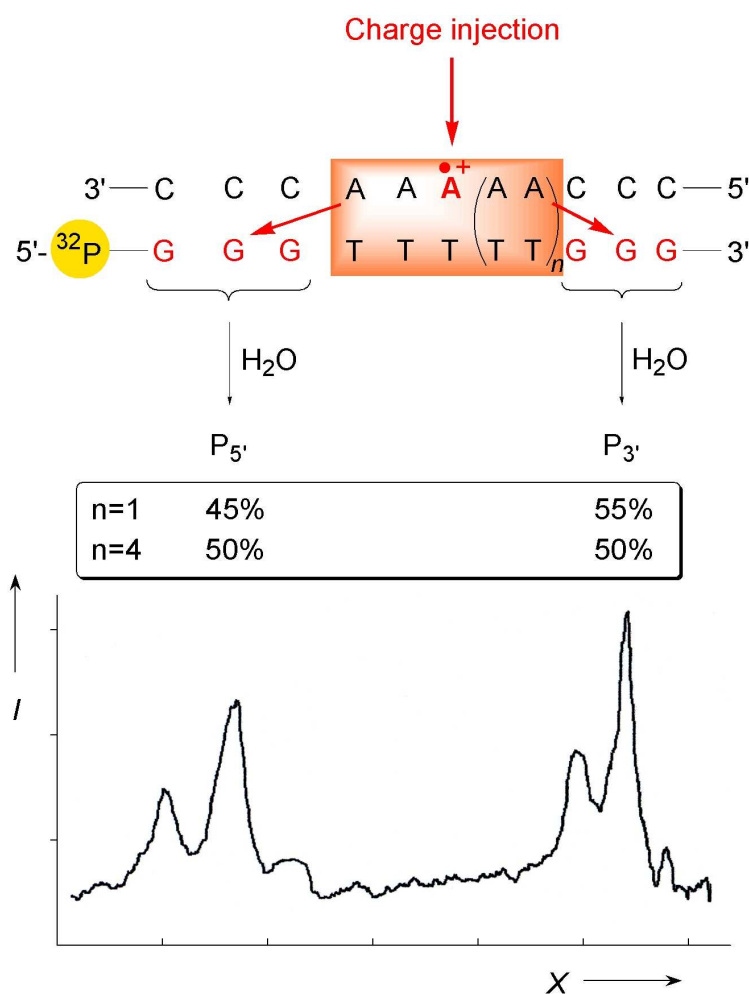
*Figure 2.1. Histogram of denaturing polyacrylamide gels, obtained by subtraction of control experiments (irradiation of unmodified strands) from irradiation experiments with the modified strand **34a** (n=1), and relative yields of the strand cleavage products at the 5'- and 3'-GGG units for strands **34a** (n=1) and **34b** (n=4).*

2.2 A First Synthesis of 4'-Pivaloyl Modified Adenosine

Kendrick's synthesis of the 4'-pivaloylated adenosine building block starts by building up a suitably functionalized 4'-pivaloyl glycoside **37**, analogously to a method developped by *Crich*.[101] The glycoside was further modified to suit the desired purpose of subsequent monomer experiments (*Scheme 2.2*) or introduction into DNA (*Scheme 2.3*).[86,100]

Scheme 2.2
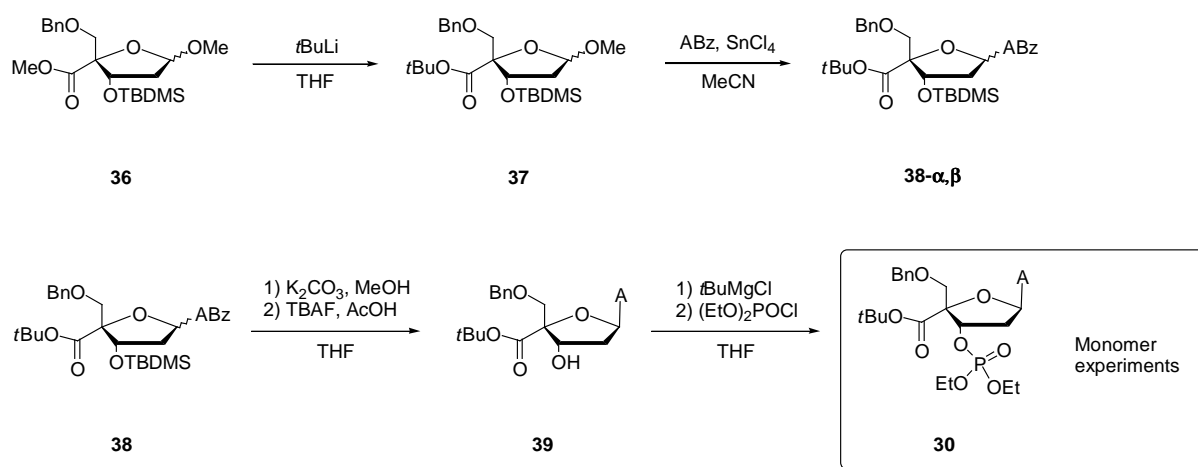
The pivaloyl group was introduced by reaction of methylester **36** with *t*-BuLi to give the photolabile pivaloyl ketone **37**. Reaction with benzoyl-protected adenine (ABz) and stannic chloride yielded nucleoside **38**. Removal of the benzoyl and silyl groups, followed by selective introduction of the phosphate group afforded compound **30**, which was used for monomer photocleavage experiments. *Crich's* synthesis assay for the 4'-acetyl glycoside **36** was incompatible with the requirements on a precursor for the automated DNA synthesis, and numerous further steps were needed in order to change the protecting groups into DNA synthesizer-compatible ones (*Scheme 2.3*). The benzyl group was removed *via* photobromination and replaced by a benzoyl group in compound **41**. Reaction with protected adenine (ABz) and stannic chloride yielded the nucleoside **42**. The 5'-benzoyl group was then

replaced by a trityl group, and the compound was desilylated and phosphorylated to afford the DNA synthesizer compound **33**.

Scheme 2.3
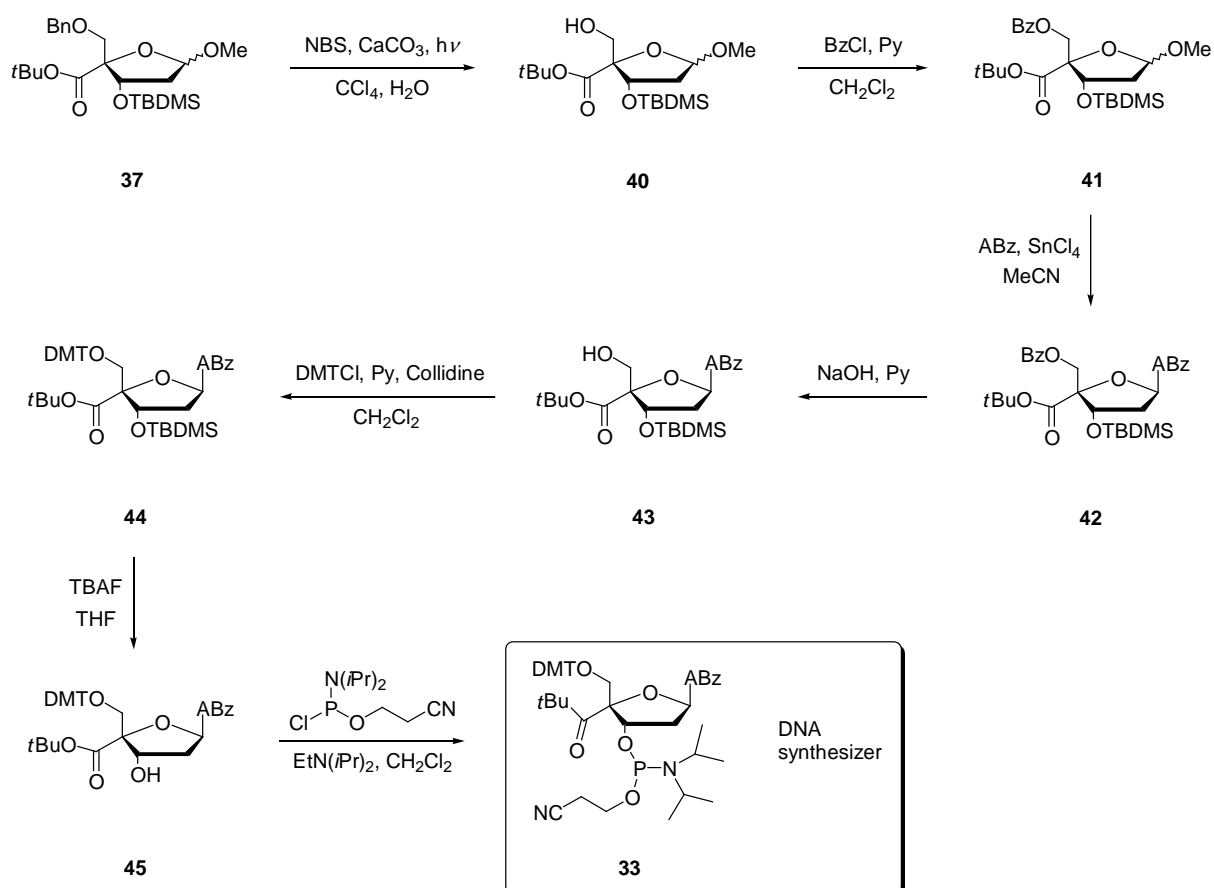
Kendrick's synthesis of the 4'-pivaloylated adenosine building block turned out not to be of further practical use due to its bad reproducibility, the use of very toxic reagents and the insufficient overall yield (approximately 0.05%) of the DNA synthesizer monomer **33**.

3 Proposal

The first part of our proposal was to develop a new, reliable synthetic route to 4'-pivaloylated adenosine building block **46**, analogous to compound **33** (*Scheme 3.1a*).

Scheme 3.1

X,Y: variable bridge (A−T / T−A / mismatch / reduced abasic site)
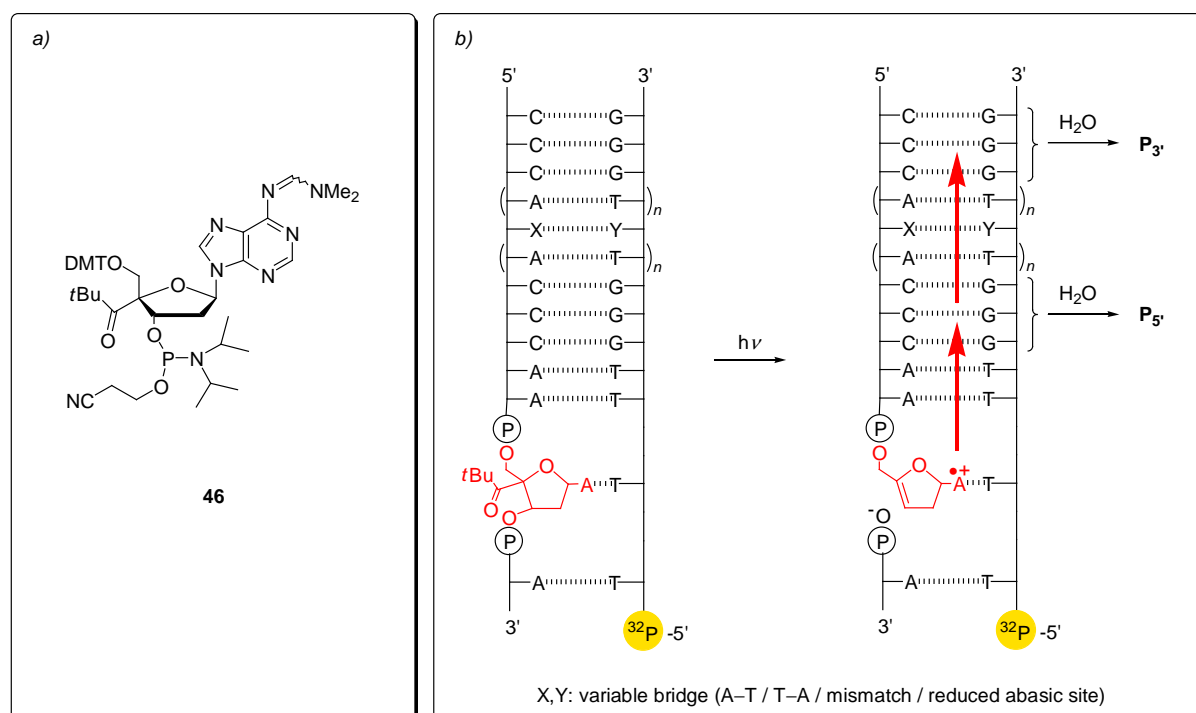
The second part of the proposal comprised:

- the determination of the pH dependence of the charge injection efficiency in single- and double-stranded DNA,
- the investigation of the distance-independent hole transfer through long $(A-T)_n$ sequences, in terms of sequence-dependence, influence of base mismatches and the dependence on the secondary structure of the DNA double helix (*Scheme 3.1b*).

4   Synthesis of 4'-Pivaloyl Modified Adenosine

4.1   Synthetic Strategy

Apart from the assay described in *Chapter 2.2*, there are two more principal assays, which lead to 4'-acylated nucleosides.[102,103] The shorter pathway *a* (*Scheme 4.1*) includes first the introduction of the pivaloyl group *via* organometallic addition of *t*-butyllithium to aldehyde **47**, followed by oxidation of the secondary alcohol. The 4'-C,C-coupling takes place at the end of the synthesis *via* an aldol addition of formaldehyde and barium hydroxide, to yield two diastereomeric nucleosides **49** and **50**. Pathway *b* also starts with aldehyde **47** and proceeds *via* an aldol reaction and subsequent reduction to diol **51**, which is converted to alcohol **52** by means of suitable protection and deprotection steps. Oxidation to aldehyde **53**, followed by introduction of the pivaloyl group, analogous to pathway *a*, leads to the target nucleoside **50**.

Scheme 4.1
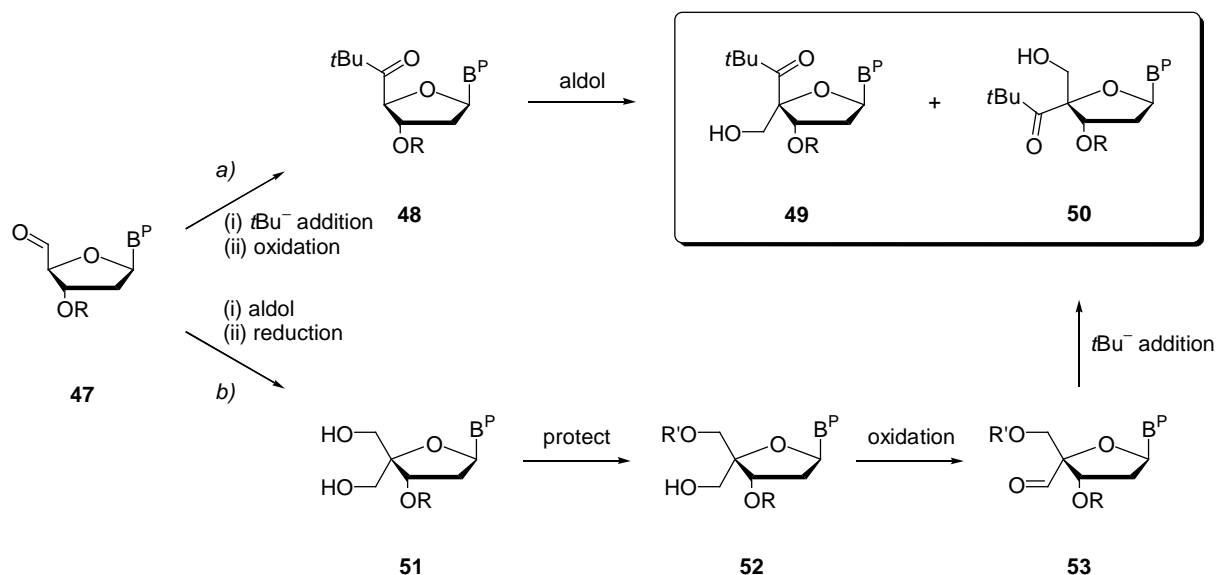
In contrast to thymine, adenine possesses a free primary amino group which must be protected during the key steps of the synthesis. This protective group should ideally be easy to introduce and should withstand the basic conditions of the aldol reaction and the conditions of the Pfitzner-Moffatt and Dess-Martin oxidation steps. Even more important is the fact that the cleavage of any protective group must not lead to acid-catalysed depurination. Depurination already occurs under slightly acidic conditions and therefore constitutes a severe limitation in purine nucleoside, particularly adenosine chemistry.[104] *Kendrick* attempted to use the benzoyl (Bz) group for adenine protection but observed very poor yields for the aldol reaction.[100] The *i*-butyryl group applied by *Spormann* to the synthesis of the 4'-pivaloyl modified guanosine[103] is not suitable for adenine.[104] Although it is slightly more stable towards basic conditions than the benzoyl group, amides generally are not stable towards coupling reagents like DCC or CMC, which are used in the Pfitzner-Moffatt oxidation.[105]

The *t*-butyl carbamate (Boc) protecting group, which shows a significantly higher stability towards basic, nucleophilic and Pfitzner-Moffatt conditions, combined with a much higher reactivity towards (Lewis) acids and heating,[105,106] was selected for the new synthetic approach. However, it was necessary to change the base protecting group before using the building block for DNA synthesis (*Scheme 4.2*).

Scheme 4.2
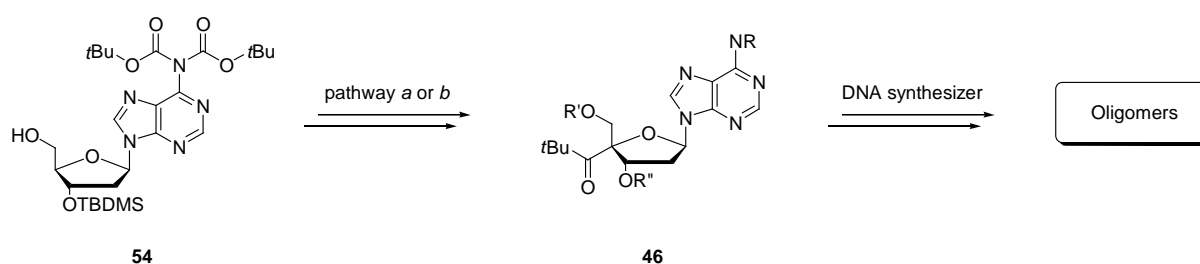
R = (dimethylamino)methylidene
R' = 4,4'-Dimethoxytrityl
R"= 2-Cyanoethyl-*N,N*-diisopropylphosphoramidite

4.2   Synthesis of the 4'-Pivaloyl Modified Adenosine DNA Building Block

A precursor suitable for both synthetic strategies was obtained in three steps. In a first step, the 3'- and 5'-hydroxy groups of 2'-deoxyadenosine **64** were protected with TBDMSCl according to a method by *Ogilvie*.[106] The free amino group of the base was subsequently protected with di-*t*-butyl-dicarboxylate (Boc),[107] and the primary TBDMS group was selectively cleaved using a mixture of TBAF and glacial AcOH in THF.[108] This afforded nucleoside **63** in 48% yield over three steps.
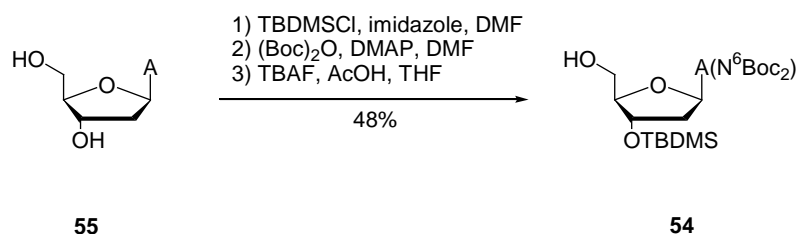
Starting from the protected nucleoside **54**, diol **56** was obtained *via* a modified Pfitzner-Moffatt oxidation,[109] followed by aldol reaction and sodium borohydride reduction. The aldol reaction is the first key step in the synthesis as it provides the C,C-coupling at the 4'-position of the deoxyribose. In contrast to the previous syntheses,[102,103] the use of DCC proved to be not useful due to separation problems during the workup. Replacement of DCC by CMC resulted in an excellent yield of 48% over three steps, the best result yet reported for this aldol reaction. Remarkably, one of the two Boc groups was cleaved during the aldol reaction, and the resulting diol **56** readily crystallized out of the crude reaction mixture in analytical purity. The loss of one Boc group did not affect any of the subsequent synthetic steps.

54   **56**
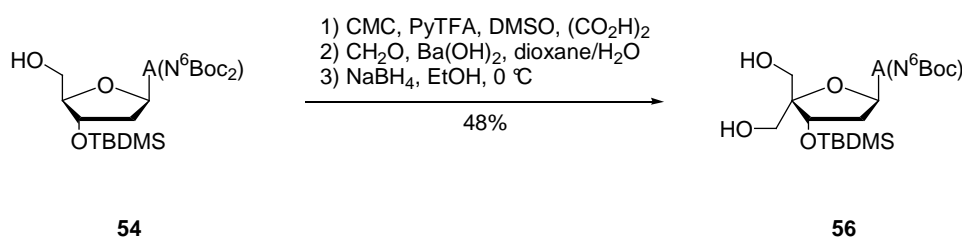
Subsequently, the diol **56** was reacted with trimethyl orthoacetate according to a method by *Müller*,[110] and the intermediary cyclic orthoester was hydrolyzed under acidic conditions. The remaining free hydroxy groups were protected with TBDMSCl, and the acetyl groups selectively cleaved with sodium methoxide, which afforded the silylated nucleosides **57a** and **57b** in 49% and 36% yield over four steps, respectively. The absolute stereochemistry of the two compounds was assigned by comparison of the glycosidic ^{1}H NMR chemical shifts with the corresponding thymine[102] and guanine[103] derivatives at this stage. Definitive verification of the stereochemistry was achieved using a [1]H-NOESY experiment of protected pivaloyl compound **59**. Dess-Martin oxidation[111] of the alcohol **57a** gave aldehyde **58** in 81% yield.

58
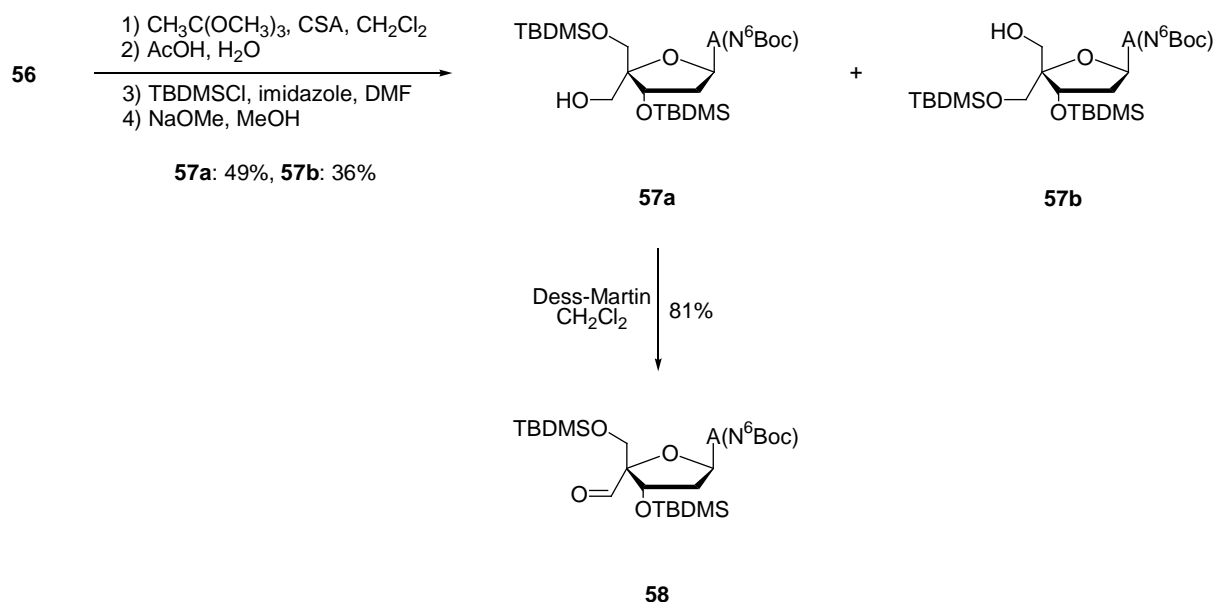
Introduction of the pivaloyl group was achieved by addidion of t-butyllithium to aldehyde **58**. The resulting alcohol was directly converted into ketone **59** *via* Dess-Martin oxidation in 25% yield over two steps.
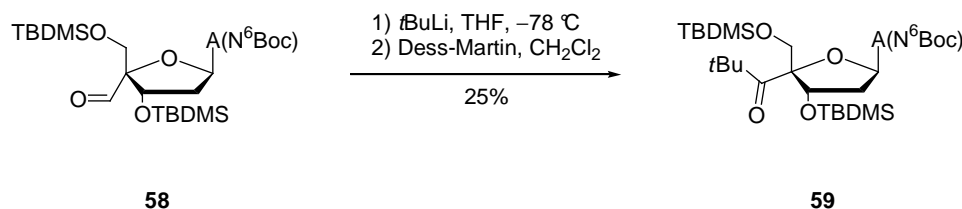
The absolute stereochemistry of compound **59** was verified by NOE measurements. Differential NOE effects between H−C(1') and the *t*-butyl group (4%) and between H_a−C(2') and the *t*-butyl group (2%) were detected (*Figure 4.1*).
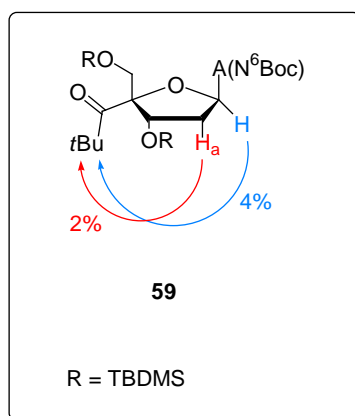
*Figure 4.1. Verification of the absolute stereochemistry of compound **59** by NOESY*

The two TBDMS groups were cleaved by reaction with TBAF, and the subsequent cleavage of the Boc group turned out to be the second key step of the synthesis. The common methods using acidic conditions or Lewis acids were unsuccessful,[112] as they all resulted in rapid depurination of the nucleoside. The priority was to screening reactions that make use of ion-exchange resins and solid-phase Lewis acids, as these were promising alternatives to the use

of protic systems. Finally, the selective cleavage of the Boc group was achieved by reacting ketone **59** with silica gel *in vacuo* at 80 °C for one week, according to a method by *Wensbo*,[113] to yield the desired 4'-modified nucleoside **60** in 37% yield over two steps.
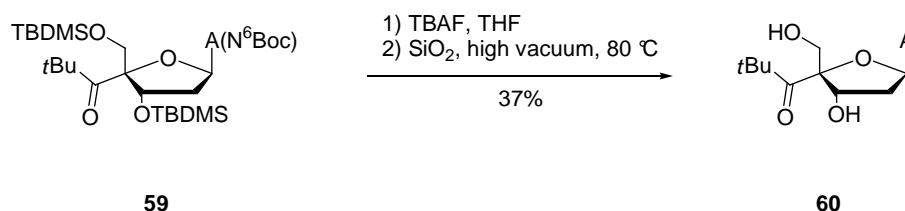
Three more modifications were needed to convert the 4'-pivaloylated nucleoside **60** into a DNA synthesizer-compatible building block. The free amino group of the base was selectively protected with a dmf group,[104,114] and the 5'-hydroxy group was selectively protected with DMTCl in collidine / DMF,[115] to give the tritylated product **61** in 55% yield over two steps. Phosphitylation was performed according to a standard procedure[116] using 2-cyanoethyl-*N,N*-(diisopropyl)-chlorophosphoramidite and Hünig's base and lead to the desired monomer **46** in 78% yield. Monomer **46** is suitable for introduction into synthetic oligonucleotides via automated solid-phase synthesis.[117]
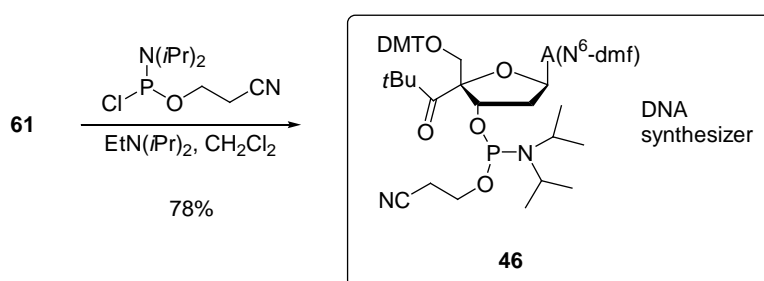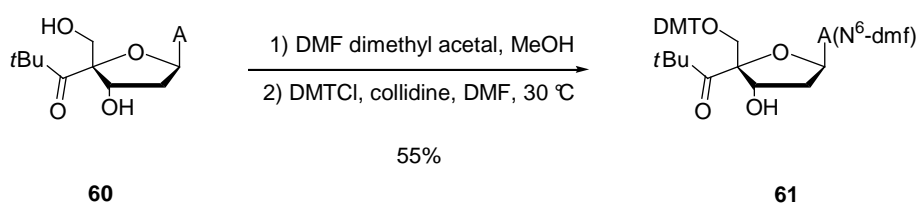
4.3   Summary

Synthesis of adenine radical precursor **46** (*Scheme 4.3*) was achieved in a similar way to the synthesis of the corresponding thymidine or guanidine compounds. Several steps had to be modified due to the higher reactivity of 2'-deoxyadenosine towards depurination. This work presents the first example where the Boc protecting group was successfully introduced to protect the primary amino function of adenine in a deoxyribonucleoside and cleaved under ultramild conditions. The shorter synthesis pathway *a via* addition of *t*-butyllithium to aldehyde **47** (*Scheme 4.1*) followed by aldol addition of formaldehyde was not pursued. The synthesis of the guanosine derivative on this pathway failed, probably due to the steric hinderance of the purine base, which is considerably larger than a pyrimidine base like thymine.[80] The 4'-position of aldehyde **47** was hydroxymethylated, which led to the important intermediary diol **56** after reduction. By means of a suitable protection group strategy, diol **56** was converted into alcohol **57** with a fairly good regioselectivity of 1.4:1 in favour of the preferred diastereomer. After subsequent oxidation, addition of *t*-butyllithium and Dess-Martin oxidation, the pivaloylated adenosine **59** was obtained. The protective groups were cleaved, and DNA synthesizer-compatible dmf and trityl protective groups were introduced. Upon conversion with 2-cyanoethyl-*N*,*N*-(diisopropyl)-chlorophosphoramidite, the 4'-pivaloylated precursor **46** (which is suitable for the introduction into synthetic oligonucleotides via automated solid-phase synthesis) was obtained in 0.5% overall yield over 10 characterized steps starting at 2'-deoxyadenosine **55**.

Scheme 4.3
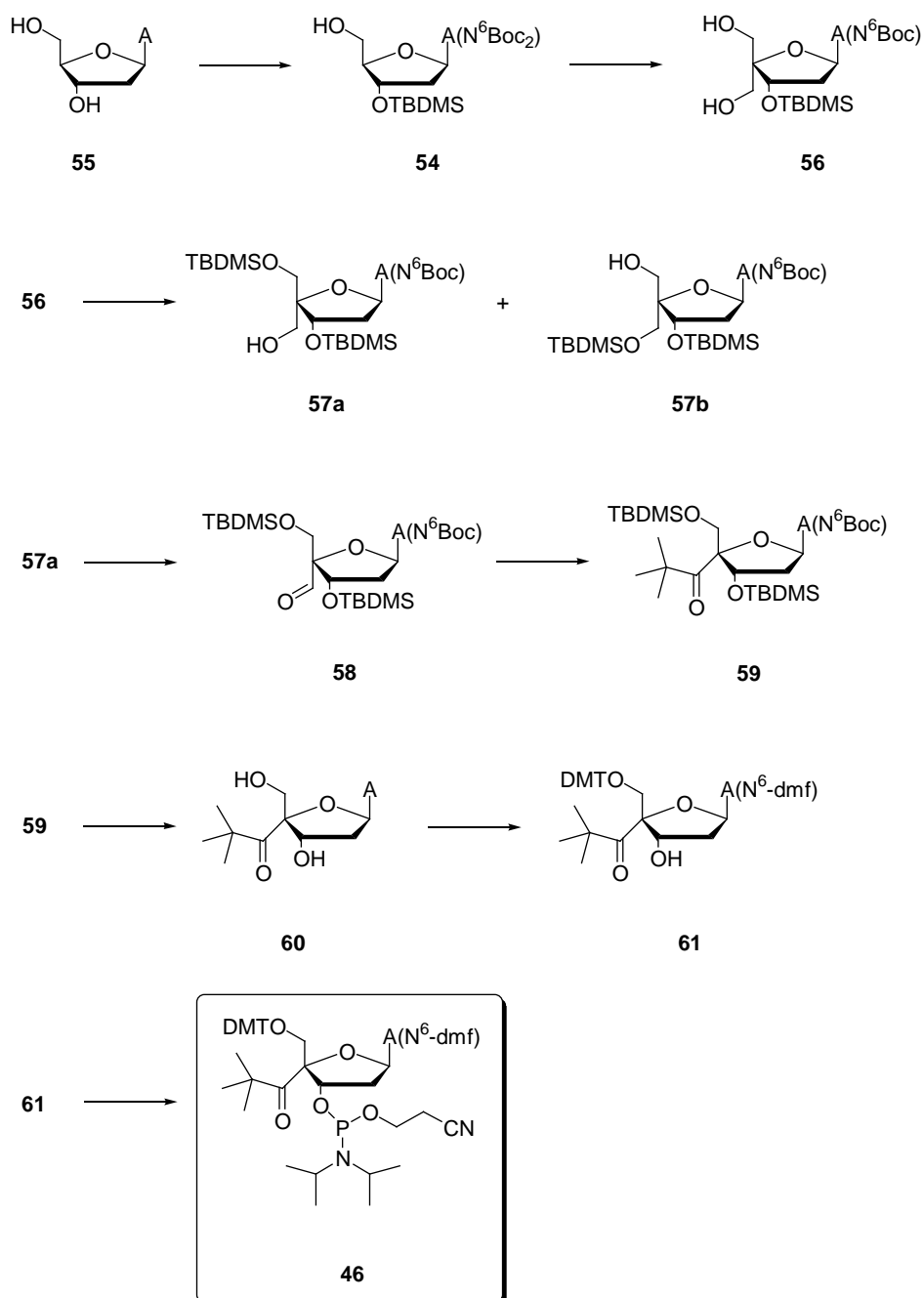
5   Investigation of the Charge Injection Efficiency within an Oligonucletide

5.1   Rate of Charge Injection into Adenine

The photocleavage experiments with monomer **30** undertaken by *Kendrick* (*Chapter 1.3.3*) demonstrated that the electron transfer from adenine (leading to the formation of enol ether) and water addition to the deoxyribose moiety (leading to several decomposition products) compete with each other at about similar rates. This was verified by addition of the rapid electron donor potassium iodide[118] to the photolysis mixtures, which raised the yield of the enol ether formed from 40% to 98%.[86] These experiments have demonstrated that a 4'-pivaloylated 2'-deoxyadenosine is indeed able of *a)* charge transfer to the base, and *b)* the results for the different bases qualitatively reflect the oxidation potentials determined by *Steenken*[22b] and others.[22a]

Scheme 5.1
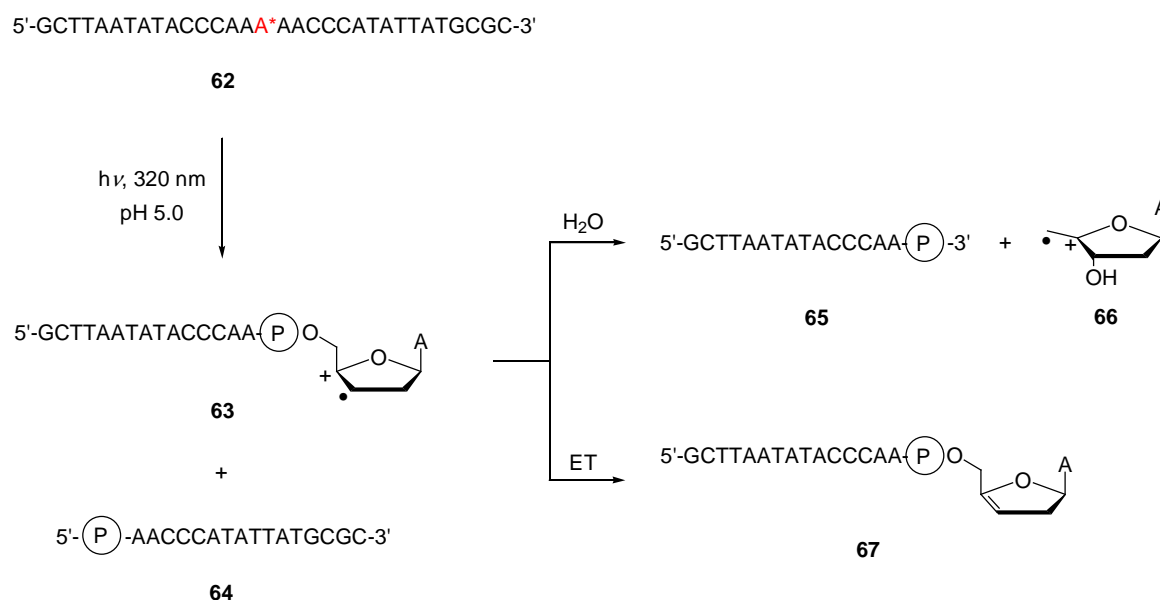
A* = 4'-pivaloyl modified adenosine

A further experiment to determine the charge injection rate within an oligonucleotide was also performed by *Kendrick*[100] using HPLC analysis (*Scheme 5.1*). The single-stranded DNA **62** was irradiated at 320 nm at pH 5.0, which led to the formation of radical cation **63** and of 5'-phosphate **64**. The radical cation **63** either undergoes water addition to form radical cation **66** and 3'-phosphate **65**, or electron transfer occurs from adenine which leads to enol ether **67**. Although no quantitative results were obtained, because the DNA fragments to be separated were all of nearly identical size, the experiment provided some qualitative information about the rate of charge injection into adenine. The ratio between enol ether **67** and 3'-phosphate **65** varied upon the concentration of KI as was the case for thymidine, whereas in similar experiments using a 4'-pivaloylated guanosine as charge injecting system, no influence of KI concentration on the ratio between enol ether and 3'-phosphate was observed.[80]

In comparing the water trapping rate (k_{trap}) with the rate of electron transfer (k_{ET}) between KI and the thymine derivative **19** (5×10^9 s^{-1}),[118] assuming a diffusion-controlled reaction of KI, a k_{trap} of about 1.1×10^8 s^{-1} was estimated.[94]

Meggers has shown that both electron transfer and water addition proceed irreversibly, and assuming that the concentration of electron donor does not change during the reaction, the ratio of the water addition products **64**–**67** against the electron transfer product **67** is given by Eq. 5-1:[40]

$$k_{ET,rel} = \frac{k_{ET}}{k_{trap}} = \frac{\mathbf{67}}{\mathbf{64\text{–}67}} \qquad (5\text{-}1)$$

For the guanine derivative **28**, *Spormann* determined a $k_{ET} \geq 5 \times 10^9$ s^{-1} and a 60-fold higher $k_{ET,rel}$ than in the case of thymine. The discrepancy can be explained by the low oxidation potential of guanine and the short distance between donor and acceptor.[103] Assuming that k_{trap} is identical for all nucleosides, *Kendrick* estimated that the electron transfer from adenine in radical cation **63** is about 1.5 times faster than the water trapping reaction (as calculated from the yields of **67** (30%) and **64** (50%)) resulting in an absolute electron transfer rate k_{ET} of about 1.6×10^8 s^{-1}.[100] This means that the electron transfer from adenine in radical cation **70** is slightly more efficient than the electron transfer from a single guanine to an adjacent

radical cation in **71** (*Scheme 5.2*), but more than at least one order of magnitude less efficient than the electron transfer from guanine in radical cation **28**. However, these values are strongly dependent on the neighbouring bases and thus may vary by several orders of magnitude from case to case.

Scheme 5.2

$k_{ET} \sim 1.6 \times 10^8 \text{ s}^{-1}$ $k_{ET} \sim 6.5 \times 10^7 \text{ s}^{-1}$ $k_{ET} \geq 5 \times 10^9 \text{ s}^{-1}$
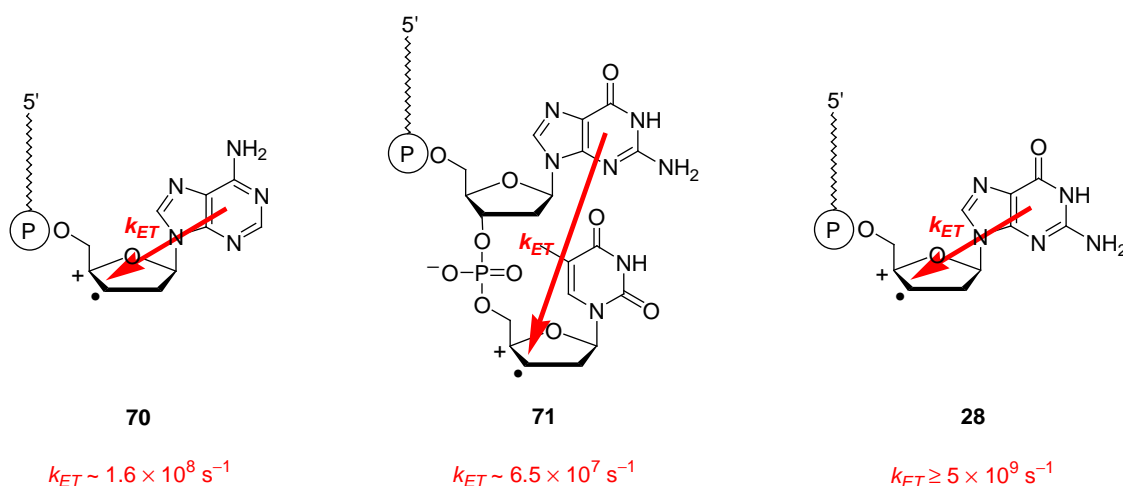
5.2   Charge Injection Efficiency in Single-Stranded DNA

For the investigation of charge injection efficiency of the 4'-pivaloylated 2'-deoxyadenosine, a new assay using ^{32}P radiolabelling and PAGE was developped. The incorporation of radical precursor **46** into DNA strands is described in detail in *Chapter 14*. Several experiments were performed with single-stranded sequences **102** and **103** in order to determine the overall charge injection efficiency and the influence of the pH value on this step. The results of these experiments should allow us to find a pH value offering maximum clevage yield, as the enol ether DNA fragment **76** (23mer) resulting from charge transfer to adenine is easily separable from the 3'-phosphate **74** (22mer) by PAGE analysis (*Scheme 5.3*). In contrast to the electron transfer experiments, the DNA strands containing the radical precursor and not the GGG units were radiolabelled in the following charge injection experiments.

Scheme 5.3
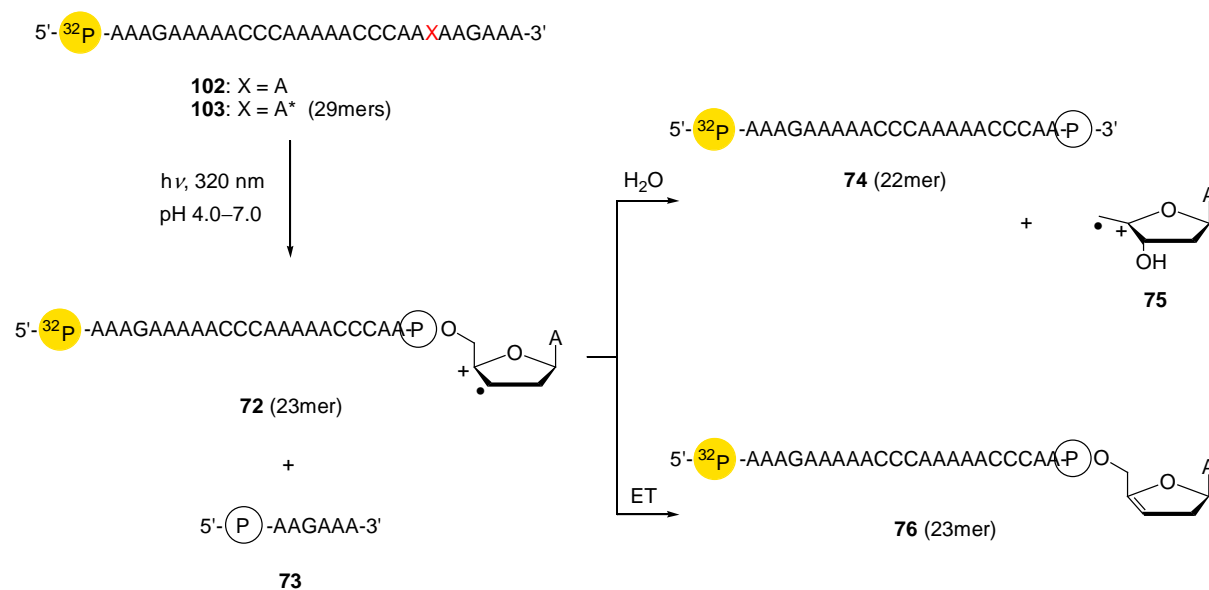
A* = 4'-pivaloyl modified adenosine

The autoradiogram of single strand **103** photolyses (left lanes) clearly shows the two radioactive products **74** and **76**, which differ in one nucleotide size (*Figure 5.1*). The yield of 3'-phosphate **74** was always higher than the yield of enol ether **76** for all examined pH values. No cleavage at all was seen in blind experiments using the unmodified strand **102** (right lanes).
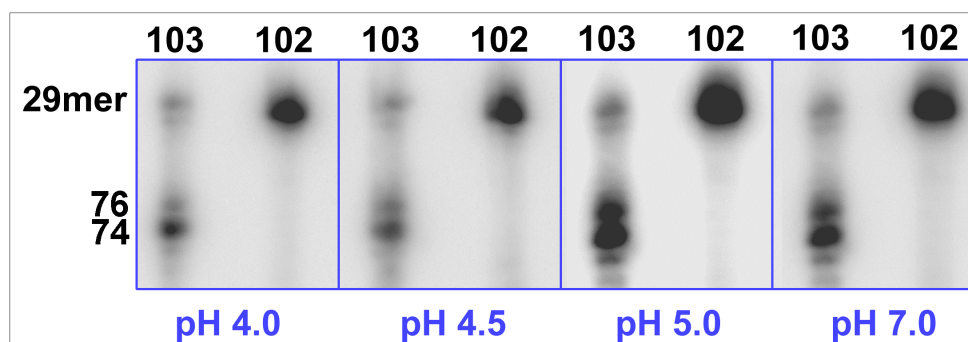
Figure 5.1. *Autoradiogram of single-strand photolyses at different pH values*

The best results were obtained at pH 5.0, which yielded enol ether **76** and 3'-phosphate **74** in 20% and 32% yield, respectively (*Figure 5.2*).
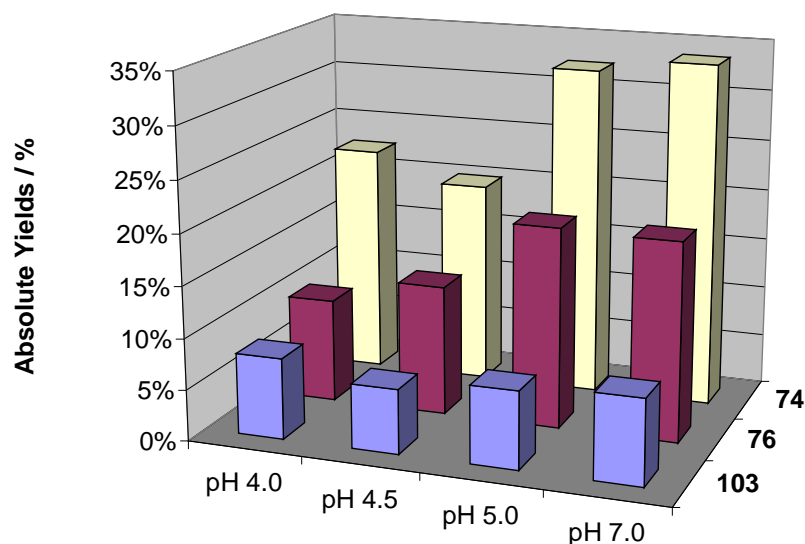
Figure 5.2. Results of single-strand photolyses at different pH values

5.3   Charge Injection Efficiency in Double-Stranded DNA

The charge injection efficiency experiments were repeated with double-stranded sequences **102**/**101** and **103**/**101**, because double-stranded DNA is much less flexible than single-stranded DNA, and the results may differ from single strand experiments. The autoradiogram again shows photocleavage products **74** and **76** for double-strand **103**/**101** photolyses, and no photocleavage products for double-strand **102**/**101** blind experiments (*Figure 5.3*).
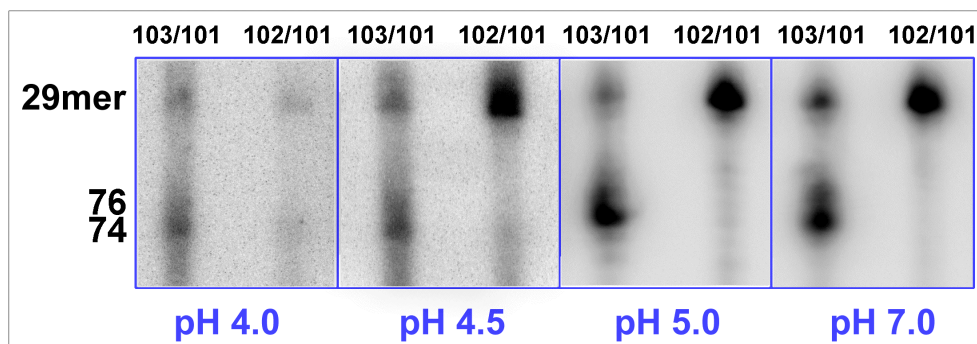
Figure 5.3. Autoradiogram of double-strand photolyses at different pH values

The best results were again obtained at pH 5.0, which yielded enol ether **76** and 3'-phosphate **74** in 19% and 30% yield, respectively. These yields are approximately identical to those in the single strand experiment. Considerable random cleavage at a range of positions was observed at lower pH (4.0 and 4.5) in the double strand experiments, which resulted in very low yields of both remainig 29mer educts **102**/**103** and potential photocleavage products enol ether **76** and 3'-phosphate **74** (*Figure 5.4*, left section).
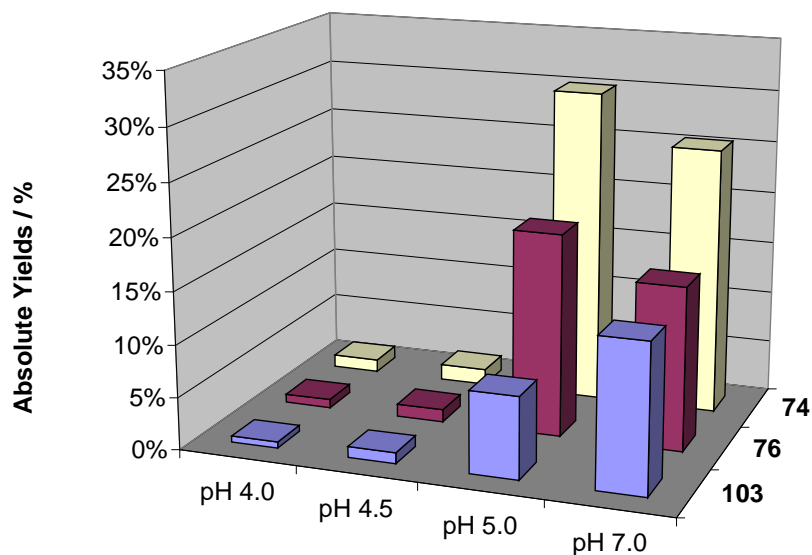
Figure 5.4. Results of double-strand photolyses at different pH values

5.4 Summary

These experiments have demonstrated that the 4'-pivaloylated adenine **46** when incorporated into an oligomer is indeed capable of promoting an electron hole into an adjacent adenine, as the formation of enol ether **76** is observed for both single- and double-stranded DNA.

Photolyses at pH 5.0 afforded the best absolute yields of enol ether **76**, which means that the charge injection into DNA is maximum under these conditions. This result is comparable to experiments by *Meggers*[40] who also found the most efficient charge injection at pH 5.0 for 4'-pivaloylated thymidine. This can be explained by the decreasing nucleophilicity of water with decreasing pH, so that electron transfer is more favourable than water addition.

The sudden drop in electron transfer product **76** at pH lower than 5.0 cannot be explained by protonation of bases because the adenine radical cation has a $pK_a \leq 1$. Even at pH 4.0 all adenines remain uncharged except the intermediary $A^{\bullet+}$.[119] However, it is known from experiments by *Erdmann*[120] that the adenosine enol ether **77** is unstable in protic aqueous solutions and decomposes to yield adenine **78** and ketoaldehyde **79** (*Scheme 5.4*).

Scheme 5.4
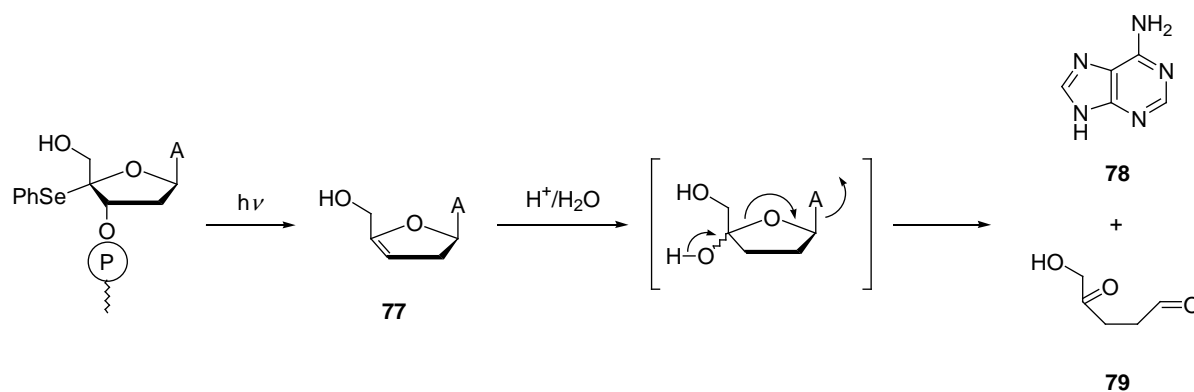
As only the radioactive products could be detected and quantified, the low yield of enol ether **76** may be explained by decomposition of the enol ether **76** at lower pH values in favour of increase of yield of the water addition product 3'-phosphate **74**. The strong, unselective decomposition of double strands at pH 4.0 and 4.5 is presumably due to acid-catalysed depurination of the A-rich strand during the annealing process at elevated temperature.

6 Adenine as Charge Carrier in the Hole Transfer Process

6.1 Köhler's Experiments

Incorporating a sequence of four or more alternating A–T pairs into the radiolabelled strand should identify any oxidative damage at adenines, if they were indeed charge carriers during the hole transfer process and thus underwent water addition. *Köhler*[121] synthesized DNA duplex **80** containing seven alternating A–T pairs between the hole donor G and hole acceptor GGG. The PAGE histogram shows strong oxidative damage at all adenines, thus demonstrating their contribution in a multistep charge transfer process (*Figure 6.1*). Although the charge transfer between adenines is supposed to be fast, water addition products were detected. An effective charge transfer over about 27 Å was observed, resulting in a yield ratio P_{GGG}/P_G of 3.7.[121]
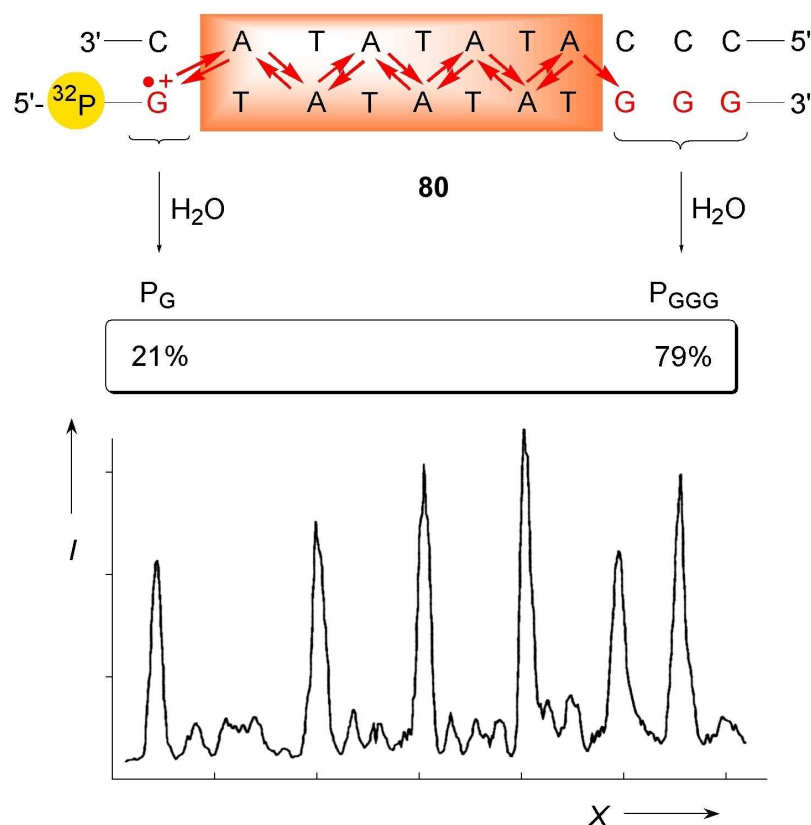
Figure 6.1. *PAGE histogram for interstrand A-hopping (n=7)*

6.2   Further Evidence

Thus far, the postulated adenosine radical cation has not been detected directly. *Dohno* and *Saito*[122] have developed a rapid hole trapping method which allows the visualization of transient oxidation within a poly-A sequence. The kinetic hole trapping moiety is a N^6-cyclopropyl-deoxyadenosine (d^{CP}A, **81**), which undergoes cyclopropane ring opening upon one-electron oxidation and forms two products **82** and **83** (*Scheme 6.1*). Incorporation of **81** into oligonucleotides resulted in a decay of the cyclopropane moiety as well as oxidative cleavage at the modified position upon photolysis, showing that the electron hole was effectively trapped by the d^{CP}A moiety.

Scheme 6.1
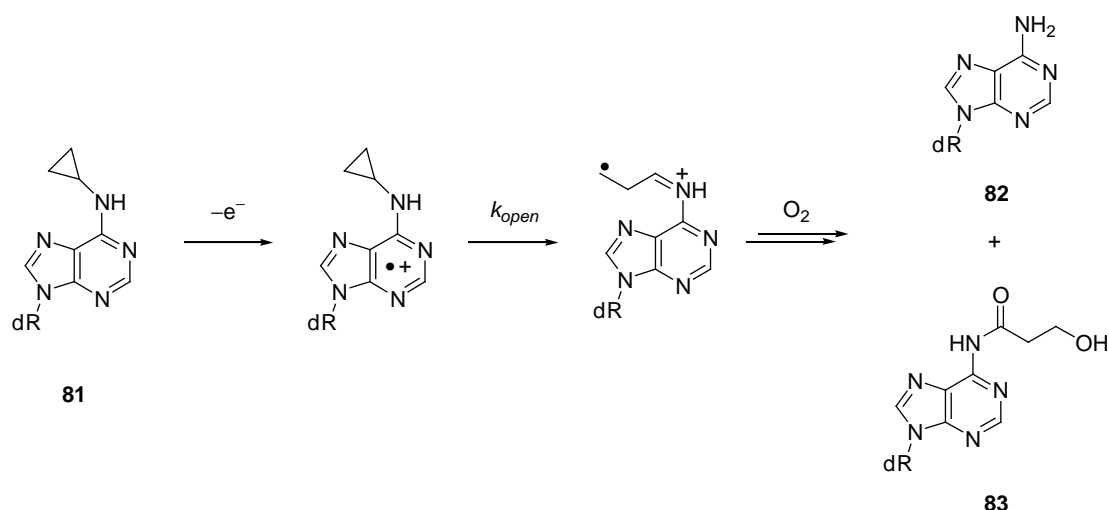
Within the scope of this research, we were able to reproduce and amplify *Köhler's* experimental results showing oxidative damage at adenines (see *Chapter 6.1*) in a comparable case. DNA duplex **111**/**109**, containing a TTATT bridge, featured little oxidative damage at adenine (≤ 10%), which *a)* also points towards an intermediate oxidized adenine, and *b)* again demonstrates that the charge is not tunneling but involves two slower *interstrand* hopping steps (*Figure 6.2*).
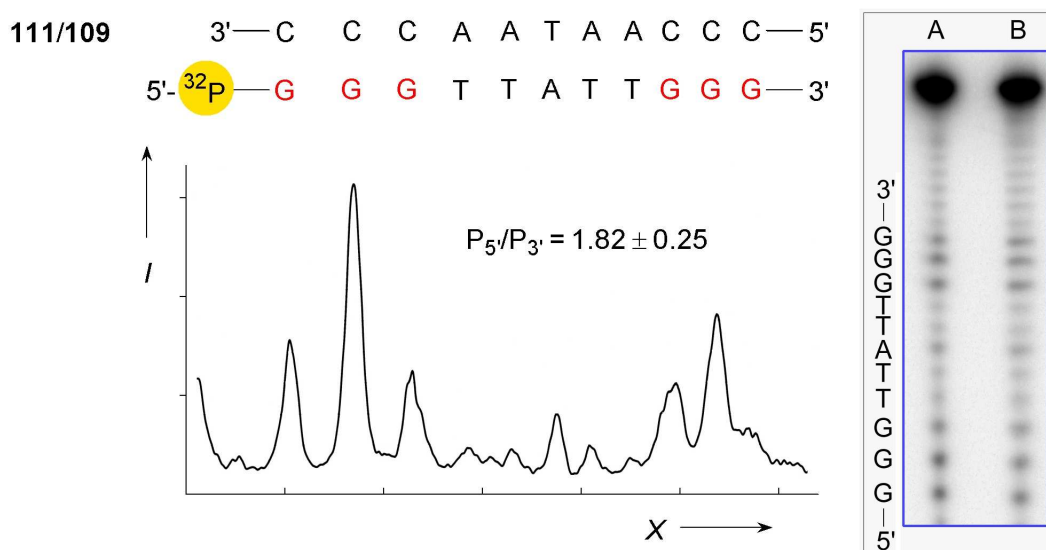
Figure 6.2. *(left) PAGE histogram obtained after subtraction of the blind experiments for interstrand A-hopping (n=5). (right) Autoradiogram of the gel electrophoresis, obtained after photolysis of duplex DNA at pH 5.0 and subsequent piperidine cleavage. Lane A, experiment* **111/109**, *lane B, blind experiment* **111/113**.

Compared to *Köhler's* experiment,[121] the damage at the central A is significantly weaker and this can be explained by a) the different charge injection assays used, b) inefficient water trapping reaction at adenines due to the rapid charge transfer, or c) inefficient strand cleavage through piperidine treatment of water-trapped adenines. Whereas *Köhler* used the 4'-pivaloylated guanosine precursor, all experiments done for this research use the 4'-pivaloylated adenosine precursor, which is assumed to inject the hole at a higher potential, thus leading to a slower water reaction from $A^{\bullet+}$ than from $G^{\bullet+}$, according to the Curtin-Hammett principle (*Figure 6.3*).[85a] This view should be extended to the charge injection system, as a higher-potential charge injection assay apparently leads to a slower water reaction at adenines.
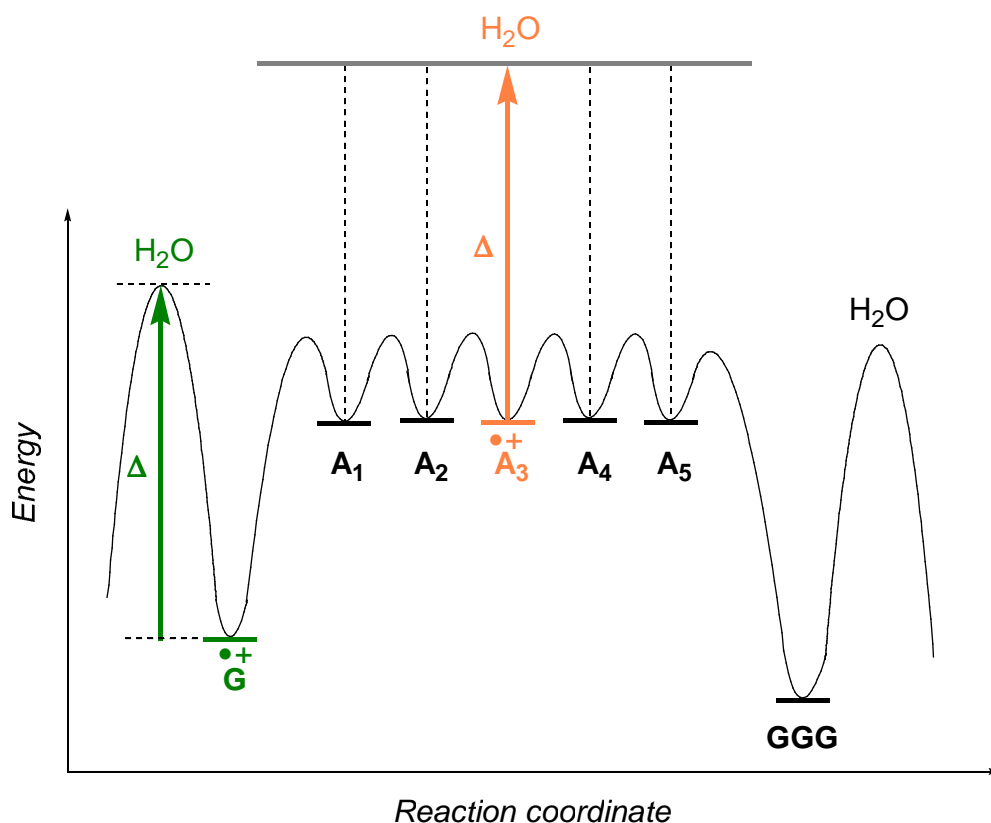
Figure 6.3. *Curtin-Hammett plot for charge transfer processes in a long $(A-T)_n$ sequence involving guanines and adenines as charge carriers. The activation barrier Δ is about the same for $G^{\bullet+}$(green) as for $A^{\bullet+}$ (orange).*

6.3   Summary

The experiments done so far have provided some information about the principle of charge transfer involving long $(A-T)_n$ sequences. The evidence includes the fact that:

a)   the hole transfer over long $(A-T)_n$ sequences involves adenines as charge carriers,

b)   very efficient and nearly distance-independent charge transfer is observed,

c)   the adenines undergo oxidative damage in this process; trapping of a hole within a poly-A sequence is possible by means of a modified adenine.

In the literature, there are speculations that the positive charge is delocalized over more than one A−T base pair so that a phonon-assisted polaron-hopping process,[96] an ion trapped in a self-generated local structural distortion,[123] might make the hole transfer in oxidized (A−T)$_n$ sequences very efficient (*Figure 6.4*). The radical cation then hops adiabatically from minimum to minimum by a thermally activated process as a result of the motions of the DNA and its solvent and counterion environment.
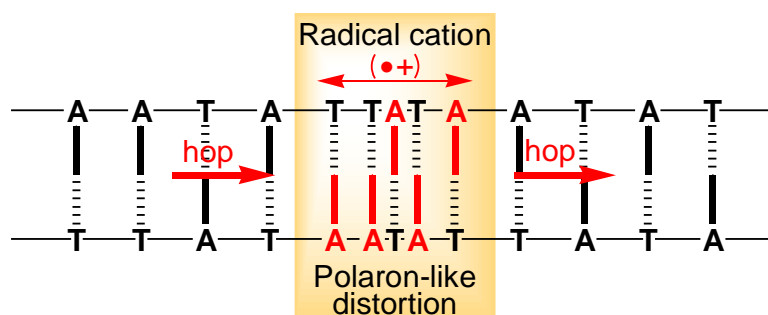
Figure 6.4. *A schematic representation of a polaron-like species in DNA. The base pairs are represented by the vertical lines; the sugar phosphate backbone is represented by the horizontal lines. The polaronic distortion is enclosed in the yellow box and extends over some number of base pairs. This is shown schematically by drawing the base-pair lines closer together. Its movement is thermally activated and proceeds as a whole from one base pair to another.*

The transition from a localized multistep A-hopping process to a polaron-mediated, delocalized charge transport is smooth. No experimental evidence of such delocalized states is available so far, although theoretical calculations by *Schuster*,[124] *Conwell*,[125] *Ratner*[126] and others[29,127] describe such processes. Three conceivable assays for probing the polaron-hopping hypothesis are:

a) measurement of the temperature dependence of the product ratio in an oligonucleotide containing a temperature-independent charge injector and a GGG−(A−T)$_n$−GGG sequence,

b) investigation of the charge transfer process in solid phase or surfactant complexes, thus avoiding ion-gating at the DNA backbone,

c) modification of the bridge by insertion of a series of kinetic traps at the adenines, which may reproduce the charge delocalization pattern.

The discussion on this topic is to be continued as soon as new experimental data is available, particularly concerning the question concerning postulated charge delocalization (or polaron), or how far this distance-independent charge transfer over long $(A-T)_n$ sequences may reach.

7 Influence of Mismatches on the Hole Transfer

7.1 Introduction

Mismatched base pairs constitute a major threat to the genetic information, as they lead to mutations when not enzymatically repaired prior to the next replication. Depending on the nature of the mismatched base pair, the geometry and hydration pattern of the DNA duplex is directly affected. This is generally reflected by a decrease of the DNA melting temperature T_m.[3] Base stacking is accompanied by reduction in UV absorption (hypochromicity), so the UV spectrum is a convenient monitor of the formation and breakdown of duplexes. If the temperature of a solution containing double-helical DNA is slowly raised, UV absorption increases suddenly at a certain temperature because ordered duplexes dissociate. The midpoint of transition is called the "melting temperature" or T_m. *Figure 7.1* shows T_m of several DNA duplexes containing no or one mismatched base pair.
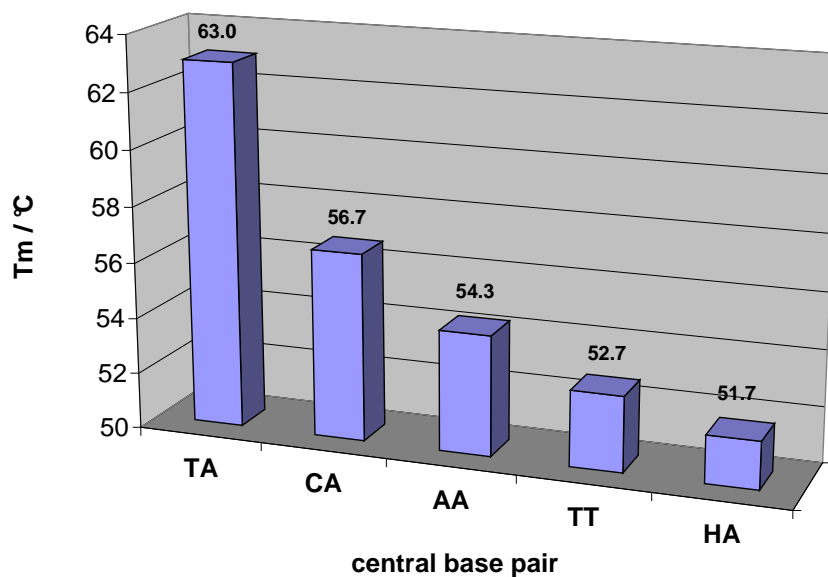
Figure 7.1. *Tm of double-stranded **101/102** containing no or one mismatched central base pair. **TA** represents the unmodified sequence, **H** represents a reduced abasic site*

All mismatches show a destabilizing effect on the DNA duplex, which is maximum for the A−[abasic site] mismatch. Since adenines play a central role in the charge transfer mechanism over long $(A-T)_n$ sequences, mismatches of the adenine−thymine (A−T) base pair should dramatically influence the efficiency of charge transport, as the adenine radical cation is a rather strong acid, but still much too weak to protonate thymine.[119] Thus, proton shifts are not expected to occur within long $(A-T)_n$ sequences, as long as the sequence does not contain any modifications. In G-hopping experiments, *Giese*[72] observed a drastic drop in charge transfer when a thymine or an abasic site was introduced opposite a guanine. In contrast, the presence of an A−A mismatch within an invervening $(A-T)_2$ bridge between guanines hardly affected the charge transfer. *Barton*[128] observed a complete suppression of long-range methylindole radical formation when an A−A mismatch was inserted into an $(A-T)_6$ sequence. The systematic investigation of mismatches within a $(A-T)_n$ sequence was performed using the following modified DNA sequences (*Scheme 7.1*), none of which contain any guanine within the $(A-T)_n$ bridge in order to exclude the G-hopping mechanism.

Scheme 7.1

3'── AAAGAA **A**•⁺ AACCCAA **X** AACCCA AAAAGAAA ──5'

5'-³²P── TTTCTTT TTGGGTT **Y** TTGGGT TTTTCTTT ──3'
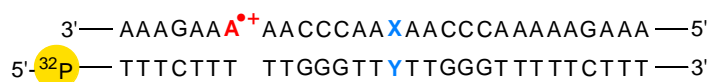
101/103: X=A, Y=T
101/109: X,Y=T
104/103: X=A, Y=H
106/103: X=A, Y=C
111/103: X,Y=A

H = reduced abasic site
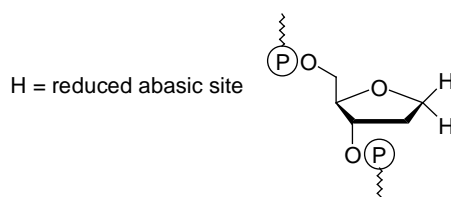
84

The reduced abasic site **84** was introduced using standard methods, and it shows the same properties as an abasic site generated by depurination (still containing its anomeric hydroxy residue) except that it is not cleaved under acidic or basic conditions.[129] This effect is visible

on PAGE histograms, as no cleavage occurs at the 3'-position of the abasic site, resulting in a slightly wider gap between the two neighbouring peaks on PAGE histograms and no peak for the abasic site itself (*Figure 7.3*, bottom right).

7.2 Partial Thermodynamic Charge Equilibration

In the faultless DNA duplex **101**/**103**, a yield ratio $P_{5'}/P_{3'}$ of 1.8 was obtained (*Figure 7.2*). This means that the water trapping of the GGG radical cation is approximately as fast as both the oxidation of adenine and subsequent charge transport over the $(A-T)_n$ sequence.
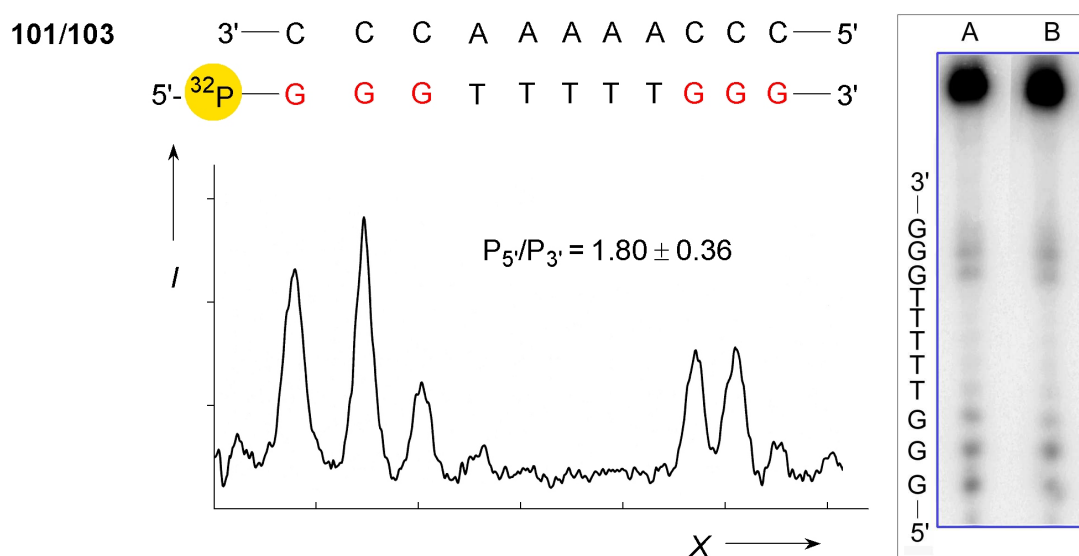
*Figure 7.2. (left) PAGE histogram obtained after subtraction of the blind experiments for intrastrand A-hopping (n=5). (right) Autoradiogram of the gel electrophoresis, obtained after photolysis of duplex DNA at pH 5.0 and subsequent piperidine cleavage. Lane A, experiment **101/103**, lane B, blind experiment **101/102**.*

Thus, the almost distance-independent efficiency of the hole transport between guanines, separated from each other by long $(A-T)_n$ sequences (as first shown in *Figure 2.1*) is not caused by a complete equilibration of the charge before the water trapping occurs. We conclude that the charge must be already partially equilibrated before being trapped by water. The weak distance effect is caused not only by the rate of the hole transport, but also by a partial, thermodynamic charge equilibration over the $(A-T)_n$ sequence.

7.3   Mismatches and DNA Structure

The results from the mismatch experiments are summarized in *Figures 7.3 − 7.4*. Introduction of an A−A mismatch in duplex **111**/**103** resulted in a literally unchanged yield ratio $P_{5'}/P_{3'}$ of 1.9, whereas introduction of a T−T (**101**/**109**) or an A−C (**106**/**103**) mismatch raised the yield ratio $P_{5'}/P_{3'}$ to 2.3 and 4.1, respectively. Introduction of an abasic site (**104**/**103**) and leaving the central adenine unpaired, resulted in the strongest effect observed of no detectable charge transfer to the distant GGG unit ($P_{5'}/P_{3'} \geq 25$).

111/103 3'—C C C A A **A** A C C C—5'

5'-^{32}P—G G G T T **A** T T G G G—3'

$P_{5'}/P_{3'} = 1.87 \pm 0.25$

101/109 3'—C C C A A **T** A A C C C—5'

5'-^{32}P—G G G T T **T** T T G G G—3'

$P_{5'}/P_{3'} = 2.32 \pm 0.47$
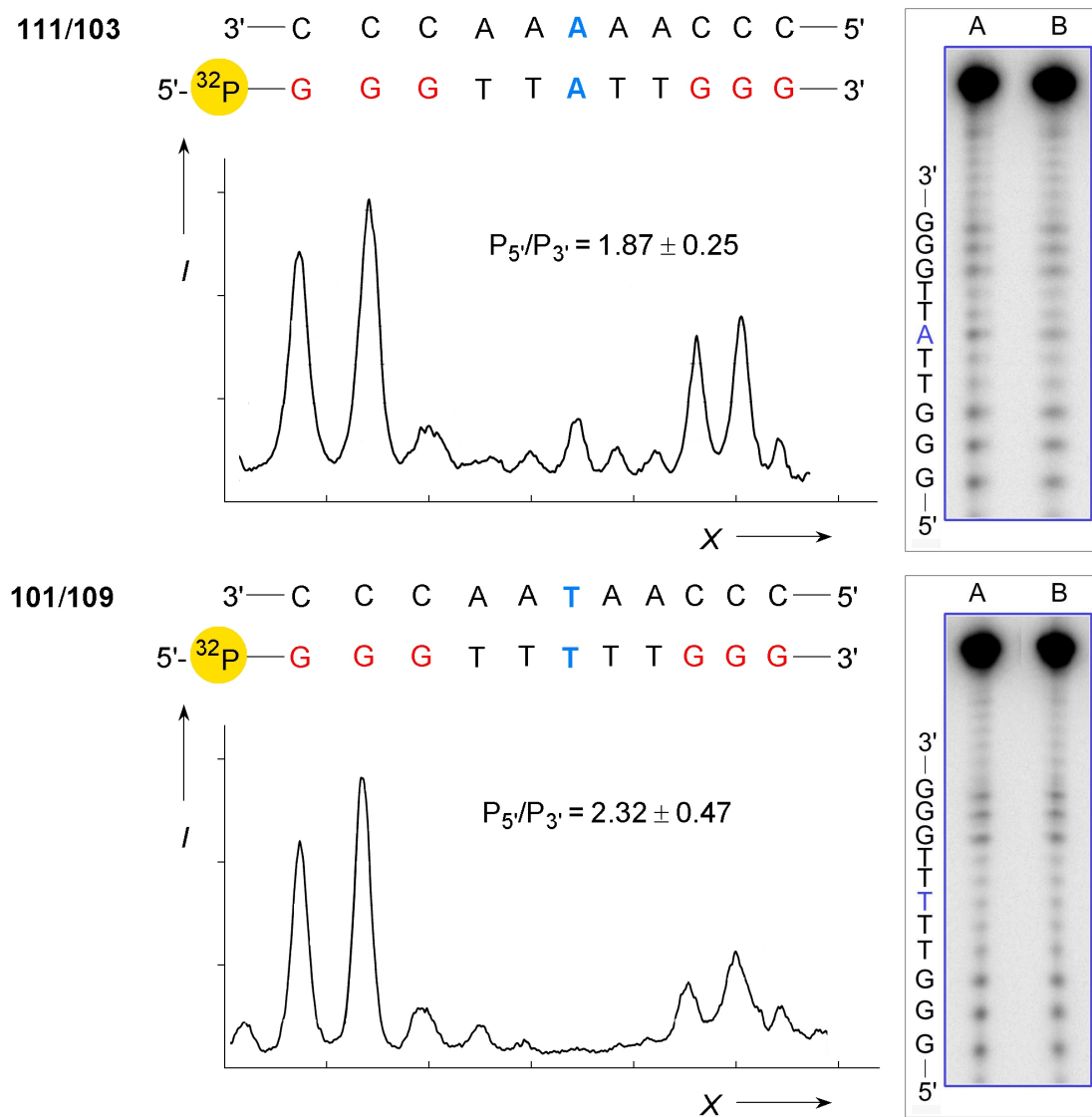
Figure 7.3. (left) PAGE histograms obtained after subtraction of the blind experiments for A–A (top) and T–T (bottom) mismatches. (right) Autoradiograms of the gel electrophoreses, obtained after photolyses of duplex DNA at pH 5.0 and subsequent piperidine cleavage. Lanes A, experiments 111/103 (top) and 101/109 (bottom), lanes B, blind experiments 111/102 (top) and 101/113 (bottom).
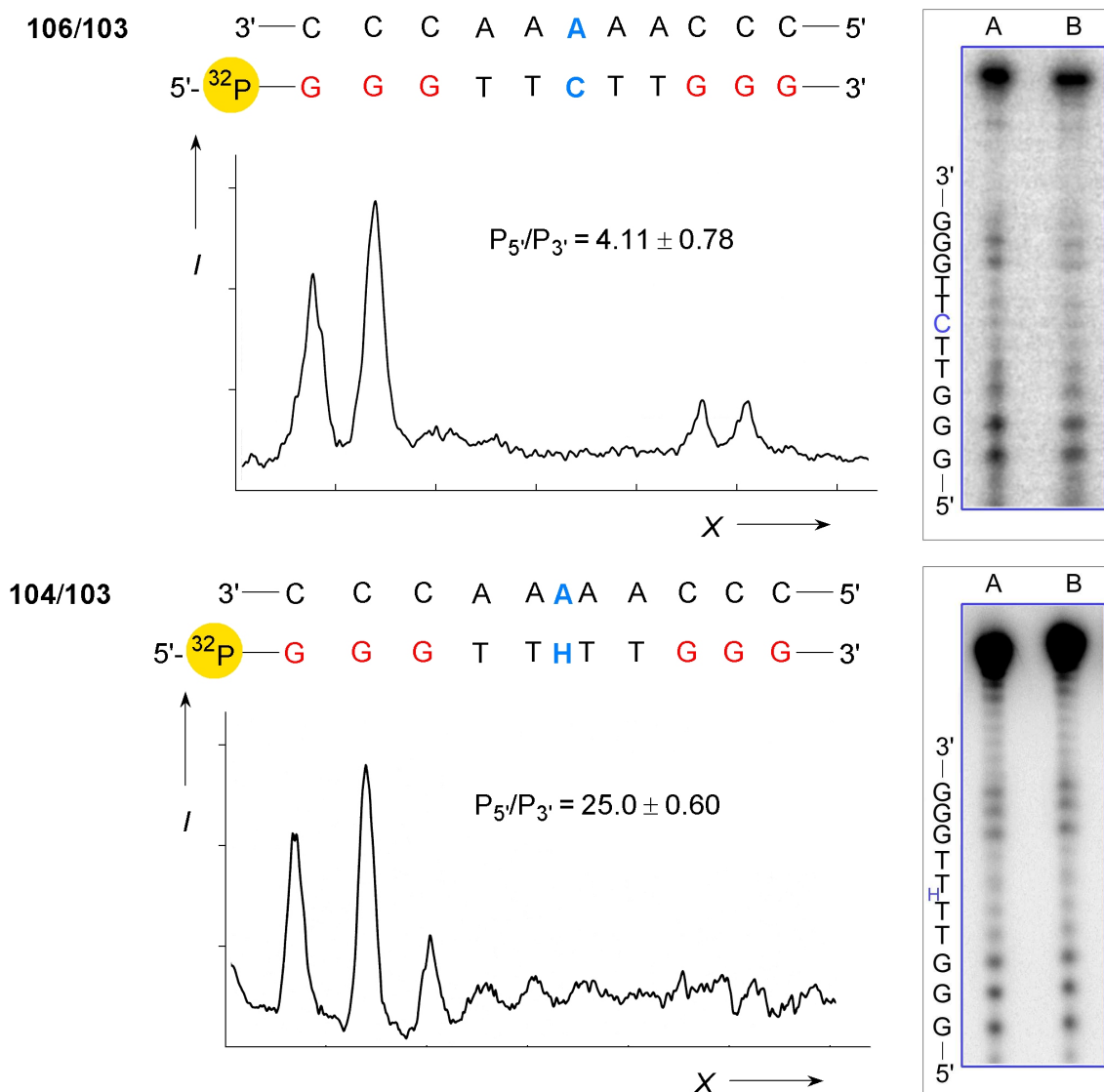
Figure 7.4. (left) PAGE histograms obtained after subtraction of the blind experiments for A−C (top) and abasic site (bottom) mismatches. (right) Autoradiograms of the gel electrophoreses, obtained after photolyses of duplex DNA at pH 5.0 and subsequent piperidine cleavage. Lanes A, experiments **106/103** (top) and **104/103** (bottom), lanes B, blind experiments **106/102** (top) and **104/102** (bottom). Note that the reduced abasic site is not cleaved by piperidine and thus does not produce any signal in the PAGE separation.

Considering the A−A mismatch, where no effect on the yield ratio is observed, we can assume that the deprotonation of A$^{•+}$ towards the mismatched A constitutes a rapid equilibrium and does not lead to charge loss. Similar observations for A−A mismatches were also made by *Giese*[130] and Schuster.[131] NMR studies by *Gervais*[132] demonstrated that an A−A mismatch as well as a T−T mismatch impose little structural change in the duplex. Both mispairs are well integrated in a B-DNA helix, and no change in conformation was observed between pH 4.7 and 9. The exchange with solvent is reported not to be enhanced by the presence of an A−A mismatch, but the bases around a T−T mismatch are reported to show enhanced exchange with bulk solvent. The A−A wobble-type base pair is postulated to adopt positions similar to those in A−T base pairs and is able to establish only one hydrogen bond, with two pseudo-symmetrical possibilities (*Figure 7.5a*).

The imino protons of the T−T wobble base pair are postulated to lie in an approximately symmetrical position about the helix axis, switching between two pseudo-symmetrical wobble-type structures with one hydrogen bond in a fairly rapid equilibrium (*Figure 7.5b*).
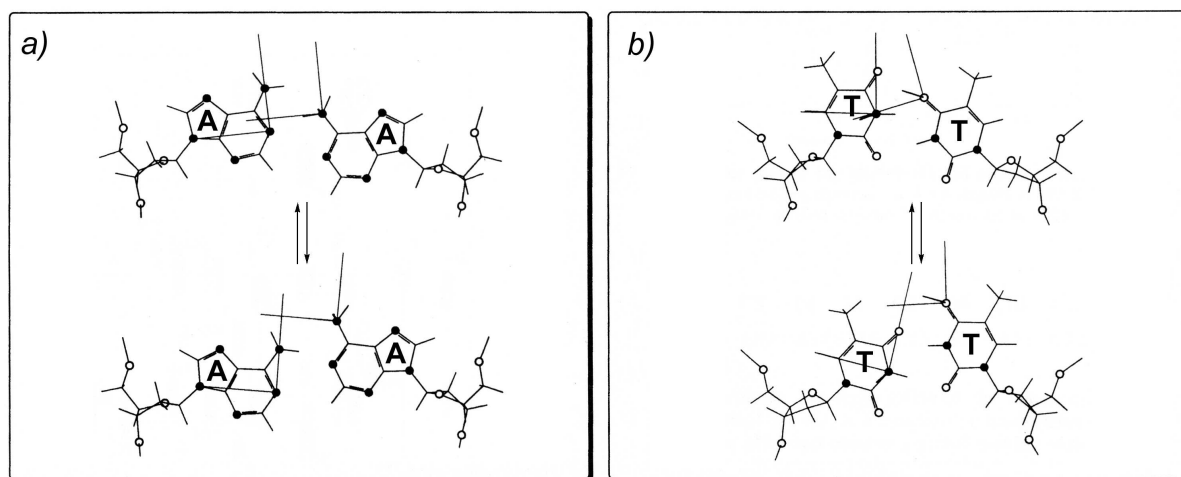
Figure 7.5. *Possible wobble structures for a) the A−A mismatch, and b) the T−T mismatch*[132]

Thus, the lower charge transfer efficiency through the T−T mismatch may be explained by the destabilization of adjacent bases, which is also reflected in the lower melting temperature of

the duplex containing the T−T mismatch. Compared to the situation with A−A, which is furthermore favourable to charge transfer by a mainly unaffected purine base stack,[132] the charge must tunnel through the T−T bridge in order to reach the second GGG unit.[131]

A somewhat different situation is implied by the A−C mismatch, which may be explained by the structural changes caused by this modification. *Brown*[133] determined the X-ray structure of an oligomer containing two isolated A−C mismatches (*Figure 7.6*).
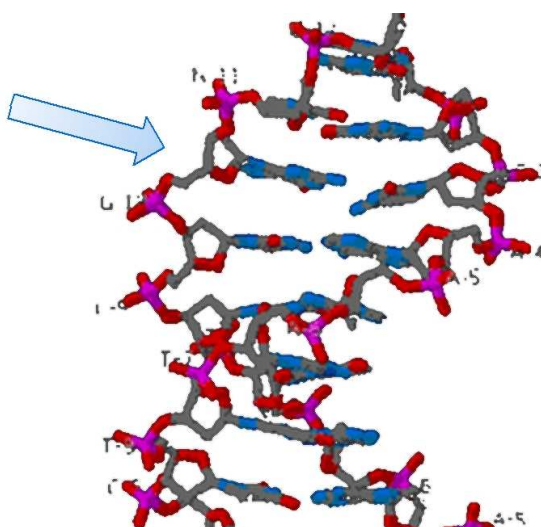
Figure 7.6. *Excerpt from the X-ray structure of an A-C mismatch within an oligonucleotide duplex. The mismatch is the third base pair from top (arrow).*[133]

Although essentially neither the B-DNA structure nor the base stacking is affected by this mispair, *Brown* located well-defined water molecules bridging the A−C pair in the major groove. Such pre-organized water molecules may constitute a pathway for a rapid hydrolytical loss of a positive charge from the A−C mispair. The N^1-position of adenine is likely to be protonated under physiological conditions with the consequent formation of a second hydrogen bond of the A-C base pair (*Figure 7.7*).[133,134]
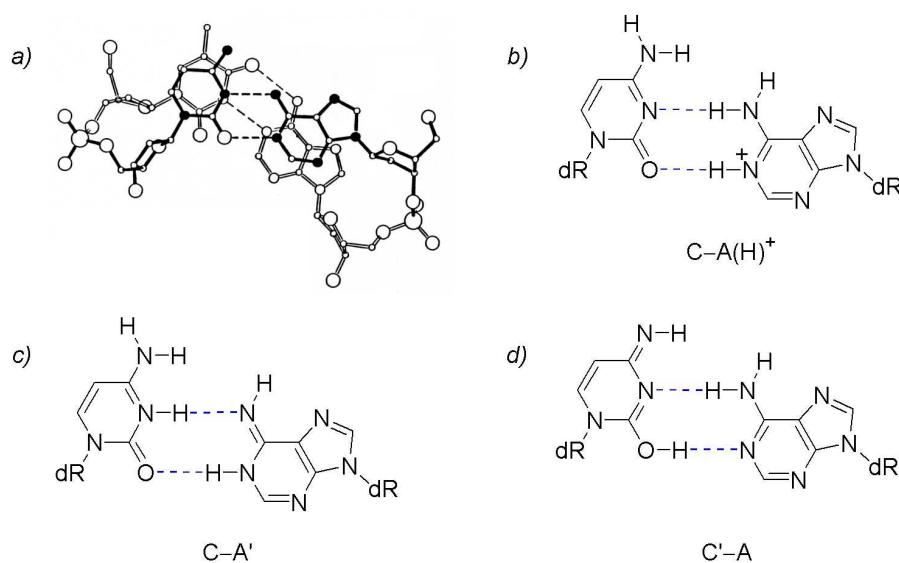
Figure 7.7. *a) and b) X-ray structure and model for the A−C mismatch in duplex DNA, c) and d) alternative hydrogen-bonding schemes for the A−C base pair involving rare tautomeric forms (marked by a prime) of the bases, although their significance is rather unlikely due to high energy of tautomerization.[133]*

The low charge transfer efficiency through the A−C mismatch is in accordance with experiments by *Barton*,[135] which provided equally low charge transfer efficiencies for any cytosine-containing mismatches. Such closed hydrogen bonds are known to confer additional stabilization.[3] *Steenken*[119] determined an equilibrium constant K_a of $10^{3.3}$ for the proton shift reaction $A^{\bullet+} + C \rightarrow A(-H)^{\bullet} + C(H)^{+}$, but an electron transfer from a protonated adenine to an adjacent adenine radical cation is not likely in this case. In conclusion, the drop in charge transfer efficiency caused by the A−C mismatch results from the combination of minor structural changes in the DNA duplex and major changes in the hydrogen-bonding properties.

7.4   Proton Transfer from the Adenine Radical Cation

Introduction of an abasic site, leaving the central adenine unpaired, efficiently suppresses any charge transport to the distant GGG unit (*Figure 7.4*, bottom) in DNA duplex **104/103**. We have already seen that adenine radical cation **85** is a rather strong acid ($pK_a \leq 1$) which can readily deprotonate and form neutral radical **86** if the base itself is either accessible for water molecules or forming a mismatch enabling proton transfer (*Scheme 7.2*).[136]

Scheme 7.2
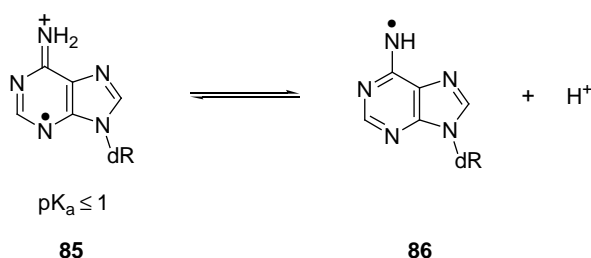
In G-hopping experiments, *Giese*[130] observed a decrease in charge transfer efficiency when an abasic site was located opposite a guanine. This decrease was avoided when the unpaired guanine was methylated and thus not able to deprotonate any more. *Bolton*[137] determined the NMR structure of a DNA duplex containing an abasic site within an (A−T)$_n$ domain. The unpaired adenine opposite the abasic site remained stacked,[138] but the curvature of the undamaged DNA (see *Chapter 8*) originating in the poly(A) domain was lost due to the presence of the abasic site. The structural continuity is disrupted giving rise to bending in the parent, undamaged DNA. The accessible surfaces of this DNA duplex were calculated with a probe radius of 1.4 Å and revealed (essentially for the β-structure) increased accessibility up to two base pairs away from the damaged site. The view from the minor groove shows that the β form contains both the abasic site and the opposing adenine residue in considerably more accessible positions than in the α form (*Figure 7.8*).[137]
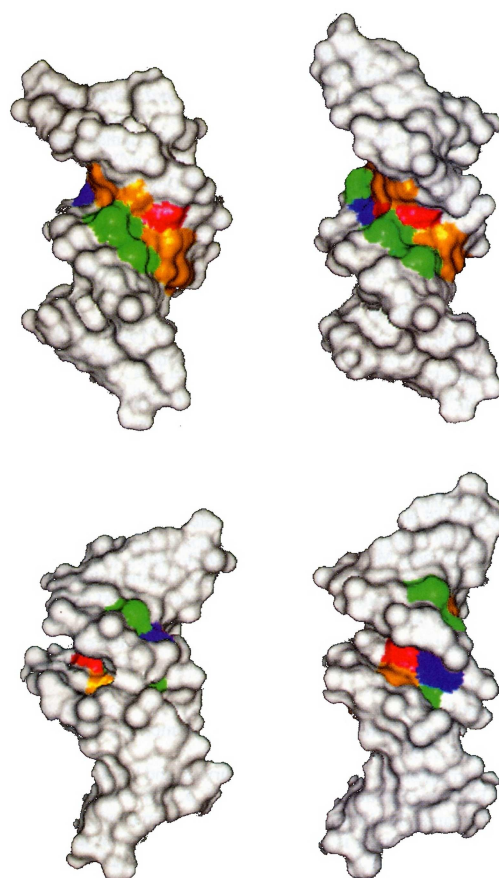
Figure 7.8. *The accessible surfaces of the α (left) and β (right) forms of the DNA duplex are viewed from the major groove (top) and the minor groove (bottom). The accessible surface is the surface calculated with a probe radius of 1.4 Å. The abasic deoxyribose hemiacetal is shown in blue, and the adenine opposite the abasic site in red. Further adenines are shown in orange and thymines are shown in green.*[137]

Other studies mention a water molecule that is postulated to occupy the gap in front of the unpaired adenine, forming hydrogen bonds between adenine and the anomeric hydroxy group of the abasic site.[139] However, the presence of this well-orientated water molecule cannot be assumed in case of a reduced abasic site. In the case of the reduced abasic site within a $(A-T)_5$ domain and leaving one adenine unpaired, we can conclude that:

a) the solvent accessibility of several base pairs neighbouring the damaged site and essentially including the gap in front of the unpaired adenine, is increased,

b) the curvature of the poly(A) domain is disrupted,

c) the adenine radical cation opposite the abasic site can readily deprotonate and thus lose its charge.

7.5 Summary

The results with long $(A-T)_n$ sequences have shown that the charge must be already partially equilibrated over the DNA sequence before being trapped by water. Thus, the weak distance effect is caused not only by the rate of the hole transport but also by the partial thermodynamic charge equilibration over the $(A-T)_n$ sequence. In order to rationalize this distance-independent efficiency, one has to assume that the rate of the charge hopping over the $(A-T)_n$ sequence depends only weakly on n. To determine the influence of the $(A-T)_n$ sequence on the hole transfer rate alone, a new assay must be found in which the trapping of the radical cation is faster than the hole transfer between guanines.

The introduction of several structural damages, including a reduced abasic site, into DNA duplexes revealed that the charge transport over long $(A-T)_n$ sequences, which is hardly distance-dependent in case for undamaged DNA, is sensitively dependent on an undisturbed structure of the DNA duplex.

Whereas a reversible proton shift from guanine radical cation to cytidine is energetically favoured and stabilizing the base pair,[140] a proton shift from the adenine radical cation to thymine is not feasible.[119b] Contrary to this, protonation of adenine increases the oxidation potential of the base, and deprotonation of the adenine radical cation leads to charge loss, resulting in a decrease or suppression of charge transfer in both cases.

8 Abnormal Distance Effects in Long (A–T)$_n$ Sequences

8.1 Introduction

The structure of a DNA duplex containing poly(A)–poly(T) homopolymers ("A-tracts") implies a close relationship to a canonical B-DNA structure but contains some intrinsic structural differences. Other DNAs of natural origin or the analogous poly(A–T) with alternating sequence, all show around 10.5 ± 0.1 base pairs per turn in aqueous solution but the A-tract duplex displays 10.1 ± 0.1 base pairs per turn. Due to the differences in its helicity, the B-DNA-like structure of poly(A)–poly(T) was called B'-DNA (*Figure 8.1*).[7]
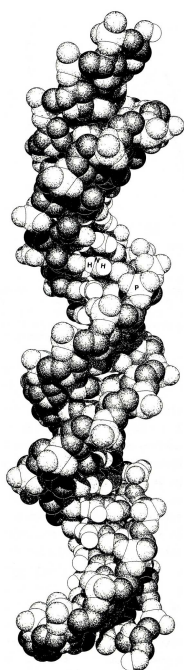
Its difference from DNAs with alternating or random distributions of bases is also evident from its resistance to transform into other helical forms, its peculiar CD spectra, and its inability to form reconstituted nucleosomes when combined with histone octamers.[3]

Figure 8.1. A space-filling structure of B'-DNA, calculated from a x-ray structure.[141] The B'-DNA features a deep, narrow minor groove, and a slightly narrowed, shallow major groove. The pitch (distance between two base pairs) is 3.2 Å for B'-DNA, in contrast to normal B-DNA, which has a pitch of 3.4 Å.

DNA molecules which contain an A-tract, or multiple A-tracts phased with respect to the helical twist of DNA, contain a significant bend in their helical axis.[142] The relationship between A-tract crystal structures and solution state studies of DNA curvature has remained controversial,[143] although several structural properties of A-tracts have been resolved, *e.g.*

high propeller twist of base pairs, a narrow minor groove and a helix pitch reduced by 0.2 Å.[144-146] There is a clear consensus about the two probable origins of helix bending by A-tracts by a) selective binding of monovalent cations to the A-tracts in the minor groove of the DNA duplex in solution, and b) the aprupt change in propeller twist at the ends of the A-tract, which forces the helix axis to bend.[147,148]

The high propeller twist of the base pairs inside the A-tract enables an enhanced base stacking. The adenine and thymine bases tend to stack in an partially eclipsed conformation (six-membered ring over six-membered ring, *Figure 8.2*) whereas the guanines in poly(G)-poly(C) tend to stack in a staggered fashion (six-membered ring over five-membered ring) and the cytosines show no overlap.[149]
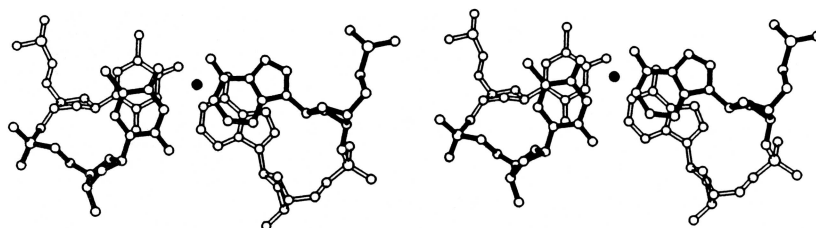
Figure 8.2. Stereo views of a typical AA−TT base step. The two base pairs, the upper in black and the lower in white, are viewed down the helix axis (illustrated by a black circle).[144]

In the context of the structural peculiarity of A-tracts and in particular its improved base stack, the effect of these structural effects on long-distance charge transfer over A-tracts was studied.

8.2   Adenine Stacking Enhances Charge Transfer

Charge transfer experiments by *Barton*[79] with long (A−T)ₙ sequences showed that yields of damage at a distant GG unit increased with the length of the intervening (A−T)ₙ bridge and

was interpreted to be due to the conformational dynamics and extensive purine stacking associated with these sequences. Unfortunately, these experiments lacked appropriate blind experiments under identical experimental conditions. We have synthesized DNA duplex **115**/**114** (*Scheme 8.1*), containing an (A–T)$_{12}$ bridge, which was subjected to photolysis and piperidine treatment with subsequent PAGE analysis.

Scheme 8.1

115/114
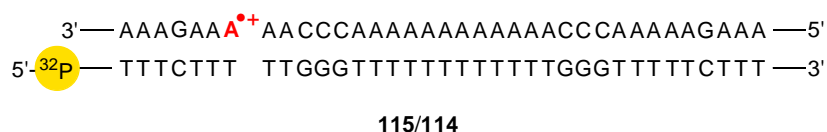
Surprisingly, a yield ratio (P$_{5'}$/P$_{3'}$ = 1.49 ± 0.09) nearly equal to the result for the (A–T)$_5$ system (P$_{5'}$/P$_{3'}$ = 1.80 ± 0.36) was obtained, taking the experimental error limits into account (*Figure 8.3*).
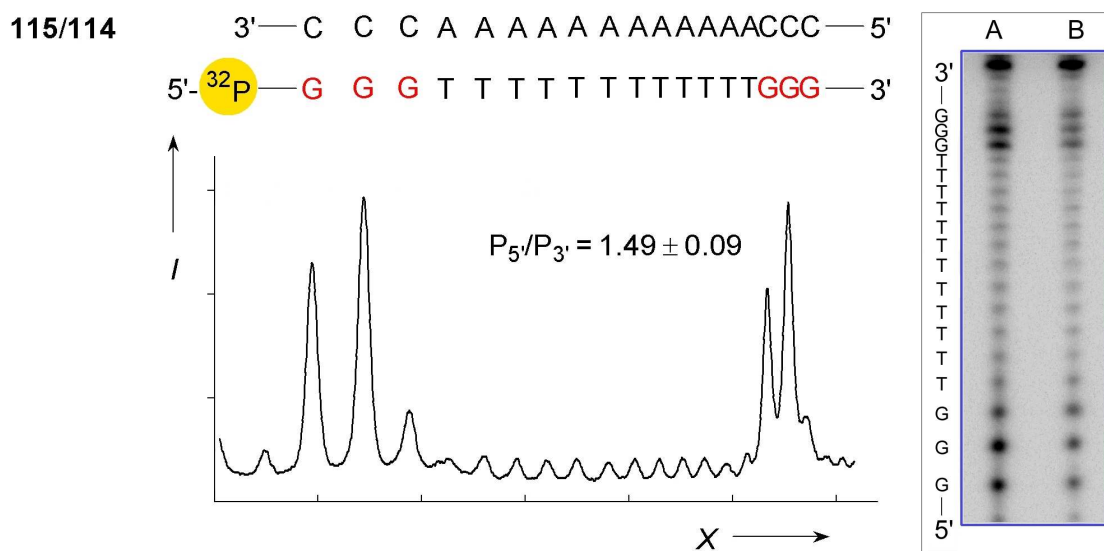
***Figure 8.3.** (left) PAGE histogram obtained after subtraction of the blind experiments for intrastrand A-hopping (n=12). (right) Autoradiogram of the gel electrophoresis, obtained after photolysis of duplex DNA at pH 5.0 and subsequent piperidine cleavage. Lane A, experiment **115/114**, lane B, blind experiment **115/116**.*

This experiment has impressively shown that $(A-T)_n$ sequences are capable of a nearly distance-independent charge transfer over long distances especially when the nucleating core contains at least four to five adenines. [144] They are only capable of charge transfer if the A-tract is not disrupted by alternating A−T pairs, structural damages or intervening G−C pairs[79] that decrease the charge transfer efficiency. Introduction of adenine analogs with increased stacking area and lowered oxidation potentials were found to enhance the long-distance charge transfer efficiency up to complete charge equilibration.[150]

8.3   Summary

The synthesis and study of the long-range charge transfer in a DNA duplex containing an $(A-T)_{12}$ domain was performed. The resulting charge transport over the A-tract proceeded with an efficiency nearly equal to the result obtained for a shorter $(A-T)_5$ sequence.

The result was explained by the intrinsic structural abnormailties of poly(A)−poly(T) homopolymers, which imply a significantly better stacking of both the purine and pyrimidine bases inside the A-tract. The distance between base pairs (pitch) is reduced by 0.2 Å, compared to canonical B-DNA, and the A−T pairs stack in a partially eclipsed fashion, whereas G−C pairs and base pairs inside random sequences tend to stack in a staggered manner.

These results underscore the complex role of sequence dependent structure and dynamics in DNA-mediated charge transfer. Certainly the observations cannot be rationalized by models in which holes hop along guanines *via* superexchange through short A−T bridges.[27,151] Nor are the results consistent with a "zig-zag" mechanism involving indiscriminate intra- and interstrand migration that is not influenced by the A−T base orientation.[27,65] The unexpectedly high charge transfer efficiency is attributed to the formation of transient, well-coupled conformations, distinct from canonical B-DNA.

9 Summary of the Work and Outlook

9.1 Summary

For the purposes of site-selective charge injection into guanine-free DNA, a new synthetic route towards a 4'-pivaloylated adenosine derivative was developped, enabling the study of long-range charge transfer in DNA. The synthesis of 4'-pivaloylated adenosine **46** succeeded in 0.5% yield over 10 steps, providing a DNA-synthesizer compatible building block.

Photolysis of single- or double-stranded 29mer **103** demonstrated that the generated ribose radical cation is most efficiently reduced by electron transfer from adenine at pH 5.0 in 20 % absolute yield. This process yields an adenine radical cation and thus promotes a positive charge into the DNA base stack.

Experiments with DNAs containing long guanine-free sequences have shown that, once the positive charge is injected into an $(A-T)_n$ sequence, a rapid and distance-independent charge transfer mechanism involving adenines as charge carriers is established. A guanine-hopping mechanism[27,151] was excluded due to lack of guanines in these DNAs. Instead, a partial thermodynamic charge distribution was observed.

The apparently highly-efficient charge transport over long $(A-T)_n$ sequences was shown to be easily disrupted by structural changes in the base-pairing. This was studied by introduction of a series of base mismatches and an abasic site opposite an adenine. Higher solvent accessibility of the damaged sites accounted for deprotonation and thus charge loss from the acidic adenine radical cation. Protonation of adenine inside an A−C wobble base pair also decreased the charge transfer efficiency.

The abnormal structural changes found in A-tracts of duplex DNA were shown to increase the charge transfer efficiency over long $(A-T)_n$ sequences as they imply an improved DNA duplex structure providing a higher stacking area and shorter base-base distances.

This work has shown that, although the field of charge transfer over long $(A-T)_n$ sequences is new and little understood, the charge transport mechanism is thought to be a rapid, multistep process involving adenines as charge carrier where the charge may hop from adenine to adenine or may be delocalized in polaron-like species.

9.2   Outlook

Some decades ago, no scientist would have expected radical reactions to proceed in the watery, buffered environment of biological systems in a rapid and highly selective manner. The unique ability to establish precise redox equilibria depending on the pH and to perform chemical conversions at non-activated sites are the reasons why nature applies radical chemistry.

Essentially, charge transfer chains in biological systems are not optimized for maximum speed but for maximum robustness, as they proceed much faster than the enzymatic turnover rate.[55] For example, the enzyme ribonucleotide reductase (RNR) catalyses the reduction of the 2'-hydroxy group of ribonucleotides to provide the essential DNA building blocks, the deoxyribonucleotides (*Scheme 9.1*).[152,153]

Scheme 9.1
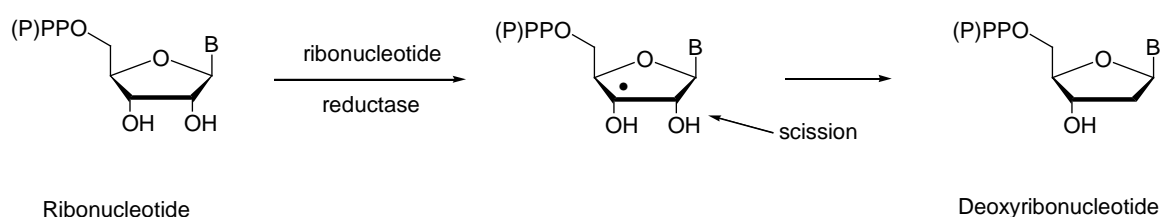
In biological systems, charge transfer processes are essentially coupled to proton transfer ("proton-coupled electron transfer", PCET), thus providing a way to modulate the redox properties of the charge transfer system.[55]

Inside RNRs, the electron is "stored" as a stable tyrosyl radical and for the catalytic reaction it is transferred over 35 Å from one subunit to another, involving a redox cascade of tunneling and thermally activated charge transfer steps (*Figure 9.1*).
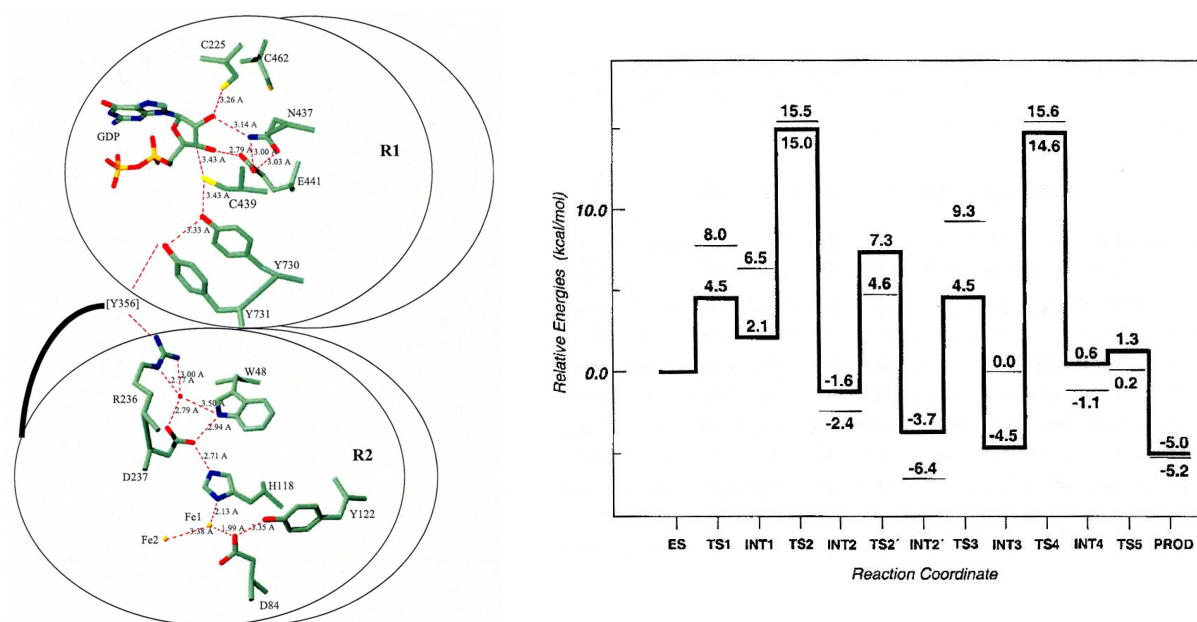
Figure 9.1. *(left) The charge transfer pathway in a Class I RNR, involving several intermediary tyrosyl and cysteyl radicals in subunits R1 and R2.[153] (right) A calculated energy diagram for the redox cascade.[154]*

Studying the molecular charge transfer mechanisms in DNA and proteins is the direct pathway to a deeper understanding of molecular recognition, catalysis and energy conversion.

Experimental Part

10 Devices and Materials used for this Work

10.1 Reaction Instruments

Photolysis Setup

Device: *Oriel 68810* photolysis stand equipped with an *Osram HBO 500 W/2 L2* high-pressure mercury arc lamp and 320 nm lowpass filter (2 mm thick) by *Schott* (*WG-320*). The device used was further equipped with an *Oriel 6123* IR cutoff filter and a thermostatically cooled sample holder. At given wavelength light transmittance is about 50%. The UV light was focused to the centre of the sample holder using an additional *Schott UG-1* UV bandpass filter and a test cuvette containing a) a solution of umbelliferone in 0.1 M sodium citrate buffer at pH 3.0, or b) a sample of bright-white paper, which both show visible fluorescence when excited at 325 nm. *Figure 10.1* shows the photolysis device, and *Figure 10.2* shows the un-filtered spectrum of the mercury arc lamp.
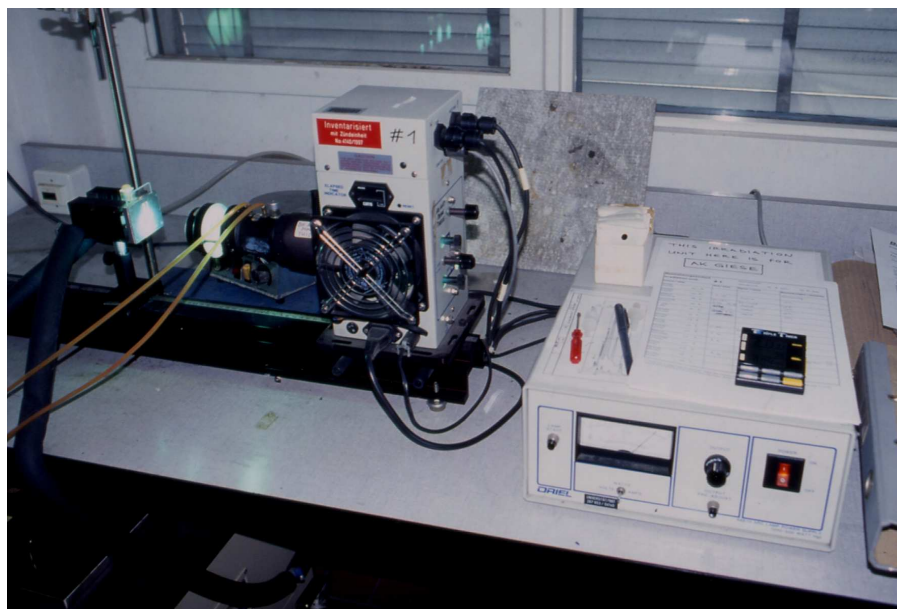
Figure 10.1. *Photolysis Device*
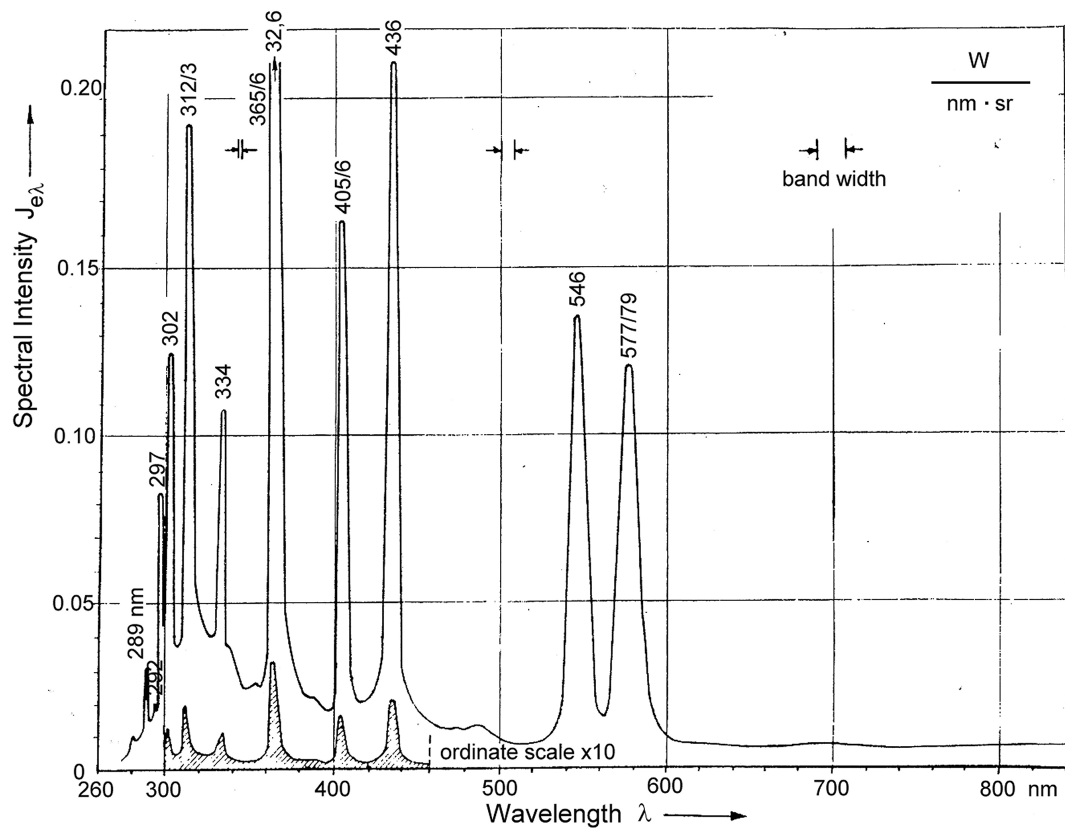
Figure 10.2. *Lamp spectrum*

Figure 10.3 shows the efficiency of the thermostated sample holder, measured under experimental conditions. This device ensures that annealed complementary DNA strands will never denature under the photolysis conditions.
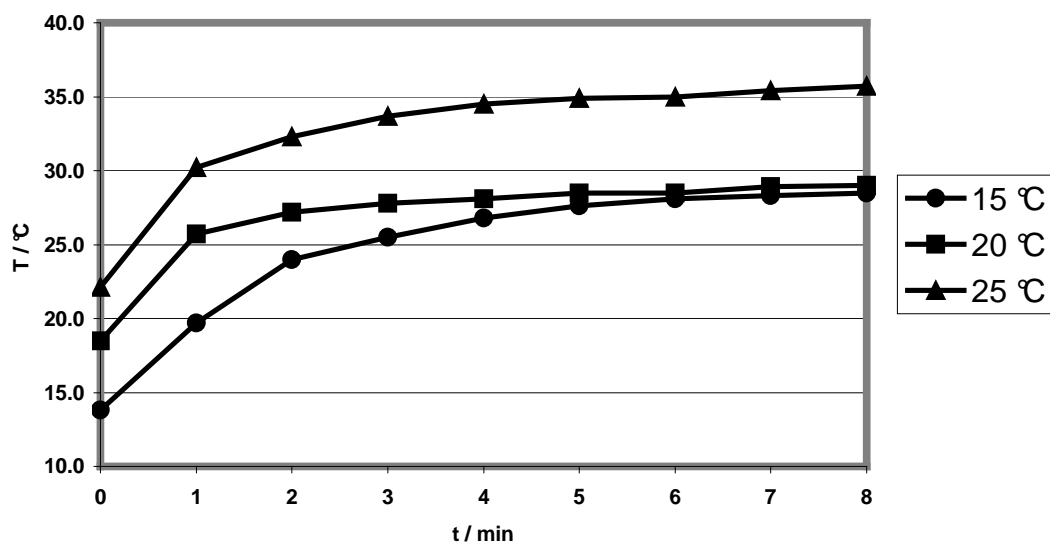
Figure 10.3. *Course of temperature inside the cuvette during irradiation*

Nucleic Acid Synthesizer

Device: *PerSeptive Biosystems Expedite 8909* nucleic acid synthesis system. The DNA synthesis related chemicals were supplied by *Glen Research*.

10.2 Physical Data

[1H] NMR spectroscopy

Devices: *Varian Gemini 300* (300 MHz), *Bruker dpx400* (400 MHz). Chemical shifts (δ) are indicated in ppm, relative to $SiMe_4$ ($\delta = 0.00$) or based on the solvent signals of the partially deuterated nuclei of chloroform-d_1 ($\delta = 7.26$) or dimethyl sulfoxide-d_6 ($\delta = 2.50$). All spectra are interpreted by first order, and the coupling constants (J) are given in Hertz (Hz). Split signals featuring defined multiplicity were characterized by the arithmetic mean of the signal lines. Free hydroxy groups are assigned by proton-deuterium exchange due to addition of

D_2O. The signals were abbreviated as follows: s = singlet, br. s = broad singlet, d = doublet, t = triplet, q = quartet, *quint.* = quintet, m = multiplet. NOE mesaurements were designated as follows (irradiated H → affected H): ++ = strong, + = medium, (+) = weak.

^{13}C NMR spectroscopy

Devices: *Varian Gemini 300* (75.5 MHz), *Bruker dpx400* (101.0 MHz). Chemical shifts (δ) are indicated in ppm and are relative to the following solvent signals: chloroform-d_1 (δ = 77.0) or dimethyl sulfoxide-d_6 (δ = 39.5). The spectra are broad-band proton decoupled, the classification of the signals was achieved by APT or DEPT.

^{31}P NMR spectroscopy

Devices: *Varian Gemini 300* (121.0 MHz), *Bruker dpx400* (162.0 MHz). Chemical shifts (δ) are indicated in ppm and are relative to the spectra reference of an external standard of 58% triphenylphosphate in chloroform (δ = −18). The spectra are broad-band proton decoupled.

Numbering of the nuclei

The protons in the ^{1}H NMR spectra are numbered with the same numbers as the related carbon atoms. Atoms within the sugar backbone are marked by an additional prime. If geminal hydrogen atoms show two distinguished signals, the high-field and the low-field shifted nuclei are told apart by an additional "a" or "b", respectively. *Scheme 10.1* demonstrates the numbering of the atoms in 2'-deoxyadenosine.

Scheme 10.1
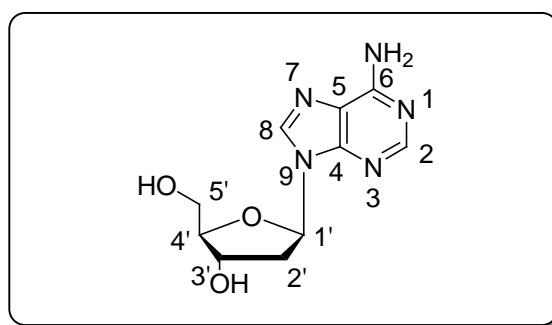
Infrared Spectroscopy (IR)

Device: *Perkin-Elmer 1600 FT-IR*. The bands are given in wavenumbers ($\tilde{\nu}/\,\mathrm{cm}^{-1}$). The spectra were acquired by addition of four single spectra, followed by subtraction of the background spectrum. Liquids and oils were measured as thin film between two sodium chloride plates, solids as potassium bromide pressings.

UV-VIS Spectroscopy

Device: *Perkin-Elmer Bio-Lambda II* spectrophotometer, featuring a *PTP-6* peltier unit. Micromolar extinction coefficients (ε_{mM}) of oligonucleotides are referred to a cell path of 1 cm at 260 nm.

Mass Spectrometry (FAB-MS)

Devices: *VG70-250* and *Finnigan MAT 312* mass spectrometers. Measurements were carried out by Dr. H. Nadig at the institute for organic Chemistry at the University of Basel. The ion generation resulted via fast-atom bombardment (FAB) using xenon atoms and 3-nitrobenzyl

alcohol as matrix and sodium chloride as additive. The data are given in mass units per charge (m/z). The spectra were recorded each with and without addition of potassium chloride.

Electrospray Mass Spectrometry (ESI-MS)

Device: *Finnigan MAT LCQ*, octapole mass spectrometer. The samples were directy injected as 0.1 mg/ml solutions in methanol. The ion source worked via electron ionization. The data are given in mass units per charge (m/z).

MALDI-TOF Mass Spectrometry (matrix-assisted laser desorption ionization time-of-flight)

Devices: *Vestec Voyager Elite* and *PerSeptive Biosystems Voyager-DE PRO*. The spectrometers were run in linear mode at 25 kV acceleration voltage for negative ions. 2,4-Dihydroxyacetophenone was used as a matrix. Probe desorption and ionization was induced by a N_2-LASER (337 nm, 3 ns pulses, 0.2 mJ per pulse, acquisition of 10 to 100 pulses). The signals are referred to the unfragmented, single negatively charged molecule ions $[M-H]^-$. The data are given in mass units per charge (m/z).

Elementary Analysis

Devices: *Leco CHN-900* (C, H, N detection), *Leco RO-478* (O detection). The elementary analyses were carried out by W. Kirsch at the institute for organic Chemistry at the University of Basel. The data are indicated in mass percents.

Melting Points

Devices: *Büchi 530* and *Hund Wetzlar V200*. The melting points are given in degrees centigrade [°C] and are uncorrected.

10.3 Separation and Purification Methods

Thin Layer Chromatography (TLC)

Merck silica gel *60 F_{254}* aluminium sheets (0.2 mm layer). The compounds were detected by two subsequent precedures:

1. fluorescence quenching detection at 254 nm,
2. dipping into a solution consisting of a) cerium(IV)sulfate tetrahydrate (10 g), b) ammonium heptamolybdate tetrahydrate (25 g), c) H_2O (900 ml), and d) conc. H_2SO_4 (100ml), followed by heating.

TLC retention factors (R_f) are indicated together with the appropriate solvent mixture in brackets.

Flash Column Chromatography (FC)

Flash column chromatography was performed under low pressure (~1.5 bar, membrane pump) on silica gel *Uetikon C560D* (40-63 μm, 230-400 mesh), or on silica gel *Merck 60* (40-63 μm, 230-400 mesh). The solvents were of technical grade and were re-distilled prior to use. The mixture ratios of solvents are referred to the parts of the volume.

High Performance Liquid Chromatography (HPLC)

Device: *Hewlett-Packard 1050* chromatograph with UV detection at 260 nm. Columns for reversed-phase HPLC: *Merck LiChroSpher 100* (RP-18e, 5 μm, 125 × 4 mm, Flow: 1.0 ml min^{-1}). As solvents were used acetonitrile 190 (*Romil*) and 0.1 M aqueous TEAA solution, puchased as 1.0 M stock solution (*Fluka*), diluted by 9 parts of nanopure water prior to use.

Ion Exchange Purification of Oligonucleotides

Mini-QuickSpin (Sephadex G-25, *F. Hoffmann−La Roche*) centrifuge columns for oligonucleotide purification were used following the enclosed procedure.

Polyacrylamide Gel Electrophoresis (PAGE)

Device: *Life Technologies Model 2* apparatus, equipped with a *Pharmacia Biotech EPS 3500* potentiostatic power unit. PAGE was performed in TBE buffer (0.1 M *Tris*-borate, pH 8.3; 2 mM EDTA) at 1500 V. Acrylamide/ bisacrylamide solution (*AccuGel*, 19:1, 40%) for gel preparation was provided by *National Diagnostics*.

10.4   Further Instruments

Centrifuge, Thermomixer and Vortexer

Devices: *Eppendorf 5415C* and *5415D* centrifuges. *Eppendorf 5436* thermomixer. *Bender & Hobein Vortex Genie 2*

Drying of DNA Containing Probes

Devices: *Savant Speed Vac Plus*, and *Eppendorf 5301*

Phosphorimager, Storage Phosphor Screens and Software

Device: *Molecular Dynamics Storm 840*. Storage phosphor screens of 35×43 cm size were provided by *Molecular Dynamics*. For quantification and visualization of the results, *Molecular Dynamics ImageQuant v5.2* and *Microsoft Excel 2000* software was used.

Scintillation Counter

Device: *Packard Tri-Carb 460 C* liquid scintillation counter. Solvent: *IrgaSafe Plus*, provided by *Zinsser Analytic*.

10.5   Solvents, Chemicals, Enzymes and Miscellaneous

Solvents

Technical grade solvents for extraction and flash column chromatography were distilled prior to use. HPLC grade solvents, provided by *Fluka*, *Romil*, *Mächler* and *J.T.Baker*, were used for flash column chromatography (acetone, ethyl acetate) and for water-containing reactions. For all other reactions in water-free environment, or for analytic purposes, absolute solvents from *Fluka* were used without further purification. The absolute THF, 1,4-dioxane and diethyl ether used for reactions still contained their chemical stabilizers.

Chemicals

2'-deoxyadenosine was purchased from *Pharma Waldhof*. Chemicals for DNA synthesis were provided by *Glen Research*. Sodium citrate and sodium phosphate buffer solutions (HPCE grade), and TEAA (1 M) stock solutions were obtained from *Fluka*. All other chemicals were provided by *Fluka*, *Aldrich* and *Acros* and were of the highest grade available.

Enzymes

T_4 polynucleotide kinase (10 000 units ml^{-1}) was provided by *New England Biolabs*.

Miscellaneous

DNA containing probes were handled using disposable 1.5 ml PE snap-cap tubes from *Treff-Lab* and screw-cap tubes from *Brand*. *Mini-QuickSpin* (Sephadex G-25) columns for oligonucleotide purification were provided from *F. Hoffmann−La Roche*. Disposable PMMA cuvettes for photolyses and optical-density measurements were purchased from *Semadeni*; their optical properties are shown below (*Figure 10.4*).
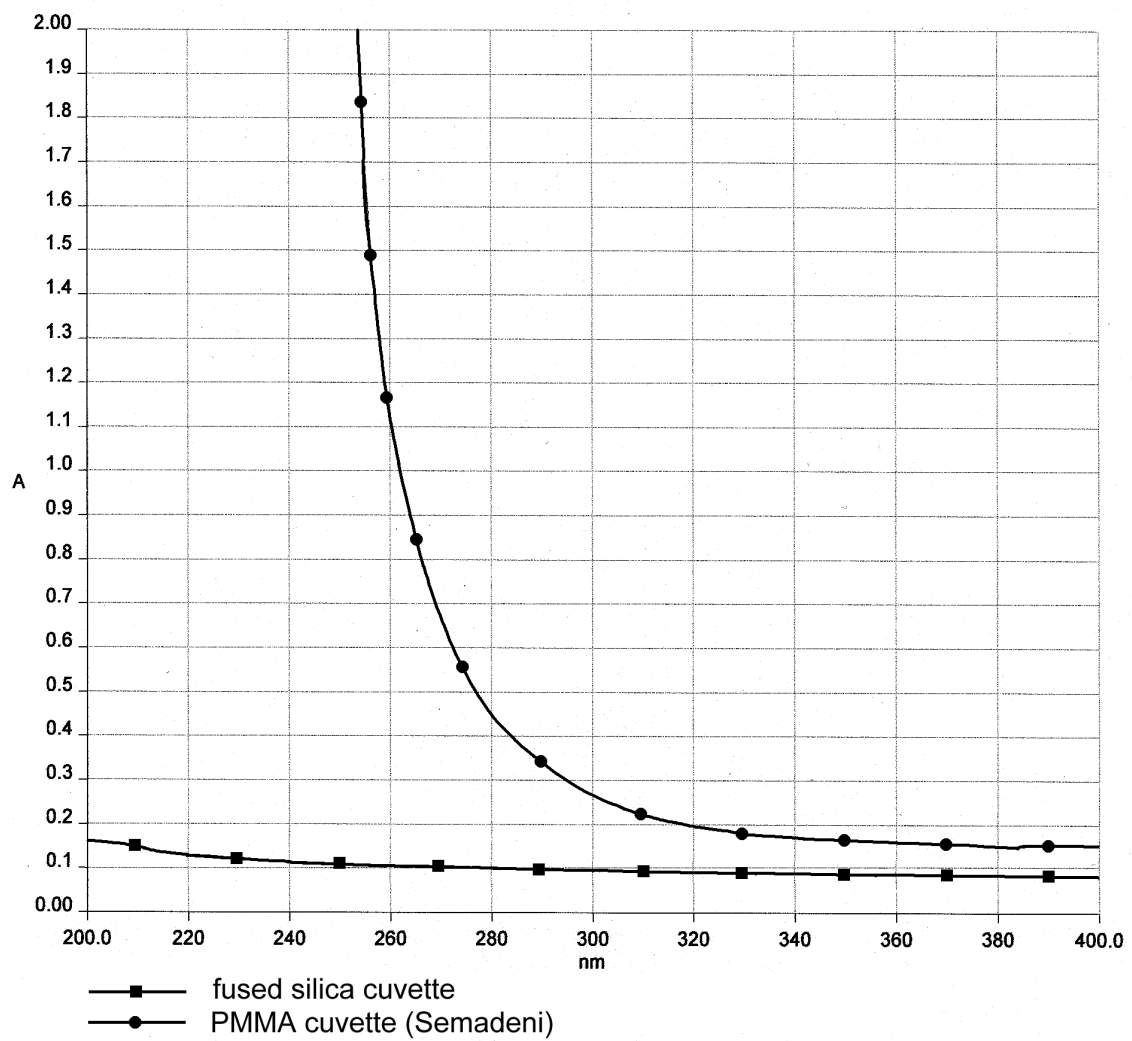
Figure 10.4. *Optical properties of a disposable PMMA cuvette. At 320 nm, the PMMA cuvette features about 50% of the transmittance of a fused silica cuvette.*

11   General Synthetic Procedures

11.1   Syntheses

All reactions were carried out in standard laboratory glassware of appropriate dimension, which was vacuum-dried at 300 °C and flushed with argon prior to use. All reactions at ambient pressure were performed under argon atmosphere.

11.2   Reversed-Phase HPLC

Generally, reversed-phase columns provided by *Merck* (*LiChroSpher* 100-5, RP-18e, 250×4 mm, Flow 1.0 ml min^{-1}) were used. Solvent A: 0.1 M triethylammonium acetate buffer (TEAA) at pH 7; Solvent B: acetonitrile 190.

For separation of oligonucleotides an acetonitrile gradient was applied, whereas detection was achieved by UV absorption at 260 nm. Most of the tritylated oligonucleotides elute at an acetonitrile fraction range between about 25% and 30%. Oligonucleotides without trityl protection group generally elute at less than 15% acetonitrile fraction. In order to avoid aggregation effects, the column temperature was always set to 55 °C.

11.3   Formation of Double-Stranded DNA

Equal amounts (0.2 nmol) of the complementary single strands were dissolved in 1.0 ml of buffer solution (pH 5.0, 20 mM sodium citrate, 100 mM NaCl), heated to 75 °C for 5 min, and then cooled to r.t. over 2 h to provide a clean annealing.

11.4   Quantification of Oligonucleotides via UV Absorption

Firstly, the micromolar extinction coefficients at 254 nm ($\varepsilon_{\mu M, 254}$) of the oligonucleotides were calculated according to a standard incremental method, which applies the following empirical equation (Eq. 11-1): [116,155]

$$\varepsilon_{\mu M,\ 254} = \{\ (8.8 \times nT) + (7.3 \times nC) + (11.7 \times nG) + (15.4 \times nA)\ \} \times 0.9 \qquad (11\text{-}1)$$

Secondly, the absorption at 254 nm of the corresponding aqueous oligonucleotide solutions was determined using an UV-transparent PMMA cuvette (d = 1.0 cm), and the amount calculated applying the Beer-Lambert law.

11.5   Photolyses

Irradiations of single- or double-stranded DNA were performed in disposable 1.5 ml PMMA cuvettes provided by *Semadeni*. As long as not otherwise indicated, irradiations were performed in citrate buffer (pH 5.0, 20 mM sodium citrate, 100 mM NaCl). Prior to irradiation, the solutions were degassed with argon 57 for 6 min. During irradiation, the argon flow through the cuvettes was sustained.

The cuvettes were thermostated to 20 °C, which limited the warming of the solution to below 30 °C during irradiation.

11.6   Mass Determination of Oligonucleotides

Probes which contained salts were de-salted by RP-HPLC prior to mass determination. A solution of the analyte (1.0 µl) was mixed on the sample plate together with matrix solution (1.0 µl, 0.5 M 2,4-dihydroxyacetophenone and 0.3 M ammonium tartrate in 3:1

water/acetonitrile) and crystallized. Synthetic and natural oligonucleotides with known mass within the same range as the probes were used as internal or external calibration of the spectrometer devices.

12 Synthesis of the 4'-Pivaloyl Modified Adenosine for Introduction into Oligonucleotides

12.1 3'-*O*-, 5'-*O*-Bis[(*tert*-butyl)dimethylsilyl]-2'-deoxyadenosine (68)
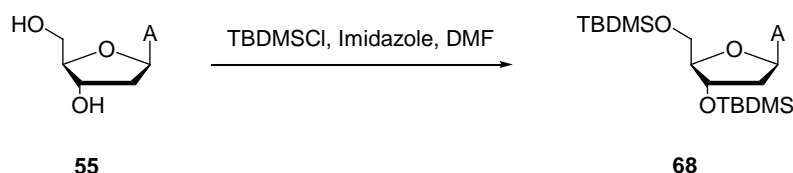
A solution of 2'-deoxyadenosine (**55**) (10.0 g, 39.8 mmol), 1*H*-imidazole (17.9 g, 263 mmol, 6.6 equiv.) and *t*-butyl-dimethylchlorosilane (19.1 g, 127 mmol, 3.2 equiv.) in anhydrous DMF (80 ml) was stirred overnight at r.t. The reaction was quenched by addition of MeOH (20 ml), and the solvent was removed *in vacuo*. The residue was dissolved in a mixture of CH_2Cl_2 (400 ml) and 0.3 M aqueous tartaric-acid solution (600 ml), and extracted with CH_2Cl_2 (2 × 300 ml). The combined organic phases were dried ($MgSO_4$), filtered, and concentrated under reduced pressure. The residue (colourless oil that tends to crystallize) was co-evaporated with toluene (2 × 15 ml) to yield crude **68** (18.9 g, 99%) as an off-white solid. This crude product was of sufficient purity for the subsequent synthetic steps. Further purification for analytical purposes was achieved by recrystallization from hexane which yielded pure **68** (14.0 g, 74%) as a white solid.

TLC:

$R_f = 0.42$ (AcOEt).

M.p.:

135°

¹H-NMR (300 MHz, CDCl₃):

8.35 (*s*, H–C(2)); 8.15 (*s*, H–C(8)); 6.45 (*t*-like, J = 6.4, H–C(1')); 5.81 (br. *s*, NH₂); 4.63–4.59 (*m*, H–C(3')); 4.01 (*q*-like, J = 3.4, H–C(4')); 3.87 (*dd*, J = 4.1, 11.2 Hz, H$_a$–C(5')); 3.77 (*dd*, J = 3.2, 11.3, H$_b$–C(5')); 2.66–2.59 (*m*, H$_a$–C(2')); 2.47–2.40 (*m*, H$_b$–C(2')); 0.91 (*s*, *t*-BuSi); 0.10, 0.09 (2*s*, 2 Me₂Si).

¹³C-NMR (75.5 MHz, CDCl₃):

155.3 (C(6)); 152.8 (C(2)); 149.6 (C(4)); 139.1 (C(8)); 87.9 (C(1')); 84.3 (C(4')); 71.9 (C(3')); 62.6 (C(5')); 41.3 (C(2')); 26.0, 25.8 (2 *Me₃*CSi); 18.4, 18.0 (2 CSi); –4.6, –4.8, –5.3, –5.5 (4 MeSi).

MS (FAB):

480 ([M + H]⁺).

IR (KBr):

3316, 3151, 2930, 2857, 1666, 1601, 1254, 1111, 837, 777.

EA:

| C₂₂H₄₁N₅O₃Si₂ (479.77) | calculated: | C 55.08, H 8.61, N 14.60. |
| | found: | C 55.20, H 8.58, N 14.60. |

12.2 6-*N*,6-*N*-Bis[(*tert*-butoxy)carbonyl]-3'-*O*,5'-*O*-bis[(*tert*-butyl)dimethylsilyl]-2'-deoxyadenosine (69)

TBDMSO ⟶ O ⟶ A ———— Boc₂O, DMAP, DMF ————▶ TBDMSO ⟶ O ⟶ A(N⁶Boc₂)

OTBDMS   OTBDMS

68   **69**
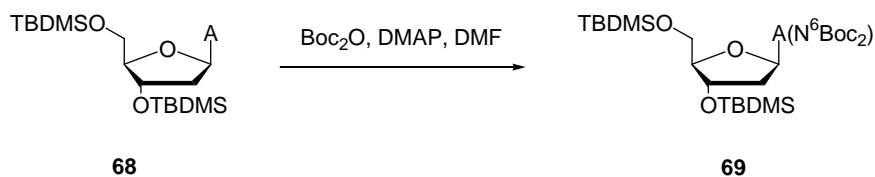
A solution of **68** (38.1 g, 79.5 mmol), Boc$_2$O (52.1 g, 239 mmol, 3.0 equiv.) and DMAP (29.2 g, 239 mmol, 3.0 equiv.) in anh. DMF (100 ml) was stirred overnight at r.t. The the solvent was removed *in vacuo*, the residue was dissolved in CH$_2$Cl$_2$ (700 ml), extracted with 0.3 M aqueous tartaric-acid solution (2 × 700 ml), and the organic phase was re-extracted with CH$_2$Cl$_2$ (700 ml). The combined organic phases were dried (MgSO$_4$), filtered, and concentrated under reduced pressure. Flash column chromatography (FC) of the crude material (hexane/AcOEt 3:1→ 2:1) afforded pure **69** (49.1 g, 91%) as a colourless oil.

TLC: R$_f$ = 0.40 (hexane/AcOEt 2:1).

^{1}H-NMR (300 MHz, CDCl$_3$):
8.87 (*s*, H−C(2)); 8.45 (*s*, H−C(8)); 6.56 (*t*-like, *J* = 6.3, H−C(1')); 4.65 (*dd*-like, *J* = 1.9, 3.6, H−C(3')); 4.09–4.04 (*m*, H−C(4')); 3.92 (*dd*, *J* = 4.6, 11.3, H$_a$−C(5')); 3.81 (*dd*, *J* = 3.2, 11.2, H$_b$−C(5')); 2.72–2.62 (*m*, H$_a$−C(2')); 2.54–2.46 (*m*, H$_b$−C(2')); 1.48 (*s*, *t*-BuO); 0.95 (*s*, *t*-BuSi); 0.14, 0.12 (2*s*, 2 Me$_2$Si).

^{13}C-NMR (75.5 MHz, CDCl$_3$):
151.9 (C(6)); 150.4 (C(2)); 143.2 (C(8)); 88.0 (CO); 84.5 (C(1')); 83.7 (C(4')); 71.7 (C(3')); 62.7 (C(5')); 41.4 (C(2')); 27.8 (*Me*C); 26.0, 25.7 (2 *Me$_3$*CSi); 18.4, 18.0 (2 CSi); −4.6, −4.8, −5.4, −5.5 (4 MeSi).

MS (FAB):
680 ([*M* + H]$^+$).

IR (CHCl$_3$):
3019, 2956, 2951, 1791, 1758, 1601, 1370, 1255, 1215, 1110, 838.

EA:
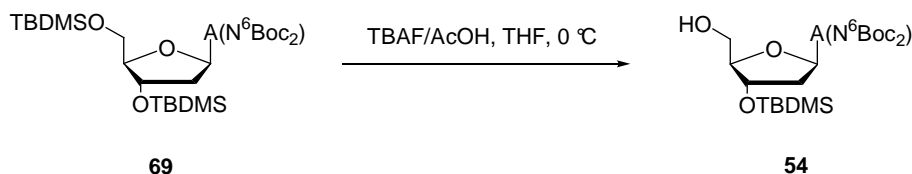C$_{32}$H$_{57}$N$_5$O$_7$Si$_2$ (680.01)   calculated: C 56.52, H 8.45, N 10.30.
                                                  found: C 56.60, H 8.49, N 10.26.

12.3 6-*N*,6-*N*-Bis[(*tert*-butoxy)carbonyl]-3'-*O*-[(*tert*-butyl)dimethylsilyl]-2'-deoxyadenosine (54)

69   **54**

To a stirred solution of **69** (37.9 g, 55.7 mmol) in THF (108 ml), a mixture of TBAF (1 M in THF, 55.7 ml, 55.7 mmol, 1.0 equiv.) and glacial AcOH (12 ml) was slowly added over 15 min at 0°. Stirring was continued for 40 min at 0°, before the soln. was warmed up to r.t. After 3 h, another 0.1 equiv. TBAF/AcOH was added, and the reaction was allowed to go to completion (5 h). Silica gel (25 g) was added, and the solvent was removed under reduced pressure. FC (hexane/AcOEt 2:1) yielded pure **54** (17.0 g, 54%) as a white solid.

TLC:

R_f = 0.24 (hexane/AcOEt 2:1).

M.p.:

156−158°.

^{1}H-NMR (300 MHz, (D$_6$)DMSO):

8.86 (*s*, H−C(2)); 8.85 (*s*, H−C(8)); 6.48 (*t*-like, *J* = 6.8, H−C(1')); 5.02 (*t*-like, *J* = 5.6, OH); 4.64 (*quint.*-like, *J* = 2.8, H−C(3')); 3.92−3.86 (*m*, H−C(4')); 3.66−3.57 (*m*, H$_a$−C(5')); 3.56−3.47 (*m*, H$_b$−C(5')); 2.91 (*ddd*, *J* = 6.0, 7.2, 13.3, H$_a$−C(2')); 2.38 (*ddd*, *J* = 3.5, 6.2, 13.3, H$_b$−C(2')); 1.39 (*s*, *t*-BuO); 0.91 (*s*, *t*-BuSi); 0.12 (*s*, Me$_2$Si).

^{13}C-NMR (75.5 MHz, (D$_6$)DMSO):

151.4 (C(6)); 150.4 (C(2)); 144.3 (C(8)); 90.3 (CO); 87.9 (C(1')); 84.0 (C(4')); 73.8 (C(3'));

63.2 (C(5')); 41.3 (C(2')); 27.8 (*Me*C); 25.8 (*Me$_3$*CSi); 18.0 (CSi); –4.7, –4.8 (2 MeSi).

MS (FAB):

604 ([*M* + K]$^+$); 566 ([*M* + H]$^+$).

IR (KBr): 3308, 2933, 2858, 1745, 1708, 1607, 1464, 1355, 1270, 1163, 1121, 1025, 930, 836, 788.
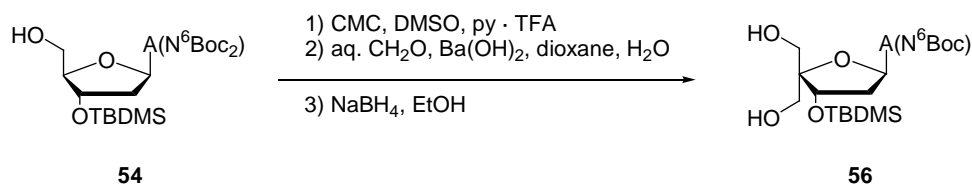
EA:

C$_{26}$H$_{43}$N$_5$O$_7$Si (565.75)	calculated:	C 55.20, H 7.66, N 12.38.
	found:	C 55.49, H 7.73, N 12.05.

12.4 6-*N*-[(*tert*-Butoxy)carbonyl]-3'-*O*-[(*tert*-butyl)dimethylsilyl]-4'-(hydroxymethyl)-2'-deoxyadenosine (56)

54 → **56**

1) CMC, DMSO, py · TFA
2) aq. CH$_2$O, Ba(OH)$_2$, dioxane, H$_2$O
3) NaBH$_4$, EtOH

Compound **54** (18.6 g, 32.9 mmol) and CMC (48.7 g, 115 mmol, 3.5 equiv.) were co-evaporated with toluene (2 ×), added to a solution of pyridinium trifluoroacetate (3.50 g, 18.1 mmol, 0.55 equiv.) in anhydrous DMSO (210 ml) and stirred for 18 h at r.t. The yellow mixture was cooled in an ice-bath, a solution of oxalic acid (1.63 g, 18.1 mmol, 0.55 equiv.) in MeOH (30 ml) was added, and the solution was stirred for another 75 min. The colourless

precipitate was filtered off and washed with cold CH_2Cl_2 (250 ml). The organic phase was washed with saturated aqueous $NaHCO_3$ solution (500 ml), and the aqueous phase was re-extracted with CH_2Cl_2 (4 × 300 ml). The combined organic phases were dried ($MgSO_4$), filtered, and concentrated under reduced pressure to yield a yellow oil, which was dissolved in a mixture of 1,4-dioxane (237 ml), H_2O (107 ml) and 36% aqueous formaldehyde (27.1 ml). Then, $Ba(OH)_2 \cdot 8 H_2O$ (14.8 g, 47.0 mmol, 1.43 equiv.) was added, and the mixture was sonicated for 5 min under vigorous shaking, stirred for 19 h at r.t., and poured into saturated aqueous NH_4Cl solution (500 ml). The aqueous phase was extracted with CH_2Cl_2 (4 × 400 ml), the combined organic phase was dried ($MgSO_4$), filtered, concentrated under reduced pressure, and co-evaporated with toluene. The residue was dissolved in anh. EtOH (120 ml), cooled to 0°, and $NaBH_4$ (1.87 g, 49.4 mmol, 1.50 equiv.) was slowly added. After stirring for 75 min at r.t., the mixture was cooled to 0°, AcOH (6 ml) was added, and the solution was concentrated. The green residue was dissolved in CH_2Cl_2 (500 ml), and the organic layer was washed with brine (400 ml). After re-extracting the aqueous phase with CH_2Cl_2 (4 × 300 ml), the combined organic phases were dried ($MgSO_4$), filtered, and concentrated *in vacuo* for 10 min. The residue was dissolved in AcOEt (23 ml) and kept at r.t. until no more precipitate was obtained (48 − 72 h). The off-white precipitate was filtered off, washed with cold AcOEt (10 ml) and hexane (20 ml), and dried under high vacuum to yield pure **56** (7.82 g, 48%) as a white solid.

TLC:
R_f = 0.39 (AcOEt).

M.p.:
208−210°.

^{1}H-NMR (300 MHz, (D_6)DMSO):
8.65 (*s*, NH, H−C(2)); 8.59 (*s*, H−C(8)); 6.45 (*t*-like, *J* = 6.6, H−C(1')); 4.99 (*t*-like, *J* = 5.5, OH); 4.70 (*quint.*-like, *J* = 3.8, H−C(3')); 4.46 (*t*-like, *J* = 5.5, OH); 3.65−3.49 (*m*, CH₂(5'),

CH_2OH); 2.99–2.89 (*m*, H$_a$–C(2')); 2.48–2.38 (*m*, H$_b$–C(2')); 1.48 (*s*, *t*-BuO); 0.91 (*s*, *t*-BuSi); 0.11 (*s*, Me$_2$Si).

^{13}C-NMR (75.5 MHz, (D$_6$)DMSO):

151.3 (C(6)); 151.0 (C(2)); 150.0 (C(4)); 142.5 (C(8)); 123.8 (C(5)); 89.6 (CO); 83.0 (C(1')); 80.1 (C(4')); 72.7 (C(3')); 61.9, 61.0 (CH$_2$OH, C(5')); 40.4 (C(2')); 28.7 (*Me*C); 25.7 (*Me$_3$*CSi); 17.7 (CSi); –4.9, –5.2 (2 MeSi).

MS (ESI):

518 ([*M* + Na]$^+$); 494 ([*M* – H]$^-$).

IR (KBr):

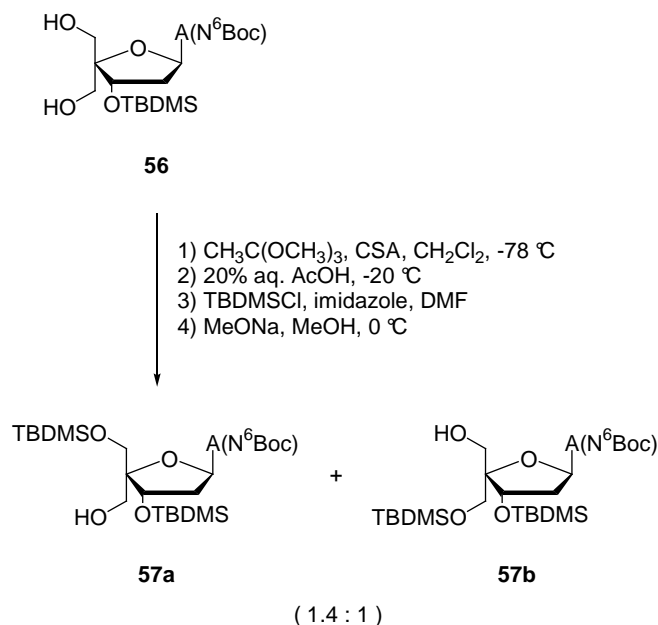3414, 3354, 2933, 2857, 1754, 1619, 1585, 1470, 1403, 1369, 1331, 1232, 1146, 1116, 1057, 1017, 950, 873, 838.

EA:

C$_{22}$H$_{37}$N$_5$O$_6$Si (495.66)   calculated: C 53.31, H 7.52, N 14.13.

                                              found: C 53.13, H 7.54, N 14.13.

12.5   6-*N*-[(*tert*-Butoxy)carbonyl]-3'-*O*,5'-*O*-bis[(*tert*-butyl)dimethylsilyl]-4'-(hydroxymethyl)-2'-deoxyadenosine (57)

After co-evaporation with toluene (2 × 10 ml), diol **56** (6.18 g, 12.5 mmol) was dissolved in anhydrous CH_2Cl_2 (60 ml) and cooled to –78°. Trimethyl orthoacetate (7.85 ml, 62.5 mmol, 5.0 equiv.) and racemic CSA (232 mg, 1.00 mmol, 0.080 equiv.) were added. After 10 min, the cooling bath was removed, and the solution was stirred for 3 h at r.t. The solution was cooled to –20°, 20% aqueous AcOH (83 ml) was added, and the biphasic mixture was stirred at –20 to 0° for 17 h. Then, CH_2Cl_2 (500 ml) and 1% aqueous NaOH solution (500 ml) were added, followed by saturated aqueous $NaHCO_3$ solution (about 600 ml) to adjust the pH to 8–9 (caution: evolution of CO_2 requires slow addition). The resulting mixture was extracted with CH_2Cl_2 (3 × 400 ml). The combined organic phase was dried ($MgSO_4$), filtered, and the solvent removed under reduced pressure. After co-evaporation with toluene (2 × 10 ml), the colourless residue was dissolved in anhydrous DMF (75 ml), 1*H*-imidazole (2.55 g, 37.5

mmol, 3.0 equiv.) and TBDMSCl (2.83 g, 18.8 mmol, 1.5 equiv.) were added, and the solution was stirred at. r.t. for 15 h. The reaction was quenched by addition of MeOH (30 ml), and the solvent was removed *in vacuo*. The residue was dissolved in CH_2Cl_2 (500 ml) and 0.3 M aqueous tartaric-acid solution (1000 ml), and extracted with CH_2Cl_2 (3 × 300 ml). The combined organic phase was dried ($MgSO_4$), filtered, and concentrated under reduced pressure. The residue was dissolved in MeOH (60 ml), chilled to 0°, and MeONa (10.3 g) was added. After stirring the white suspension for 30 min at 0°, CH_2Cl_2 (500 ml) and saturated aqueous NH_4Cl soln. (850 ml) were added. Then, the solution was adjusted to pH ≈ 5 by addition of glacial AcOH. The mixture was extracted with CH_2Cl_2 (4 × 300 ml), the combined organic phase was dried ($MgSO_4$), filtered, and the solvent was removed under reduced pressure. FC (hexane/AcOEt 2:1 → AcOEt) yielded pure diastereoisomers **57a** (3.74 g, 49%) and **57b** (2.77 g, 36%) as white foams, in a ratio of **57a**/**57b** 14 : 10.

Data for **57a**:

TLC:
$R_f = 0.10$ (hexane/AcOEt 1:1).

M.p.:
61−62°.

^{1}H-NMR (300 MHz, (D$_6$)DMSO):
8.59, 8.58 (2*s*, NH, H−C(2), H−C(8)); 6.44 (*t*-like, *J* = 6.5, H−C(1')); 4.75 (*t*-like, *J* = 5.3, OH); 4.50 (*t*-like, *J* = 5.2, H−C(3')); 3.69 (*s*-like, CH$_2$(5')); 3.66 (*dd*, *J* = 4.3, 11.5, CH$_a$−C(4')); 3.51 (*dd*, *J* = 6.2, 11.5, CH$_b$−C(4')); 3.07−2.98 (*m*, H$_a$−C(2')); 2.51−2.40 (*m*, H$_b$−C(2')); 1.47 (*s*, *t*-BuO); 0.90, 0.84 (2*s*, 2 *t*-BuSi); 0.11, 0.10 (2*s*, 2 MeSi); 0.01, −0.01 (2*s*, 2 MeSi).

^{13}C-NMR (75.5 MHz, (D$_6$)DMSO):
151.5 (C(6)); 151.3 (C(2)); 150.0 (C(4)); 142.5 (C(8)); 123.8 (C(5)); 88.9 (CO); 82.7 (C(1'));

80.1 (C(4')); 72.3 (C(3')); 62.6, 60.5 (CH$_2$OH, C(5')); 39.0 (C(2')); 27.8 (*Me*C); 25.7, 25.6 (2 *Me$_3$*CSi); 18.0, 17.7 (2 CSi); –4.8, –5.3, –5.5, –5.6 (4 MeSi).

MS (FAB):

610 ([*M* + H]$^+$).

IR (KBr):

3420, 3256, 2955, 2931, 2858, 1753, 1613, 1584, 1525, 1470, 1392, 1368, 1329, 1255, 1231, 1147, 1083, 951, 837.

EA:

C$_{28}$H$_{51}$N$_5$O$_6$Si$_2$ (609.92)   calculated: C 55.14, H 8.43, N 11.48.

                                                   found: C 55.17, H 8.36, N 11.31.

Data for **57b**:

TLC:

R$_f$ = 0.27 (hexane/AcOEt 1:1).

M.p.:

109–111° (liquid crystal).

^{1}H-NMR (300 MHz, (D$_6$)DMSO):

8.65 (*s*, NH, H–C(2)); 8.58 (*s*, H–C(8)); 6.43 (*t*-like, *J* = 6.6, H–C(1')); 5.02 (*t*-like, *J* = 5.5, OH); 4.75 (*t*-like, *J* = 5.8, H–C(3')); 3.75 (*d*, *J* = 10.7, H$_a$–C(5')); 3.69 (*d*, *J* = 10.7, H$_b$–C(5')); 3.57–3.46 (*m*, C*H$_2$*OH); 2.90–2.81 (*m*, H$_a$–C(2')); 2.52–2.43 (*m*, H$_b$–C(2')); 1.47 (*s*, *t*-BuO); 0.89, 0.88 (2*s*, 2 *t*-BuSi); 0.09, 0.08 (2*s*, 2 MeSi); 0.05, 0.04 (2*s*, 2 MeSi).

^{13}C-NMR (75.5 MHz, (D$_6$)DMSO):

151.6 (C(6)); 151.4 (C(2)); 150.0 (C(4)); 142.6 (C(8)); 123.8 (C(5)); 89.1 (CO); 83.1 (C(1'));

80.1 (C(4')); 72.2 (C(3')); 63.1, 61.8 (CH$_2$-OH, C(5')); 40.4 (C(2')); 27.8 (*Me*C); 25.8, 25.6 (2

*Me$_3$*CSi); 18.1, 17.7 (2 CSi); –4.8, –5.3, –5.5, –5.6 (4 MeSi).

MS (FAB):

610 ([*M* + H]$^+$).

IR (KBr):

3419, 2955, 2930, 2857, 1753, 1612, 1524, 1467, 1393, 1367, 1330, 1255, 1147, 1082, 953,

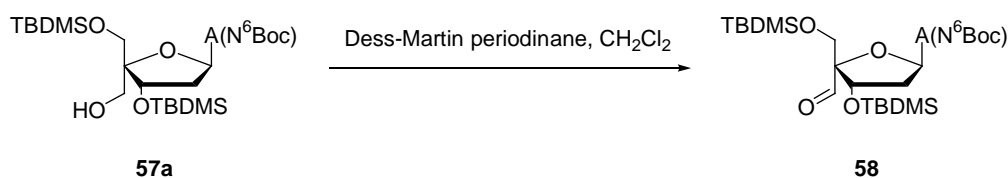837.

EA:

C$_{28}$H$_{51}$N$_5$O$_6$Si$_2$ (609.92) calculated: C 55.14, H 8.43, N 11.48.

found: C 55.17, H 8.29, N 11.41.

12.6 6-*N*-[(*tert*-Butoxy)carbonyl]-3'-*O*,5'-*O*-bis[(*tert*-butyl)dimethylsilyl]-4'-formyl-2'-deoxyadenosine (58)

A solution of **57a** (9.70 g, 15.9 mmol) and 1,1,1-triacetoxy-1,1-dihydro-1,2-benziodoxol-3(1*H*)-one (*Dess − Martin* reagent; 16.9 g, 39.8 mmol, 2.5 equiv.) in anhydrous CH_2Cl_2 (200 ml) was stirred at r.t. for 6 h. *t*-BuOMe (500 ml) was added, and the mixture was extracted with 0.3 M NaOH (3 × 300 ml) containing $Na_2S_2O_3$ (15 g each). The organic phase was washed with brine (300 ml). The aqueous phase was re-extracted with *t*-BuOMe (300 ml), the combined organic phase was dried ($MgSO_4$), filtered, and concentrated under reduced pressure. FC (hexane/AcOEt 3:1 → 1:1) yielded pure **58** (7.84 g, 81%) as a white foam.

TLC:
R_f = 0.32 (hexane/AcOEt 1:1).

M.p.:
64°.

^{1}H-NMR (300 MHz, CDCl$_3$):
9.68 (*s*, CHO); 8.76 (*s*, H−C(2)); 8.29 (*s*, H−C(8)); 8.01 (br. *s*, NH); 6.78 (*t*-like, *J* = 6.9, H−C(1')); 4.88 (*t*-like, *J* = 4.2, H−C(3')); 4.06 (*d*, *J* = 11.3, H$_a$−C(5')); 3.93 (*d*, *J* = 11.3, H$_b$−C(5')); 2.90−2.83 (*m*, H$_a$−C(2')); 2.57−2.52 (*m*, H$_b$−C(2')); 1.57 (*s*, *t*-BuO); 0.90, 0.89 (2*s*, 2 *t*-BuSi); 0.11, 0.10 (2*s*, 2 MeSi); 0.08, 0.07 (2*s*, 2 MeSi).

^{13}C-NMR (75.5 MHz, CDCl$_3$):
200.9 (CHO); 153.0 (C(6)); 149.9 (C(2)); 149.6 (C(4)); 141.0 (C(8)); 121.8 (C(5)); 93.3 (CO); 85.5 (C(4')); 82.3 (C(1')); 75.9 (C(3')); 63.9 (C(5')); 41.6 (C(2')); 28.1 (*Me*C); 25.9, 25.6 (2 *Me$_3$*CSi); 18.3, 17.9 (2 CSi); –4.7, –5.3, –5.5, –5.6 (4 MeSi).

MS (FAB):
646 ([*M* + K]$^+$); 608 ([*M* + H]$^+$).

IR (KBr):
3421, 3178, 2955, 2858, 1742, 1610, 1465, 1329, 1257, 1229, 1145, 1096, 945, 838.

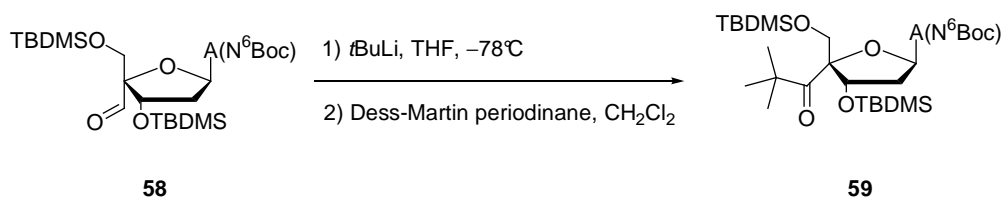EA:

C$_{28}$H$_{49}$N$_5$O$_6$Si$_2$ (607.90)   calculated: C 55.32, H 8.12, N 11.52.

                                    found: C 55.33, H 8.07, N 11.36.

12.7   6-*N*-[(*tert*-Butoxy)carbonyl]-3'-*O*,5'-*O*-bis[(*tert*-butyl)dimethylsilyl]-4'-(2,2-dimethylpropanoyl)-2'-deoxyadenosine (59)

58   **59**

Compound **58** (9.56 g, 15.7 mmol) was co-evaporated with toluene (2 × 10 ml), dissolved in anhydrous Et$_2$O (200 ml) and cooled to –78°. Cold *t*-BuLi solution (1.5 M in pentane, 52.4 ml, 78.6 mmol, 5.0 equiv.) was added within 3 min, and the brown mixture was stirred for another 10 min. Then the reaction was quenched by addition of saturated aqueous NH$_4$Cl solution (95 ml), the pale yellow mixture was warmed to r.t., treated with H$_2$O (400 ml), and extracted with CH$_2$Cl$_2$ (5 × 300 ml). The combined organic phase was dried (MgSO$_4$), filtered, concentrated under reduced pressure, and co-evaporated with toluene (2 × 10 ml). The resulting yellow foam was dissolved in anhydrous CH$_2$Cl$_2$ (150 ml), treated with 1,1,1-triacetoxy-1,1-dihydro-1,2-benziodoxol-3(1*H*)-one (*Dess−Martin* reagent; 16.6 g, 39.3 mmol, 2.5 equiv.), and stirred at r.t. for 25 h. Then *t*-BuOMe (500 ml) was added, and the mixture was extracted with 0.3 M aqueous NaOH solution (3 × 300 ml) containing Na$_2$S$_2$O$_3$ (15 g each). The organic phase was washed with brine (300 ml), and the aqueous phase was re-extracted with *t*-BuOMe (300 ml). The combined organic phase was dried (MgSO$_4$),

filtered, concentrated under reduced pressure, and co-evaporated with toluene. FC (hexane/AcOEt 7:2 → 2:1) yielded pure **59** (2.62 g, 25%) as a white foam.

TLC:

$R_f = 0.27$ (hexane/AcOEt 2:1).

M.p.:

70–72°.

^{1}H-NMR (300 MHz, CDCl$_3$):

8.76 (*s*, H–C(2)); 8.42 (*s*, H–C(8)); 8.11 (br. *s*, NH); 6.76 (*dd*, *J* = 5.4, 9.5, H–C(1')); 4.56 (*d*-like, *J* = 4.6, H–C(3')); 3.99 (*d*, *J* = 10.5, H$_a$–C(5')); 3.87 (*d*, *J* = 10.5, H$_b$–C(5')); 2.70 (*ddd*, *J* = 4.7, 9.4, 13.0, H$_a$–C(2')); 2.48 (*dd*-like, *J* = 5.5, 12.9 Hz, H$_b$–C(2')); 1.54 (*s*, *t*-BuO); 1.22 (*s*, *t*-Bu–CO); 0.88, 0.87 (2*s*, 2 *t*-BuSi); 0.11, 0.08, 0.07, 0.06 (4*s*, 4 MeSi); NOE [*t*-BuC=O → H–C(8): (+); H–C(1'): ++ ; H–C(3'): (+); H$_b$–C(5'): ++ ; H$_a$–C(2'): (+).

^{13}C-NMR (75.5 MHz, CDCl$_3$):

213.5 (*t*-Bu*C*O); 153.1 (C(6)); 149.7 (C(2)); 149.6 (C(4)); 140.9 (C(8)); 121.7 (C(5)); 100.4 (NCO); 85.5 (C(4')); 82.2 (C(1')); 75.6 (C(3')); 69.2 (C(5')); 45.1 (Me$_3$*C*–CO); 42.9 (C(2')); 28.3, 28.2, 28.1 (*Me$_3$*C–O); 26.3, 25.9, 25.8, 25.7, 25.5 (2 *Me$_3$*CSi, *Me$_3$*C–CO); 18.4, 18.0 (2 *C*Si); –4.9, –5.2, –5.4, –5.5 (4 MeSi).

MS (FAB):

702 ([*M* + K]$^+$); 664 ([*M* + H]$^+$).

IR (KBr):

3422, 3246, 3181, 2957, 2931, 2859, 1758, 1721, 1703, 1610, 1463, 1366, 1329, 1257, 1225, 1144, 941, 836.

EA:

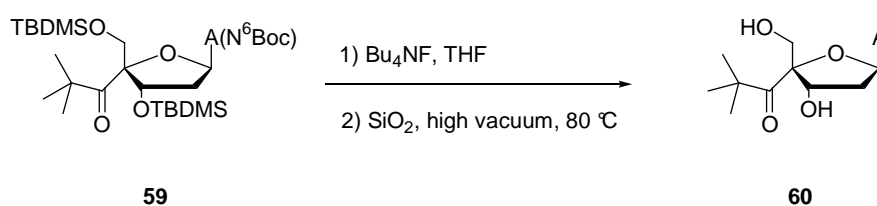C$_{32}$H$_{57}$N$_5$O$_6$Si$_2$ (664.01)   calculated: C 57.88, H 8.65, N 10.55.

                                            found: C 58.01, H 8.67, N 10.18.

12.8   4'-(2,2-Dimethylpropanoyl)-2'-deoxyadenosine (60)

A mixture of **59** (2.27 g, 3.42 mmol) and TBAF (1 M in THF, 34.2 ml, 34.2 mmol, 10 equiv.) was stirred for 1 h at 0° and for 80 min at r.t. Silica gel (11 g) was added, and the solvent was removed under reduced pressure. The reagent was removed by passing the mixture through a short column of silica gel (AcOEt). Toluene (10 ml) and silica gel (4.0 g, activated at 80° *in vacuo* for 24 h) were added, and the mixture concentrated under reduced pressure (26 mbar). The mixture was heated to 70° *in vacuo* (about 4×10^{-2} mbar) for 65 h, then, the temperature was raised to 80° for another 72 h. The mixture was cooled to r.t., extracted with DMF (30ml) and MeOH (30 ml), filtered, and concentrated *in vacuo*. Purification by FC (AcOEt → acetone) yielded pure **60** (75.0 mg, 37%) as clear, light amber crystals.

TLC:

R$_f$ = 0.21 (AcOEt/MeOH 9:1).

M.p.:

87–90° (liquid crystal).

^{1}H-NMR (300 MHz, CDCl$_3$):

8.30 (*s*, H–C(2)); 7.94 (*s*, H–C(8)); 7.18–7.13 (*m*, NH$_2$); 6.42 (*dd*, *J* = 5.1, 10.3, H–C(1')); 5.96 (br. *s*, 2 OH); 4.88 (*d*-like, *J* = 4.9, H–C(3')); 3.97 (*d*, *J* = 11.4, H$_a$–C(5')); 3.89 (*d*, *J* = 11.4, H$_b$–C(5')); 3.22 (*ddd*, *J* = 4.9, 10.3, 13.0, H$_a$–C(2')); 2.36 (*dd*-like, *J* = 5.2, 12.9, H$_b$–C(2')); 1.21 (*s*, *t*-BuC).

^{13}C-NMR (75.5 MHz, CDCl$_3$):

217.5 (*t*-Bu*C*O); 156.3 (C(6)); 152.3 (C(2)); 148.4 (C(4)); 140.3 (C(8)); 121.2 (C(5)); 102.5 (C(4')); 88.4 (C(1')); 75.7 (C(3')); 68.2 (C(5')); 45.5 (Me$_3$*C*–CO); 39.6 (C(2')); 25.7 (*Me$_3$*C–CO).

MS (FAB):

374 ([*M* + K]$^+$); 336 ([*M* + H]$^+$).

IR (KBr):

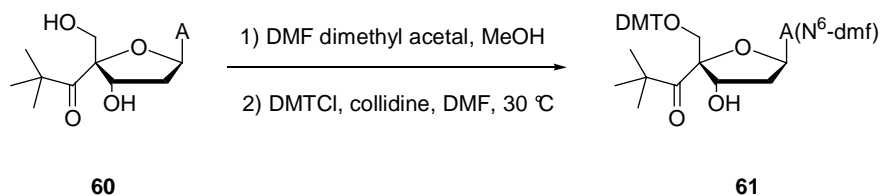3342, 3189, 2962, 2869, 1691, 1647, 1601, 1481, 1371, 1256, 1212, 1103, 944, 907.

EA:

C$_{15}$H$_{21}$N$_5$O$_4$ (335.37)	calculated:	C 53.72, H 6.31, N 20.88.
	found:	C 53.45, H 6.50, N 20.75.

12.9 5'-*O*-[Bis(4-methoxyphenyl)(phenyl)methyl]-6-*N*-[(dimethylamino)methylidene]-4'-(2,2-dimethylpropanoyl)-2'-deoxyadenosine (61)

60   **61**

After co-evaporation with toluene (2 × 2 ml), compound **60** (20 mg, 59.6 µmol) was suspended in anhydrous MeOH (5 ml), *N*-(dimethoxymethyl)-*N*,*N*-dimethylamine (= dimethyl acetal of DMF; 39.7 µl, 298 µmol, 5.0 equiv.) was added, and the mixture was stirred at r.t for 16 h. The clear solution was concentrated under reduced pressure, then co-evaporated with MeOH/toluene 1:1 (3 × 3 ml), and dried *in vacuo*. DMF (3 ml), DMTCl (30.3 mg, 89.4 µmol, 1.5 equiv.) and collidine (79.0 µl, 596 µmol, 10 equiv.) were added, and the mixture was stirred at 30° for 17 h. MeOH (2 ml) was added, and the solution concentrated under reduced pressure. The residue was co-evaporated with toluene (2 × 2 ml) and subjected to FC (silica gel *Merck 60*, AcOEt/Et₃N 99:1 → acetone/Et₃N 99:1) to yield **61** (12.8 mg, 55%) as an off-white foam.

TLC:
R_f = 0.36 (acetone/Et$_3$N 99:1).

M.p.:
125–127°.

^{1}H-NMR (300 MHz, CDCl$_3$):

8.92 (*s*, H–C(2)); 8.46 (*s*, H–C(8)); 7.96 (*s*, *H*–CNMe$_2$); 7.36–7.19, 6.80–6.77 (2*m*, arom. H); 6.72 (*dd*, *J* = 5.3, 9.7, H–C(1')); 4.71 (*d*-like, *J* = 4.6, H–C(3')); 3.77 (*s*, MeO); 3.55 (*d*, *J* = 9.8, H$_a$–C(5')); 3.42 (*d*, *J* = 9.6, H$_b$–C(5')); 3.26, 3.21 (2*s*, Me$_2$N); 2.92 (*ddd*, *J* = 5.1, 9.6, 13.5, H$_a$–C(2')); 2.53 (*dd*-like, *J* = 5.3, 13.2, H$_b$–C(2')); 1.21 (*s*, *t*-BuC).

^{13}C-NMR (75.5 MHz, CDCl$_3$):

217.0 (*t*-Bu*C*O); 158.6 (*C*NMe$_2$); 158.0, 152.7, 151.6, 143.9, 140.1, 135.1, 130.1, 128.3, 128.2, 127.9, 127.0, 113.1 (arom. C); 98.6 (C(4')); 87.2 (Ar$_3$*C*); 85.2 (C(1')); 76.0 (C(3')); 67.8 (C(5')); 55.2 (MeO); 45.7 (Me$_3$*C*-CO); 41.2 (C(2')); 38.7, 35.2 (2 MeN); 26.1 (*Me$_3$*C-CO).

MS (ESI):

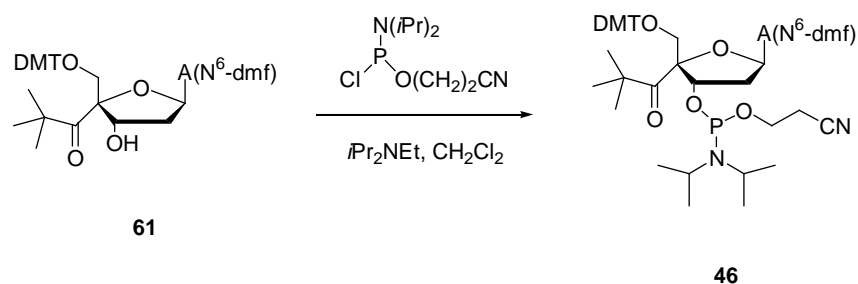715 ([*M* + Na]$^+$); 693 (*M*$^+$).

IR (KBr):

3424, 2959, 2925, 2854, 1702, 1637, 1561, 1509, 1459, 1420, 1352, 1250, 1177, 1112, 1033, 937, 829.

EA:

An accurate combustion analysis could not be obtained.

12.10 5'-*O*-[Bis(4-methoxyphenyl)(phenyl)methyl]-6-*N*-[(dimethylamino)methylidene]-4'-(2,2-dimethylpropanoyl)-2'-deoxyadenosine-3'-*O*-[(2-cyanoethyl)-*N,N*-diisopropylphosphoramidite] (46)

Well-dried **61** (56.7 mg, 81.7 µmol) was dissolved in anhydrous CH$_2$Cl$_2$ (2.0 ml), *i*-Pr$_2$NEt (*Hünig* base; 75.5 µl, 441 µmol, 5.4 equiv.) and 2-cyanoethyl-*N,N*-(diisopropyl)-chlorophosphoramidite (54.7 µl, 245 µmol, 3.0 equiv.) were added, and the solution was stirred at r.t. for 3.5 h. The mixture was poured into saturated aqueous NaHCO$_3$ solution (20 ml), which was extracted with CH$_2$Cl$_2$ (3 × 20 ml). The combined organic phase was dried (Na$_2$SO$_4$), filtered, and concentrated under reduced pressure. The residue was purified by FC (silica gel *Merck 60*, hexane/acetone/Et$_3$N 49.5 :49.5 :1) to afford **46** (57.1 mg, 78%) as a colourless solid, which was used without further purification for oligonucleotide synthesis.

Mixture of two diastereoisomers:

^{1}H-NMR (400 MHz, CDCl$_3$):
8.91, 8.90 (*s*, H−C(2)); 8.48, 8.44 (*s*, H−C(8)); 7.92, 7.91 (*s*, *H*C−NMe$_2$); 7.32–7.19, 6.76–6.73 (2*m*, arom. H); 6.71–6.65 (*m*, H−C(1')); 4.23–4.07 (*m*, H−C(3'), CH$_2$OP); 3.75 (*s*,

MeO); 3.55–3.44 (*m*, H$_a$–C(5'), H$_b$–C(5'), Me$_2$C*H*); 3.24, 3.19 (2*s*, Me$_2$N); 2.76–2.72 (*m*, H$_a$–C(2'), C*H*$_2$CN); 2.60–2.57 (*m*, H$_b$-C(2')); 1.27–1.14 (*m*, *Me$_2$*CH, Me$_3$C–CO).

^{13}C-NMR (101 MHz, CDCl$_3$):

218.1 (*t*-Bu*C*O); 158.7 (*C*NMe$_2$); 157.3, 153.2, 152.0, 144.8, 140.1, 135.1, 130.2, 129.0, 128.1, 127.7, 127.0, 116.8, 113.1 (arom. C, CN); 97.0 (C(4')); 87.1 (Ar$_3$*C*); 85.9 (C(1')); 77.2 (C(3')); 70.8 (C(5')); 58.1, 58.0 (MeO); 55.1 (*C*H$_2$OP); 46.9 (Me$_3$*C*–CO); 45.6 ((Me$_2$*C*H)$_2$NH); 41.3 (C(2')); 37.2, 35.1 (Me$_2$N); 26.0 (*Me$_3$*C–CO); 22.9, 22.8, 22.7, 22.6 ((*Me$_2$*CH)$_2$NH); 20.0, 19.1 (*C*H$_2$CN).

^{31}P-NMR (162 MHz, CDCl$_3$):

149.1, 147.4.

MS (ESI):

915 ([*M* + Na]$^+$); 893 ([*M* + H]$^+$).

13 Oligonucleotide Syntheses

## 13.1 Principle of the Automated DNA Solid-Phase Synthesis

Synthetic oligonucleotides are usually built up in 3' to 5' direction and the first building block is covalently bound to the solid phase *via* a base-labile succinyl linker. The connection to the solid phase is *via* an amide bond and the 5' hydroxy group is protected by an acid-labile DMT ether. Generally, the solid phase has a loading density of 20 to 30 µmol of the starting nucleotide per gram of solid phase. Solid phase amino functionalized borosilicates (CPG – controlled pore glass) are widely used, which offer a range of pore widths from 500 to 2000 Å. Solid phase material featuring a pore width larger than 1000 Å is of particular advantage for longer oligonucleotides (> 30mers). Pre-loaded flow-through columns for automated DNA syntheses span a synthesis scale range from 40 nmol up to 10 µmol. For this work, only 500 Å pore width CPG columns in 0.2 µmol synthesis scale were used.

The monomeric nucleotide building blocks carry temporary protection groups, which get cleaved before each coupling step. They also contain permanent protection groups for the amino functions of A, C and G, as well as for the phosphite function, which are only cleaved after completion of the oligonucleotide synthesis. The DMT group is used for the protection of all 5' hydroxy groups. The amino groups of A, C, and G are protected as amides or amidines, and the phosphites are protected by the 2-cyanoethyl group.

The first step of oligonucleotide synthesis is the deprotection of the terminal DMT group by 2% trichloroacetic acid. The following, tetrazole-activated nucleotide then couples with this free hydroxy group. The amidite building blocks are added in approximately 20-fold excess for the coupling steps. In the next step, unreacted 5' hydroxy groups are capped in a fast and quantitative reaction as acetates, in order to terminate any further synthesis of fault sequences. The subsequent oxidation of the labile P(III) compound to the phosphate is achieved by reaction with a iodine/water/pyridine mixture. With the cleavage of the DMT group the next synthesis cycle starts. The amount of cleaved trityl cation is monitored photometrically or conductometrically, as this serves as a scale for coupling efficiency. Upon completion of the synthesis, the oligonucleotide is manually cleaved off the solid phase by treatment with 30%

aqueous ammonia solution at 55 °C for 8 h. All permanent protection groups are also cleaved in this step with exception of the terminal DMT group (*Scheme 13.1*).

Scheme 13.1
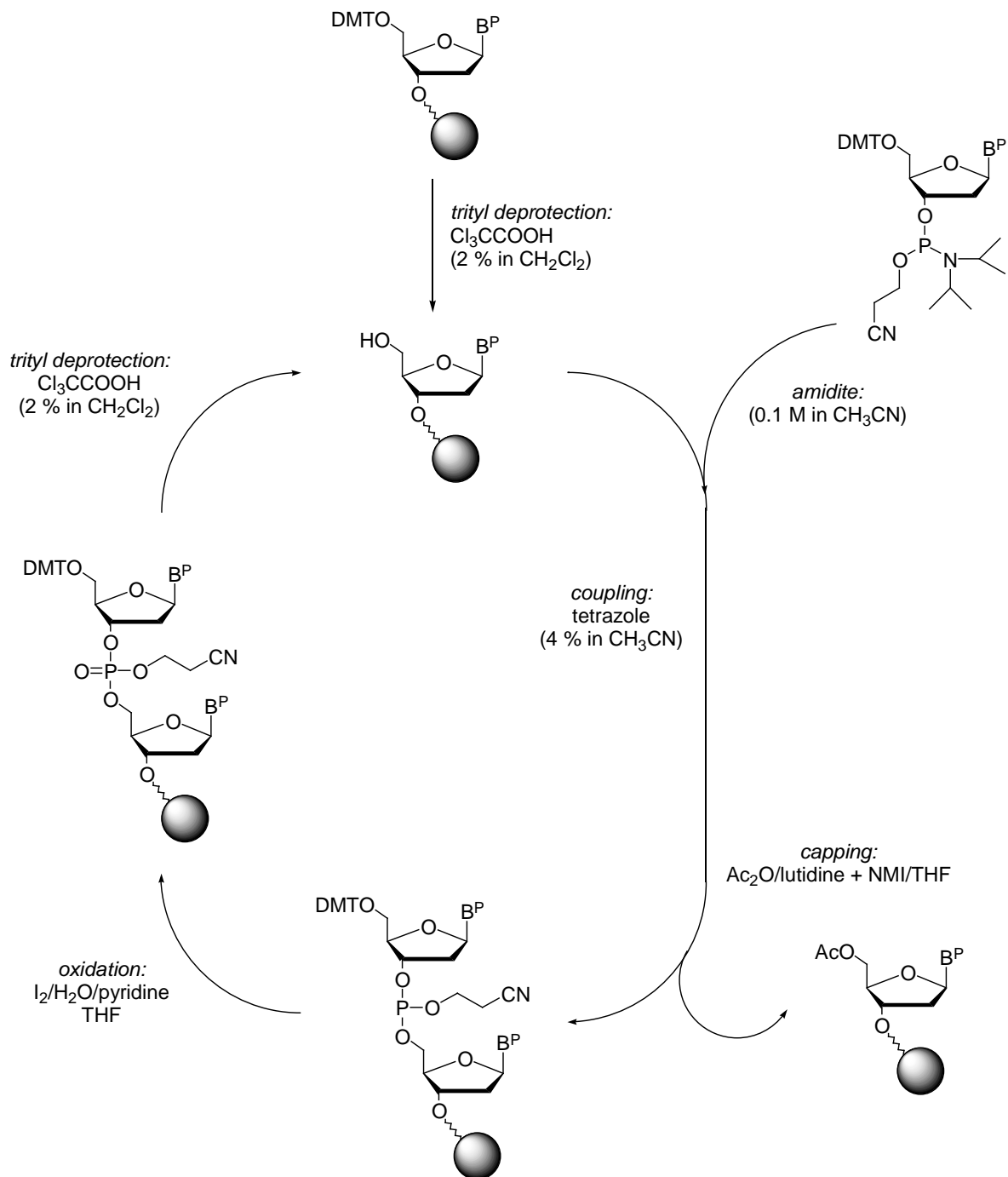
13.2 Introduction of the 4'-Pivaloylated Adenosine 46

Freshly-prepared 4'-pivaloylated nucleoside **46** was dried *in vacuo* and was dissolved in absolute CH_3CN to give a 0.1 M solution. Solid-phase syntheses were carried out at 0.2 μmol scale using standard columns (CPG, 500 Å pore width, Glen Research). The synthesizer was performing in standard mode except for the coupling of the modified nucleosides which were manually coupled using the following procedure:

- instead of "monomer 5" install anh. AcCN at the synthesizer
- manually stop synthesis when it starts pumping "monomer 5"
- remove column from synthesizer, wash with anh. AcCN. Attach two 1ml syringes, one containing 0.2ml A* solution, one containing 0.2 ml Activator solution
- pump these solutions through the column for 20 min. Let the synthesizer proceed without column until the end of the coupling procedure, stop again
- wash column with anh. AcCN, proceed with the synthesis cycle
- when deblocking has ended, stop again and remove column. Add one empty syringe, and one containing 0.5 ml of deblock mix, manually deblock for another 2-3 min, until the solution does not get cloudy any more when pumped through
- thoroughly wash with anh. AcCN, re-mount and proceed with automated synthesis

This procedure proved to afford coupling yields which were absolutely comparable to those of unmodified nucleosides ($> 98\%$), and nearly no loss of the modified nucleoside. All syntheses were carried out in trityl-ON mode. Upon completion of the syntheses, the columns were dried in an argon flow, and were incubated by 30% aqueous ammonia solution (1 ml) overnight. After lyophilization, the crude oligonucleotide was extracted with TEAA buffer (0.9 ml, 0.1 M, pH 7) and filtered through a 0.2 μm syringe filter for subsequent HPLC purification.

13.3   Workup and Purification of the Oligonucleotides

The crude trityl-ON oligonucleotide mixtures in TEAA buffer were purified by RP-18 HPLC (see *Chapter 11.2*). The following HPLC gradient was applied: 15% to 40% CH₃CN in 25 min., which led to elution of the desired oligonucleotides within 9 to 14 min. The collected fractions were lyophilized. For trityl deprotection, 80% aqueous acetic acid (200 µl) was added to the dry fractions. After 20 min at r.t., aqueous NaOAc solution (3 M, 50 µl) and *i*-PrOH (300 µl) were added, and the mixture was vigorously shaken, centrifuged and lyophilized to dryness.

For the trityl-OFF purification, the deprotected oligonucleotides were dissolved in water and filtered through a 0.2 µm syringe filter. The following HPLC gradients were applied: for oligonucleotides < 30mer, 6% to 13% CH₃CN in 20 min., which led to elution of the desired oligonucleotides after about 15 to 19 min. For oligonucleotides > 30mer, 6% to 15% CH₃CN in 27 min., which led to elution of the desired oligonucleotides after about 15 to 23 min. Oligonucleotides containing many T bases generally eluted later than oligonucleotides containing many A bases.

13.4   Data for the Synthesized Oligonucleotides

The identity of all oligonucleotides was verified by MALDI-TOF MS. Their purity was verified by RP-18 HPLC, as well as by MALDI-TOF MS. All oligonucleotides used in photolyses were of 97% purity at least. The unmodified strands were purchased from Microsynth and Qiagen/Operon, and were purified by PAGE and RP-18 HPLC.

Sequence	ε_{260} (μm^{-1} cm^{-1})	$[M-H]^-$ calculated	$[M-H]^-$ found
101: 5'-TTTCTTTTTGGGTTTTTGGGTTTTTCTTT-3'	242.6	8879.0	8877.6
102: 5'-AAAGAAAAACCCAAAAACCCAAAAAGAAA-3'	351.5	8905.9	8908.9
103: 5'-AAAGAAAAACCCAAAAACCCAAA*AAGAAA-3'	351.5	8990.0	8990.8
104: 5'-TTTCTTTTTGGGTT[sp-d]TTGGGTTTTTCTTT-3'	233.4	8754.7	8748.4
105: 5'-TTTCTTTTTGGG[sp-d]TTT[sp-d]GGGTTTTTCTTT-3'	225.5	8630.6	8630.2
106: 5'-TTTCTTTTTGGGTTCTTGGGTTTTTCTTT-3'	239.9	8863.8	8872.3
107: 5'-TTTCTTTTTGGGCTTTCGGGTTTTTCTTT-3'	238.6	8848.8	8856.5
108: 5'-AAAGAAAAAC CCAAAGAAACCCAAA*AAGAAA-3'	373.7	9634.4	9634.7
109: 5'-AAAGAAAAACCCAATAACCCAAA*AAGAAA-3'	343.5	8981.0	8987.7
110: 5'-TTTCTTTTTGGGTTTCTTTGGGTTTTTCTTT-3'	255.7	9472.2	9473.2

111:

5'-TTTCTTTTTGGGTTATTGGGTTTTTCTTT-3'   247.2   8887.8   8887.8

112:

5'-AAAGAAAAACCCAAAGAAACCCAAAAAGAAA-3' 373.7   9550.3   9553.8

113:

5'-AAAGAAAAACCCAAAGAAACCCAAAAAGAAA-3' 343.5   8898.9   8907.1

114:

5'-AAGAAAACCC

AAAAAAAAAAAACCCAAA*AAGAAA-3'   418.3   10558.1   10564.7

115:

5'-TTTCTTTTTG

GGTTTTTTTTTTTGGGTTTTCTT-3'   280.7   10399.8   10405.3

116:

5'-AAGAAAACCC

AAAAAAAAAAAACCCAAAAAGAAA-3'   418.3   10474.0   10482.7

117:

5'-AAAGAAAAC

CCAAACAAACCCAAA*AAGAAA-3'   369.8   9594.4   9596.3

118:

5'-TTTCTTTTTGGGTTTGTTTGGGTTTTTCTTT-3'   259.6   9512.2   9522.8

119:

5'-AAAGAAAAC

CCAAACAAACCCAAAAAGAAA-3'   369.8   9510.3   9516.9

120:

5'-AAGAAAACCC

AAAAAAAAACCCAAA*AAGAAA-3'   379.3   9618.4   9624.0

abbreviations:

A* 4'-pivaloyl modified adenosine

[sp-d] reduced abasic site (3-hydroxy-2-[hydroxymethyl]tetrahydrofurane)

13.5 DNA Melting Temperatures

Prior to the DNA melting temperature (T_m) measurements, the desired two complementary strands (0.2 nmol each) were dissolved in 1.0 ml buffer solution (pH 5.0, 20 mM sodium citrate, 100 mM NaCl) and annealed according to the procedure described in *Chapter 11.3*. T_m measurements were carried out at 260 nm and a temperature gradient of 1 °C min^{-1}. The values given are the mean of the heating and cooling curves.

Duplex	T_m / °C	Duplex	T_m / °C
101/102	63.0	**103/106**	55.5
101/103	58.4	**103/107**	55.4
101/109	51.3	**103/111**	53.3
101/113	52.7	**108/110**	58.8
102/104	51.8	**109/111**	57.6
102/105	46.2	**110/112**	61.3
102/106	56.7	**111/113**	59.5
102/107	56.6	**114/115**	60.0
102/111	54.3	**115/116**	61.2
103/104	49.9	**117/118**	60.5
103/105	45.2	**118/119**	61.3

14   Photolyses with Subsequent PAGE Analysis

14.1   Radioactive Labelling of Oligonucleotides

To a solution of oligonucleotide (20 pmol) in kinase buffer (4 µl, 70 mM Tris · HCl pH 7.6, 10 mM MgCl$_2$, 5 mM dithiothreitol) were added [γ-^{32}P]-ATP (2 pmol), T$_4$ polynucleotide kinase (10 units), and nanopure H$_2$O (for a total volume of 40 µl). After incubation (45 min at 37 °C), the labelled oligonucleotide was purified by centrifugation *via* a *mini-QuickSpin* column. All oligonucleotides were used for experiments within 14 h after labelling in order to minimize decomposition caused by radiation and radioactive decay.

14.2   Photolyses and Piperidine Cleavage

Double-stranded DNA was generated by mixing the 4'-modified oligonucleotide (6.7 pmol) with 1.5 equiv. of the corresponding ^{32}P-labelled complementary strand in citrate buffer (980 µl, pH 5, 20 mM citrate, 100 mM NaCl) and heating to 75° for 5 min, followed by cooling slowly to r.t (≥ 2 h). The identical procedure was applied to the non-modified control oligonucleotide.

Argon was bubbled through the solution in the cuvette for 6 min before irradiation. Double-stranded DNA solution (200 µl) was irradiated at 320 nm for 5 min (the cuvettes were thermostated to 20°) to obtain cleavage yields at the modified position of 38% to 45%.

A portion of the irradiated solution (40 µl) was mixed with 1.0 M aqueous piperidine solution (200 µl; prepared from freshly re-distilled piperidine), and was shaken at 90° for 30 min, then lyophilized.

14.3 Maxam-Gilbert Sequencing

The following procedures, derived from the original procedures by *Maxam* and *Gilbert*,[156] were applied in order to create DNA reference ladders on the gels:

- for random cleavage at all G positions: to the remains of the labelled oligonucleotide (about 1 pmol) were added phosphate buffer (50 µl, pH 7.0) and dimethyl sulfate (0.5 µl). After 15 min at r.t., 1.0 M aqueous piperidine solution (200 µl; prepared from freshly re-distilled piperidine) was added and the mixture was shaken at 90° for 15 min, then lyophilized.

- for random cleavage at all C and T positions: to the remains of the labelled oligonucleotide (about 1 pmol) were added hydrazine hydrate (20 µl) and nanopure H_2O (5.0 µl). The mixture was shaken at 40 °C for 20 min, and was evaporated to dryness at 60 °C for ≥ 3 h. Then, 1.0 M aqueous piperidine solution (200 µl; prepared from freshly re-distilled piperidine) was added and the mixture was shaken at 90° for 30 min, and lyophilized.

14.4 Polyacrylamide Gel Electrophoresis (PAGE)

14.4.1 Preparation of Gels

The 12% denaturing polyacrylamide gels were cast according to standard procedures[157] using urea (50 g), nanopure H_2O (20 ml), 10 × TBE buffer (10 ml), and *AccuGel 19:1* (30 ml). The gel mixture was degassed by a water-jet vacuum pump for 12 min, and filtered, then polymerization was initiated by addition of TMEDA and 10% ammonium persulfate (80 µl each) and the gel cast at a thickness of 0.4 mm. For this purpose, a custom-designed gel-casting device was used (*Figure 14.1*). All gels were prepared at least 3 h before use.

Figure 14.1. *Gel casting device*

14.4.2 Preparation of Probes and Gel Loading

The dried and piperidine-cleaved irradiation residue was dissolved in a mixture of loading buffer (20 µl, 90% formamide, 10% TBE buffer, some bromphenol blue) and H_2O (20 µl) by shaking at 40 °C for 30 min, then β–radiation intensity was standardized by liquid scintillation of samples (5.0 µl; mixed with 8.0 ml *IrgaSafe Plus*) from every probe in order to ensure that every lane on the gel contained an identical amount of radioactivity. Generally, the radioactivity of the 5.0 µl samples ranged between 30 000 and 70 000 CPM. The best resolution was achieved by application of 75 000 CPM for the probe lanes, and 150 000 CPM for the Maxam-Gilbert lanes. However, the volumes applied to the gel had to range between 3 and 18 µl due to the limited size of the gel loading pockets.

14.4.3 Electrophoresis, Workup and Analysis

Gels were processed at 1500 V for 130 to 170 min, then transferred onto chromatography paper (*Whatman 3 MM Chr*), wrapped into *Saran* foil and exposed to a storage phosphorus

screen for 14 to 17 h. After exposure, the gels were dried for storage purposes at reduced pressure for 3 h at 80 °C.

Relative yields were calculated by volume integration of single spots, histograms were obtained by line integration along the lanes. All results and histograms are the calculated differences between experiments containing 4'-modified oligonucleotides and control probes containing unmodified strands (see *Chapters 10.3−10.4*). The calculated data are the mean values of at least three experiments each.

14.5 Data for the Irradiated Radioactive Oligonucleotides

14.5.1 Photocleavage Efficiency Tests

Several experiments were done with single- or double-stranded sequences **101**, **102** and **103** in order to determine the photocleavage efficiency at different pH values. The results of these prelimiary experiments were used to find a pH value which offers the best yield of enol ether **76**. In contrary to the electron transfer experiments, for these cleavage experiments the A^*-containing strands were radioactively labelled. For both single- and double-strand experiments, pH 5.0 afforded the highest absolute yields for enol ether **76**.

Sequence (single)	pH	P_{29mer} / %	$P_{enol\ ether\ 76}$/ %	$P_{3'-phosphate\ 74}$/ %
102	4.0	61.1	0.4	0.4
103	4.0	7.9	10.2	22.5
102	4.5	47.8	0.6	0.8
103	4.5	6.3	12.7	19.9
102	5.0	66.3	0.5	0.5
103	5.0	7.6	19.6	32.3
102	7.0	71.2	0.6	0.5
103	7.0	8.3	19.4	33.6

Sequence (double)	pH	P_{29mer} / %	$P_{enol\ ether\ \mathbf{76}}$/ %	$P_{3'\text{-phosphate}\ \mathbf{74}}$/ %
102/101	4.0	0.8	0.4	0.7
103/101	4.0	0.6	0.8	1.2
102/101	4.5	6.6	0.5	0.8
103/101	4.5	1.0	1.2	1.5
102/101	5.0	63.7	0.8	0.7
103/101	5.0	7.8	19.4	30.1
102/101	7.0	62.8	0.5	0.4
103/101	7.0	14.1	15.6	25.5

14.5.2 Charge Transfer Experiments

Measured radioactivity of charge transfer experiments after the irradiation. The data given is weighted with the total radioactivity of the corresponding lane, and the control experiments were subtracted as well. The number of the radiolabelled strand is indicated first.

Experiment	$P_{5'}$	$P_{3'}$	$P_{5'}$ / $P_{3'}$
101/103	123.8	68.95	1.80 ± 0.36
101/109	133.7	57.62	2.32 ± 0.47
104/103	1952	79.45	25.0 ± 0.60
106/103	130.9	31.86	4.11 ± 0.78
111/103	117.3	62.71	1.87 ± 0.25
111/109	135.1	74.21	1.82 ± 0.25
115/114	91.80	61.61	1.49 ± 0.09

15   Literature

1.   L. Stryer, *Biochemie*, Spektrum Akademischer Verlag, Heidelberg, Berlin, **1994**.

2.   J. D. Watson, F. H. Crick, *Nature* **1953**, *171*, 737 and 964.

3.   W. Saenger, *Principles of Nucleic Acid Structure*, Springer Verlag, Berlin, Heidelberg, New York, **1984**.

4.   J. M. Benevides, G. J Thomas, *Nucleic Acids Res.* **1983**, *11*, 5747.

5.   R. D. Wells, S. C. Harvey, *J. Biol. Chem.* **1988**, *263*, 1095.

6.   A. Rich, A. Nordheim, A. H. Wang, *Annu. Rev. Biochem.* **1984**, *53*, 791.

7.   a) S. Arnott, D. W. L. Hukins, *Biochem. Biophys. Res. Commun.* **1972**, *47*, 1504. b) S. Arnott, E. Selsing, *J. Mol. Biol.* **1974**, *88*, 509.

8.   E. T. Kool, *Chem. Rev.* **1997**, *97*, 1437.

9.   N. Arora, B. Jayaram, *J. Phys. Chem. B* **1998**, *102*, 6139.

10. a) J. Šponer, J. Leszczynski, P. Hobza, *J. Phys. Chem.* **1996**, *100*, 5590. b) J. Bertran, A. Oliva, L. Rodriguez-Santiago, M. Sodupe, *J. Am. Chem. Soc.* **1998**, *120*, 8159.

11. a) J. Florian, J. Šponer, A. Warshel, *J. Phys. Chem.* **1999**, *103*, 884. b) J. Šponer, J. Leszczynski, P. Hobza, *Biopolymers* **2001**, *61*, 3.

12. a) O. Sinanoglu, S. Abdulnur, *Fed. Proc 24*, **1965**, *15*, 12. b) O. Sinanoglu, *Molecular Association in Biology*, Academic Press, New York, **1968**. c) D. M. Crothers, D. I. Ratner, *Biochemistry* **1968**, *7*, 1823.

13. R. Wehner, W. Gehring, *Zoologie*, Georg Thieme Verlag, Stuttgart, New York, **1995**.

14. L. Strobel, *The Case For Faith*, Zondervan Publishing House, Grand Rapids, Michigan, **2000**.

15. F. W. Gonzalez, *Mutation Research* **1972**, *15*, 303.

16. J. K. Setlow, R. B. Setlow, *Nature* **1963**, *197*, 560.

17. P. J. Dandliker, R. E. Holmlin, J. K. Barton, *Science* **1997**, *275*, 1465.

18. B. Giese, B. Carl, T. Carl, T. Carell, C. Behrens, U. Hennecke, O. Schiemann, E. Feresin, *Angew. Chem. Int. Ed.* **2004**, *43*, 1848.

19. P. J. McHugh, J, Knowland, *Nucleic Acids Res.* **1995**, *23*, 1664.

20. W. C. Orr, R. S. Sohal, *Science* **1994**, *263*, 1128.

21.   T. Finkel, H. J. Holbrook, *Nature* **2000**, *408*, 239.

22.   a) C. A. M. Seidel, A. Schulz, M. H. M. Sauer, *J. Phys. Chem.* **1996**, *100*, 5541. b) S. Steenken, S. L. Jovanovic, *J. Am. Chem. Soc.* **1997**, *119*, 617.

23.   a) C. J. Burrows, J. G. Muller, *Chem. Rev.* **1998**, *98*, 1109. b) S. Raoul, M. Berger, G. W. Buchko, P. C. Joshi, B. Morin, M. Weinfeld, J. Cadet, *J. Chem. Soc., Perkin Trans. 2*, **1996**, 371.

24.   C. Sheu, C. S. Foote, *J. Am. Chem. Soc.* **1995**, *117*, 6439.

25.   K. Kino, I. Saito, *J. Am. Chem. Soc.* **1998**, *120*, 7373.

26.   B. Halliwell, J. M. C. Gutteridge, *Free Radicals in Biology and Medicine,* Oxford University Press, Oxford, **1999**.

27.   E. Meggers, M. E. Michel-Beyerle, B. Giese, *J. Am. Chem. Soc.* **1998**, *120*, 12950.

28.   M. E. Nunez, D. B. Hall, J. K. Barton, *Chem. Biol.* **1999**, *6*, 85.

29.   P. T. Henderson, D. Jones, G. Hampikian, Y. Z. Kan, G. B. Schuster, *Proc. Natl. Acad. Sci. U.S.A.* **1999**, *96*, 8353.

30.   C. Behrens, L. T. Burgdorf, A. Schwögler, T. Carell, *Angew. Chem. Int. Ed.* **2002**, *41*, 1763.

31.   a) H. Sugiyama, I. Saito, *J. Am. Chem. Soc.* **1996**, *118*, 7063. b) F. Prat, K. N. Houk, C. S. Foote, *J. Am. Chem. Soc.* **1998**, *120*, 845.

32.   D. G. Lowy, B. M. Willumsen, *Ann. Rev. Biochem.* **1993**, *62*, 851. b) S. P. Hussain, *Oncogene* **1994**, *9*, 2277.

33.   I. Saito, T. Nakamura, K. Nakatani, Y. Yoshioka, K. Yamaguchi, H. Sugiyama, *J. Am. Chem. Soc.* **1998**, *120*, 12686.

34.   T. R. Cech, *Angew. Chem.* **2000**, *112*, 34.

35.   S. H. Cross, A. P. Bird, *Curr. Opin. Genet. Dev.* **1995**, *5*, 309.

36.   A. Heller, *Faraday Discuss.* **2000**, *116*, 1.

37.   H. S. Kaplan, *Nature* **1978**, *272*, 379.

38.   A. P. Dussy, *Dissertation* **1998**, University of Basel.

39.   T. Linker, M. Schmittel, *Radikale und Radikalionen in der Organischen Synthese*, Wiley-VCH, Weinheim, New York, **1998**.

40.   E. Meggers, *Dissertation*, University of Basel, **1999**.

41. D. D. Eley, D. I. Spivey, *Trans. Faraday Soc.* **1962**, *58*, 411.

42. D. N. Beratan, S. Priyadarshy, S. M. Risser, *Chem. Biol.* **1997**, *4*, 3.

43. C. J. Murphy, M. R. Arkin, Y. Jenkins, N. D. Ghatlia, S. H. Bossmann, N. J. Turro, J. K. Barton, *Science* **1993**, *262*, 1025.

44. E. J. C. Olson, D. Hu, A. Hörmann, P. F. Barbara, *J. Phys. Chem. B* **1997**, *101*, 299.

45. a) A. M. Brun, A. Harriman, *J. Am. Chem. Soc.* **1992**, *114*, 3656. b) A. M. Brun, A. Harriman, *J. Am. Chem. Soc.* **1994**, *116*, 10383.

46. T. J. Meade, J. F. Kayyem, *Angew. Chem. Int. Ed. Engl.* **1995**, *34*, 352.

47. for reviews see: a) T. L. Netzel, *J. Chem. Ed.* **1997**, *74*, 646. b) U. Diederichsen, *Angew. Chem. Int. Ed. Engl.* **1997**, *36*, 2317.

48. K. Fukui, K. Tanaka, *Angew. Chem. Int. Ed.* **1998**, *37*, 158.

49. a) H.-W. Fink, C. Schönenberger, *Nature* **1999**, *398*, 407. b) A. Y. Kasumov, M. Kociak, S. Guéron, B. Reulet, V. T. Volkov, D. V. Klinov, H. Bouchiat, *Science* **2001**, *291*, 280.

50. D. Porath, A. Bezryadin, S. de Vries, C. Dekker, *Nature* **2000**, *403*, 635.

51. H. B. Weber, M .Mayor, *Physik in unserer Zeit* **2003**, *34*, 272.

52. B. Giese, *Top. Curr. Chem.* **2004**, *236*, 27.

53. R. A. Marcus, N. Sutin, *Biochim. Biophys. Acta* **1985**, *811*, 265.

54. P. W. Atkins, *Physikalische Chemie,* 2. Auflage, VCH, Weinheim, New York, **1996**.

55. V. Balzani, *Electron Transfer in Chemistry, Vol. 3, Biological and Artificial Supramolecular Systems,* Wiley-VCH, Weinheim, **2001**.

56. V. G. Levich, *Adv. Electrochem. Electrochem. Eng.* **1966**, *4*, 249.

57. a) N. R. Kestner, J. Jortner, *J. Phys. Chem.* **1974**, *78*, 2148. b) J. Ulstrup, J. Jortner, *J. Chem. Phys.* **1976**, *63*, 4358.

58. P. Sliders, R. A. Marcus, *J. Am. Chem. Soc.* **1981**, *103*, 741.

59. R. A. Marcus, P. Sliders, *J. Phys. Chem.* **1982**, *86*, 622.

60. N. S. Hush, *Coord. Chem. Rev.* **1985**, *64*, 135.

61. J. R. Miller, L. T. Calcaterra, G. L. Closs, *J. Am. Chem. Soc.* **1984**, *106*, 3047.

62. O. Farver, I. Pecht, *J. Biol. Inorg. Chem.* **1997**, *2*, 387.

63. D. N. Beratan, J. N. Onuchic, J. J. Hopfield, *J. Chem. Phys.* **1987**, *86*, 4488.

64. M. D. Newton, *Chem. Rev.* **1991**, *91*, 767.

65. J. Jortner, M. Bixon, M. E. Michel-Beyerle, *Proc. Natl. Acad. Sci. U.S.A.* **1998**, *95*, 12759.

66. a) C. C . Moser, C. C. Page, X. Chen, P. L. Dutton, *J. Biol. Inorg. Chem.* **1997**, *2*, 293. b) S. S. Skourtis, D. N. Beratan, *J. Biol. Inorg. Chem.* **1997**, *2*, 378. c) R. J. P. Williams, *J. Biol. Inorg. Chem.* **1997**, *2*, 373. d) N. Y. Sardesai, J. K. Barton, *J. Biol. Inorg. Chem.* **1997**, *2*, 762.

67. a) F. D. Lewis, T. F. Wu, Y. F. Zhang, R. L. Letsinger, S. R. Greenfield, M. R. Wasielewski, *Science* **1997**, *277*, 673. b) F. D. Lewis, M. R. Wasielewski, *Top. Curr. Chem.* **2004**, *236*, 45.

68. E. Meggers, D. Kusch, M. Spichty, U. Wille, B. Giese, *Angew. Chem. Int. Ed.* **1998**, *37*, 460.

69. S. Wessely, *Dissertation*, University of Basel, **2002**.

70. B. Giese, J. Amaudrut, A.-K. Köhler, M. Spormann, S. Wessely, *Nature* **2001**, *412*, 318.

71. Y. A. Berlin, I. V. Kurnikov, D. Beratan, M. A. Ratner, A. L. Burin, *Top. Curr. Chem.* **2004**, *237*, 1.

72. B. Giese, S. Wessely, *Angew. Chem. Int. Ed.* **2000**, *39*, 3490.

73. K. Nakatani, I. Saito, *Top. Curr. Chem.* **2004**, *236*, 163.

74. Y. A. Berlin, A. L. Burin, M. A. Ratner, *Chem. Phys.* **2002**, *275*, 61.

75. M. Bixon, J. Jortner, *Chem. Phys.* **2002**, *281*, 393.

76. T. Renger, R. A. Marcus, *J. Phys. Chem. A* **2003**, *107*, 8404.

77. B. Giese, S. Wessely, M. Spormann, U. Lindemann, E. Meggers, M. E. Michel-Beyerle, *Angew. Chem. Int. Ed.* **1999**, *38*, 996.

78. a) D. Ly, L. Sanii, G. B. Schuster, *J. Am. Chem. Soc.* **1999**, *121*, 9400. b) G. B. Schuster, *Acc. Chem. Res.* **2000**, *33*, 253.

79. T. T. Williams, D. T. Odom, J. K. Barton, *J. Am. Chem. Soc.* **2000**, *122*, 9048.

80. M. Spormann, *Dissertation*, University of Basel, **2002**.

81. A. K. Felts, W. T. Pollard, R. A. Friesner, *J. Phys. Chem.* **1995**, *99*, 2929.

82. A. Okada, V. Chernyak, S. Mukamel, *J. Phys. Chem. A* **1998**, *102*, 1241.

83. D. Segal, A. Nitzan, W. B. Davis, M. R. Wasielewski, M. A. Ratner, *J. Phys. Chem. B* **2000**, *104*, 3817.

84. F. C. Grozema, Y. A. Berlin, L. D. A. Siebbeles, *J. Am. Chem. Soc.* **2000**, *122*, 10903.

85. a) B. Giese, M. Spichty, *ChemPhysChem* **2000**, *1*, 195. b) B. Giese, M. Spichty, S. Wessely, *Pure Appl. Chem.* **2001**, *73*, 449.

86. T. Kendrick, B. Giese, *Chem. Commun.* **2002**, 2016.

87. a) K. Kawai, T. Takada, S. Tojo, T. Majima, *J. Am. Chem. Soc.* **2003**, *125*, 6842. b) T. Takada, K. Kawai, X. Cai, A. Sugimoto, M. Fujituks, T. Majima, *J. Am. Chem. Soc.* **2004**, *126*, 1125.

88. W. B. Davis, M. R. Wasielewski, M. A. Ratner, V. Mujica, A. Nitzan, *J. Phys. Chem.* **1997**, *101*, 6158.

89. a) B. Giese, X. Beyrich-Graf, P. Erdmann, L. Giraud, P. Imwinkelried, S. N. Müller, U. Schwitter, *J. Am. Chem. Soc.* **1995**, *117*, 6146. b) B. Giese, X. Beyrich-Graf, P. Erdmann, M. Petretta, U. Schwitter, *Chem. Biol.* **1995**, *2*, 367.

90. N. C. Yang, E. D. Feit, *J. Am. Chem. Soc.* **1968**, *90*, 504.

91. R. Glatthar, M. Spichty, A. Gugger, R. Batra, W. Damm, M. Mohr, H. Zipse, B. Giese, *Tetrahedron* **2000**, *56*, 4117.

92. B. Giese, P. Erdmann, L. Giraud, T. Göbel, M. Petretta, T. Schäfer, M. von Rauner, *Tetrahedron Lett.* **1994**, *35*, 2683.

93. A. Gugger, R. Batra, P. Rzadek, G. Rist, B. Giese, J. Am. Chem. Soc. 1997, 119, 8740.

94. E. Meggers, A. Dussy, T. Schäfer, B. Giese, *Chem. Eur. J.* **2000**, *6*, 485.

95. M. A. O'Neill, J. K. Barton, *Top. Curr. Chem.* **2004**, *236*, 67.

96. G. B. Schuster, U. Landmann, *Top. Curr. Chem.* **2004**, *236*, 139.

97. K. Nakatani, C. Dohno, I. Saito, *J. Org. Chem.* **1999**, *64*, 6306.

98. T. Takada, K. Kawai, S. Tojo, T. Majima, *J. Phys. Chem. B* **2003**, *107*, 14052.

99. K. Kawai, T. Majima, *Top. Curr. Chem.* **2004**, *236*, 117.

100. T. Kendrick, *Dissertation*, University of Basel, **2003**.

101. D. Crich, X. Hao, *J. Org. Chem.* **1999**, *64*, 4016.

102.   A. Marx, P. Erdmann, M. Senn, S. Körner, T. Jungo, M. Petretta, P. Imwinkelried, A. Dussy, K. J. Kulicke, L. Macko, M. Zehnder, B. Giese, *Helv. Chim. Acta* **1996**, *79*, 1980.

103.   M. Spormann, B. Giese, *Synthesis* **2001**, 2156.

104.   S. L. Beaucage, R. P. Iyer, *Tetrahedron* **1992**, *48*, 2223.

105.   T. W. Greene, P. G. M. Wuts, *Protective Groups in Organic Synthesis*, 3rd ed., Wiley-Interscience, New York, **1999**.

106.   K. K. Ogilvie, Can. J. Chem. 1973, 51, 3799.

107.   A. Farèse, N. Patino, R. Condom, S. Dalleu, R. Guedj, *Tetrahedron Lett.* **1996**, *37*, 1413.

108.   A. B. Smith III, G. R. Ott, *J. Am. Chem. Soc.* **1996**, *118*, 13095.

109.   a) K. E. Pfitzner, J. G. Moffatt, *J. Am. Chem. Soc.* **1963**, *85*, 3027. b) G. H. Jones, M. Tamiguchi, D. Tegg, J. G. Moffatt, *J. Org. Chem.* **1979**, *44*, 1309.

110.   S. Müller, *Dissertation*, University of Basel, **1996**.

111.   R. L. Ireland, L. Liu, *J. Org. Chem.* **1993**, *58*, 2899.

112.   The following reagents and methods proved to be incompatible with 2'-deoxyadenosine chemistry: a) $SnCl_4$: H. Miel, S. Rault, *Tetrahedron Lett.* **1997**, *38*, 7865. b) TMSI: R. S. Lott, V. S. Chauhan, C. H. Stammer, *Chem. Commun.* **1979**, 495. c) TBDMSCl / MeOH: F. Cavalier, C. Enjalbal, *Tetrahedron Lett.* **1996**, *37*, 5131. d) HCl / AcOEt: F. S. Gibson, S. C. Bergmeier, H. Rapoport, *J. Org. Chem.* **1994**, *59*, 3216. e) TMSCl / phenole: E. Kaiser, F. Picart, T. Kubiak, J. P. Tam, R. B. Merrifield, *J. Org. Chem.* **1993**, *58*, 5167. f) TFA: M. Ubukata, K. Isono, *Tetrahedron Lett.* **1986**, *27*, 3907. g) $AlCl_3$ / CH_2Cl_2: D. S. Bose, V. Lakshminarayana, *Synthesis* **1999**, *1*, 66. h) $AlCl_3$ / anisole / CH_2Cl_2 / CH_3NO_2: K. D. James, A. D. Ellington, *Tetrahedron Lett.* **1998**, *39*, 175. i) Kaolinitic clay / Montmorillonite K10: N. S. Shaikh, A. S. Gajare, V. H. Deshpande, A. V. Bedekar, *Tetrahedron Lett.* **2000**, *41*, 385.

113.   T. Apelqvist, D. Wensbo, *Tetrahedron Lett.* **1996**, *37*, 1471.

114.   P. Kung, R. A. Jones, *Tetrahedron Lett.* **1992**, *33*, 5869.

115. the reaction conditions were modified on the basis of the following procedures: a) Harald Strittmatter, *Dissertation*, University of Basel, **1999**. b) S. K. Chaudhary, O. Hernandez, *Tetrahedron Lett.* **1979**, *2*, 95.

116. N. D. Sinha, J. Biern, J. McManus, H. Köster, *Nucl. Acids Res.* **1984**, *12*, 4539.

117. F. Eckstein, *Oligonucleotides and Analogues, A Practical Approach*, IRL Press at Oxford University Press, Oxford, **1991**.

118. R. D. Cannon, *Electron Transfer Reactions*, Butterworths, London, Boston, **1980**.

119. a) S. Steenken, *Chem. Rev.* **1989**, *89*, 503. b) S. Steenken, *Biol. Chem.* **1997**, *378*, 1293.

120. P. Erdmann, *Dissertation*, University of Basel, **1996**.

121. A.-K. Köhler, *Dissertation*, University of Basel, **2004**.

122. C. Dohno, A. Ogawa, K. Nakatani, I. Saito, *J. Am. Chem. Soc.* **2003**, *125*, 10154.

123. G. L. Sewell, *Polarons and Excitations*, Plenum Press, New York, **1962**.

124. C.-S. Liu, R. Hernandez, G. B. Schuster, *J. Am. Chem. Soc.* **2004**, *126*, 2877.

125. E. M. Conwell, S. V. Rakhmanova, *Proc. Natl. Acad. Sci. U.S.A.* **2000**, *97*, 4556.

126. M. A. Ratner, Y. A. Berlin, A. L. Burin, *J. Am. Chem. Soc.* **2001**, *123*, 260.

127. a) D. Henning, J. Archilla, J. Agarwal, *Physica D* **2000**, 1. b) G. Kalosakas, K. Ø. Rasmussen, A. R. Bishop, *Synthetic Metals* **2004**, *141*, 93.

128. J. Yoo, S. Delaney, E. D. A. Stemp, J. K. Barton, *J. Am. Chem. Soc.* **2003**, *125*, 6640.

129. a) J. Lhomme, J.-F. Constant, M. Demeunynck, *Biopolymers* **1999**, *52*, 65. b) y. Coppel, N. Berthet, C. Coulembeau, C. Coulembeau, J. Garcia, J. Lhomme, *Biochemistry* **1997**, *36*, 4817.

130. B. Giese, S. Wessely, *Chem. Commun.* **2001**, 2108.

131. N. W. Schlientz, G. B. Schuster, *J. Am. Chem. Soc.* **2003**, *125*, 15732.

132. V. Gervais, J. A. H. Cognet, M. Le Bret, L. C. Sowers, G. V. Fazakerley, *Eur. J. Biochem.* **1995**, *228*, 279.

133. W. N. Hunter, T. Brown, N. N. Anand, O. Kennard, *Nature* **1986**, *320*, 552.

134. S. Ravindranathan, S. E. Butcher, J. Feigon, *Biochemistry* **2000**, *39*, 16026.

135. P. K. Bhattacharya, J. K. Barton, *J. Am. Chem. Soc.* **2001**, *123*, 8649.

136. A. J. S. C. Vieira, S. Steenken, *J. Phys. Chem.* **1987**, *91*, 4138.

137.   a) K. Y. Wang, S. A. Parker, I. Goljer, P. H. Bolton, *Biochemistry* **1997**, *36*, 11629. b) R. D. Beger, P. H. Bolton, *J. Biol. Chem.* **1998**, *273*, 15565.

138.   a) M. W. Kalnik, C. N. Chang, A. P. Grollmann, D. J. Patel, *Biochemistry* **1988**, *27*, 924. b) M. W. Kalnik, C. N. Chang, F. Johnson, A. P. Grollmann, D. J. Patel, *Biochemistry* **1989**, *28*, 3373.

139.   I. Goljer, S. Kumar, P. H. Bolton, *J. Biol. Chem.* **1995**, *270*, 22980.

140.   M. Hutter, T. Clark, *J. Am. Chem. Soc.* **1996**, *118*, 7574.

141.   S. Diekmann, D. A. Zarling, *Nucl. Acids Res.* **1987**, *15*, 6063.

142.   P. J. Hagerman, *Annu. Rev. Biochem.* **1990**, *59*, 755.

143.   a) J. G. Nadeau, D. M. Crothers, *Proc. Natl. Acad. Sci. U.S.A.* **1989**, *86*, 2622. b) R. E. Dickerson, D. S. Goodsell, M. L. Kopka, *J. Mol. Biol.* **1996**, *256*, 108. c) R. M. Gaunis, H. Guo, T. D. Tullius, *Biochemistry* **1996**, *35*, 13729. d) D. Sprous, W. Zacharias, Z. A. Wood, S. C. Harvey, *Nucl. Acids Res.* **1995**, *23*, 1816.

144.   H. C. M. Nelson, J. T. Finch, B. F. Luisi, A. Klug, *Nature* **1987**, *330*, 221.

145.   D. G. Alexeev, A. A. Lipanov, I. Y. Skuratowskii, *Nature* **1987**, *325*, 821.

146.   M. Schatzky-Schwartz, N. D. Arbuckle, M. Eisenstein, D. Rabinovich, A. Bareket-Samish, T. E. Haran, B. F. Luisi, Z. Shakked, *J. Mol. Biol.* **1997**, *267*, 595.

147.   N. V. Hud, V. Sklenář, J. Feigon, *J. Mol. Biol.* **1999**, *286*, 651.

148.   H.-S. Koo, H.-M. Wu, D. M. Crothers, *Nature* **1986**, *320*, 501−506. b) V. P. Chuprina, *Nucleic Acids Res.* **1987**, *15*, 293.

149.   M. McCall, T. Brown, O. Kennard, *J. Mol. Biol.* **1985**, *183*, 385.

150.   A. Okamoto, K. Tanaka, I. Saito, *J. Am. Chem. Soc.* **2003**, *125*, 5066.

151.   M. Bixon, J. Jortner, *J. Phys. Chem. B* **2000**, *104*, 3906.

152.   B.-M. Sjöberg, *Struct. Bonding* **1997**, *88*, 139.

153.   M. Kolberg, K. R. Strand, P. Graff, K. K. Andersson, *Biochim. Biophys. Acta* **2004**, *1699*, 1.

154.   V. Pelmenschikov, K.-B. Cho, P. E. M. Siegbahn, *J. Comput. Chem.* **2004**, *25*, 311.

155.   C. R. Cantor, M. M. Warshaw, H. Shapiro, *Biopolymers* **1970**, *9*, 1059.

156.   A. M. Maxam, W. Gilbert, *Methods Enzymol.* **1980**, *65*, 499.

157.   J. Sambrook, E. F. Fritsch, T. Maniatis, *Molecular Cloning Vol. 1−3, A Laboratory Manual*, 2nd ed., Cold Spring Harbor Laboratory Press, New York, **1989**.

16   Subject Index

Oxidation Potentials of Nucleobases

The oxidation potentials indicated are measured for nucleosides in solution.[22] Within DNA, the oxidation potentials alter depending on the nature of the base pairing and the neighbouring bases.

Nucleoside	Structure	Oxidation Potential / (V *vs.* NHE)
2'-Deoxyadenosine		$+1.96^a$ / $+2.03^b$
Thymidine		$+2.11^a$
2'-Deoxyguanosine		$+1.49^a$ / $+1.58^b$
2'-Deoxycytidine		$+2.14^a$

^{a} Data from [22a], measured in AcCN. ^{b} Data from [22b], measured in aqueous solution.

Dipl. Chem. Ernst Furrer

Eidesstattliche Erklärung

Ich erkläre hiermit, dass ich die Dissertation „On the Distance-Independent Hole Transfer over Long $(A-T)_n$-Sequences in DNA" nur mit der darin angegebenen Hilfe und bei keiner anderen Fakultät eingereicht habe.

Basel, den 1. September 2004

(Ernst Furrer)

The following lecturers of the University of Basel contributed to my education:

T. Bickle	H.-C. Im Hof	J. Seelig
Th. Boller	U. Jenal	U. Séquin
E. Constable	M. Jungen	I. Sick
J. Engel	T. A. Kaden	H. Sigel
W. Gehring	A. Keller	L. Tauscher
G. Gescheidt	J. P. Maier	C. Ullrich
B. Giese	W. Meier	T. Wirth
H.-P. Hauri	M. Neuburger-Zehnder	J. Wirz
P. C. Hauser	M. Oehme	W.-D. Woggon
A. Herrmann	A. Pfaltz	A. D. Zuberbühler
C. Housecroft	G. Schatz	
H. Huber	P. Schiess	